Geobag Stability for Riverbank Erosion Protection Structures

by

Angela Thompson

A thesis submitted in partial fulfillment of the requirements for the degree of

Master of Science

in

Water Resources Engineering

Department of Civil and Environmental Engineering

University of Alberta

Abstract

Erosion along the banks of the Brahmaputra River in Bangladesh and India leads to both the loss of infrastructure and land, consequently forcing many of those who live along the riverbanks into poverty. Because of the limited availability of hard materials that are traditionally used to protect riverbanks, such as rock, geotextile sand filled bags (geobags) have emerged as an economic solution to this devastating problem. Over the last twenty years geobags have been used to create revetments which have begun to systematically stabilize large reaches of the Brahmaputra river system. Geobags are required to be stable against current loading in order to avoid failure of these erosion preventing structures, which can be many kilometers long. While flexible geobags have been studied extensively for coastal applications, there are limited studies regarding their stability in rivers. This study was designed to address the problem: when do geobags undergo incipient motion under current loading? Using a combination of physical and numerical models, this study approached the problem of incipient motion via the method of permissible velocity, as well as, the method of critical shear stress. The physical model study, performed at Northwest Hydraulic Consultants laboratory in Vancouver, Canada, used scaled geobags which are large enough to replicate the flexibility of the bags used in the field. Results from the physical model study were used to improve the current sizing formula by using the thickness rather than the cube root of the volume as the characteristic diameter. Additionally, the stability coefficient was suggested to be a function of the filling percentage of the geobags because the stability of the bag appears to be dependent on the flexibility and fill of the bag. The physical model study was recreated in a three dimensional numerical model, which was then used to find the shear stresses on the geobag surface.

There was not enough data to confidently find a Shields parameter for geobags to use in a design capacity; however, first results imply the value to be around 0.09. These first results also imply that the Shields parameter varies with fill percentage of the geobags.

Preface

Chapter 1 is taken from: Thompson, A., Oberhagemann, K., She, Y., Haque, A.M.A., 2018. The behavior of self-launching geotextile bag aprons – latest investigations from the Lower Brahmaputra in Bangladesh. 9th International Conference on Scour and Erosion, Taipei.

Chapter 2 is taken from: Thompson, A., Oberhagemann, K., She, Y., Submitted for publishing in the Journal of Geotextiles and Geomembranes. Geobag stability for riverbank erosion protection structures: Physical model study.

Chapter 3 is to be submitted for publication: Thompson, A. and She, Y. Geobag stability for riverbank erosion protection structures: Numerical model study.

Acknowledgements

I would like to thank Dr. Yuntong She and Knut Oberhagemann for their guidance throughout this research work. I would also like to thank Northwest Hydraulic Consultants Ltd for their financial and technical support, as well as the use of their laboratory facilities. I extend my gratitude to both the Natural Sciences and Engineering Research Council of Canada and Mitacs for financial support of this research. I would also like to acknowledge the Flood and Riverbank Erosion Risk Management Investment Program, implemented by the Bangladesh Water Development Board, with financial support for the Asian Development Bank. Thank you to both Mr. Saleh Adib Turash for his help processing data and to Dr. Rajaratnam for his valuable advice.

Finally, I would like to thank my family for their support throughout my studies.

Table of Contents

List of symbols xiii

1 Introduction 1

1.1 Development of geobag revetments 1

1.2 Dimensioning geobags 5

1.3 This thesis 9

2 Geobag stability for riverbank erosion protection structures: Physical model study ... 11

2.1 Introduction 11

2.2 Geobag revetments on the Brahmaputra River 16

2.2.1 The Brahmaputra River 16

2.2.2 Implementation of geobag revetments 17

2.2.3 Current design methodology 18

2.3 Experimental set up and method 19

2.3.1 Scaling geobags 19

2.3.2 Experimental set up 22

2.4 Results and Discussion 25

2.4.1 Incipient motion 25

2.4.2 Review of USACE formula 30

2.5 Conclusion 37

2.6 References 39

3 Geobag stability for riverbank erosion protection structures: Numerical model study 43

3.1 Introduction ... 43

3.2 Methodology ... 47

3.2.1 Flume experiment ... 47

3.2.2 Numerical model description ... 48

3.3 Results and Discussion ... 52

3.3.1 Discussion of shear stresses ... 52

3.3.2 Hydraulic forces acting on a geobag surface ... 54

3.3.3 Shields parameter ... 59

3.3.4 Contemplating the roughness of a geobag surface ... 62

3.4 Conclusions ... 65

3.5 References ... 66

4 Treatment of the boundary layer in the numerical model ... 70

5 Conclusion ... 74

References ... 77

Appendix A: Differential images ... 84

List of Tables

Table 1-1: Historical use of geobags in the Brahmaputra basin 3

Table 1-2: Summary of systematically built underwater works alongside the braided Brahmaputra. 5

Table 1-3: Overview of geobag sizes used in the Brahmaputra basin 9

Table 2-1: Four different sized geobags used in the physical model experiment 20

Table 2-2: The five experiment series performed 23

Table 3-1: Details of the geobags used in the flume experiments (using a scaled of 1:7) 47

Table 3-2: Numerical models created and measured data from the flume experiments (Thompson et al. submitted) 50

Table 3-3: Mesh independence using 250 kg cloth bags for Case 2 51

Table 3-4: Summary of forces, stresses and Shields parameters from CFD results 60

Table 3-5: Field multibeam data used to analyze geobag surface roughness 64

Table 3-6: Surface roughnesses (flume Nikuradse roughnesses scaled to prototype height) 65

Table 4-1: Differences between the boundary layer mesh of the two models being compared 71

Table 4-2: Mesh independence study for the wall function approximation model 71

List of Figures

Figure 1-1: Map of locations of geobag revetments within the Brahmaputra river basin. 4

Figure 2-1: Schematic diagram of geobag revetments (Oberhagemann and Hossain 2011) 11

Figure 2-2: Surface velocity distributions from float track survey data over seven different geobag revetments located in the Lower Brahmaputra 14

Figure 2-3: The Lower Brahmaputra Basin, with 1150 km of braided Brahmaputra River system (note that the river changes its name as it crosses country borders and joins with tributaries) 17

Figure 2-4: Four different sized geobags used in the physical model experiment (the orange bag was used in the 2010 NHC study) 20

Figure 2-5: Flexibility of geobags with varying bag dimensions (measured in meters), degrees of fill percentage and material (circled points show the bags used in the flume tests, NHC (2010) bag is 0.047 x 0.038 m) 22

Figure 2-6: Schematic of flat-bed flume experiment, where an 'x' marks a measurement point 24

Figure 2-7: Differential image of the before and after bed elevations of an experimental run (left) and the corresponding measured velocity profiles (right) for Series 2 with dumped bags 26

Figure 2-8: Differential image of the before and after bed elevations of an experimental run (left) and the corresponding measured velocity profiles (right) for Series 1 with placed bags 27

Figure 2-9: Percentage of elements moved and the corresponding depth averaged velocity 29
Figure 2-10: Experimental results for rock and its comparison with historic data and the USACE relationship with a stability coefficient of 0.30 (where y represents the vertical axis and x represents the horizontal axis) 31
Figure 2-11: Experimental results for geobags and its comparison to previous studies and the USACE relationship with a stability coefficient of 0.31 (where y represents the vertical axis and x represents the horizontal axis) 32
Figure 2-12: Measured and theoretical volumes of geobags (percentages show the fill percentage of the bags) 33
Figure 2-13: Dumped geobag incipient motion results presented with thickness, t, used as the characteristic diameter (where y represents the vertical axis and x represents the horizontal axis) 35
Figure 2-14: Placed geobag incipient motion results presented with thickness, t, used as the characteristic diameter (where y represents the vertical axis and x represents the horizontal axis) 35
Figure 2-15: Relationship between stability coefficient and filling percentage 36
Figure 3-1: Forces acting on a submerged geobag under current loading 45
Figure 3-2: Domain and boundary conditions of the numerical models 50
Figure 3-3: Example longitudinal cross section of flume showing loss in resolution from using a 2 cm grid 51
Figure 3-4: Calibrated velocity profiles for Case 1 and 2 51
Figure 3-5: Total shear stress from the CFD model for each element section 53

Figure 3-6: Velocity, pressure (both side view), and drag force (top view), over 250 kg cloth geobags for Case 2, where flow is from right to left 55
Figure 3-7: Velocity, pressure (both side view), and drag force (bottom view) over 250 kg cloth geobags for Case 1, where flow is from right to left 56
Figure 3-8: Surface of each element section in the flume experiment 57
Figure 3-9: Image of the bed before and after velocity run and the difference in bed elevation for Case 2 (top) and Case 1 (bottom) where stresses on numbered bags are shown in the following figure (flow from top to bottom) 58
Figure 3-10: The correlating total shear stress for a number of failed and stable geobags (bag locations are shown in the previous figure) 59
Figure 3-11: Corresponding Shields parameter for the stable and unstable geobag sections (the 250 kg geotextile bag was not stable in either Case 1 or 2; however, it was stable in the lower velocity runs) 61
Figure 3-12: Multibeam image of underwater geobag apron 64
Figure 4-1: Comparison of the turbulent kinetic energy of the two models and the measured values. 72

List of symbols

Symbol	Units	Description
A	m^3	Area
b	m	Width of flume
C_D	-	Drag coefficient
C_s	-	Stability coefficient
C_T	-	Thickness coefficient
C_v	-	Vertical velocity distribution coefficient
D	m	Characteristic diameter for uniformly sized material
D_{30}	m	Characteristic diameter for graded material where 30% material is finer
F_D	N	Drag force
g	m/s^2	Acceleration due to gravity
h	m	Length of geobag fabric
k	m^2/s^2	Turbulent kinetic energy
k_s	m	Nikuradse roughness
K_1	-	Side slope correction factor
m	kg	Mass
n	-	Manning roughness factor
R	m	Hydraulic radius
S_f	-	Safety factor
S_F	-	Friction slope
t	m	Thickness
u'	m/s	Fluctuations of the velocity component in the x direction
u*	m/s	Shear velocity
v'	m/s	Fluctuations of the velocity component in the y direction
V	m/s	Velocity
V_{cr}	m/s	Critical velocity
w	m	Width of geobag fabric
w'	m/s	Fluctuations of the velocity component in the z direction
y	m	Depth
θ	-	Shields parameter
μ	kg/m·s	Dynamic viscosity
ρ	kg/m^3	Density
ρ_s	kg/m^3	Saturated density of the protective elements
ρ_w	kg/m^3	Density of water
τ	Pa	Shear stress
τ_{bed}	Pa	Shear stress acting on the bed of the flume
τ_{cr}	Pa	Critical shear stress for the onset of incipient motion
τ_{wall}	Pa	Shear stress actin on the walls of the flume
ϕ	o	Degree of flexibility
ω	s^{-1}	Turbulence eddy frequency
∀	m^3	Geobag volume

1 Introduction

1.1 Development of geobag revetments

The Brahmaputra combines two major challenges for the designers of riverbank protection works: highly unpredictable erosion patterns and deep, rapid scouring. It has built the deltaic landscape of Bangladesh over hundreds of thousands of years through the agents of flood waters and sediment. The sediment is shed from the southern Himalayan slopes and consists of fine, non-cohesive sands and silts, which are easily erodible. More than 30 m of vertical erosion has been measured during one season. In addition, the Brahmaputra has widened rapidly in Bangladesh from an average width of 8 km to 12 km since the late 1960s. The resulting loss of fertile floodplain land and a lack of a defined boundary between floodplain and river has negative developmental impacts on large parts of the country, which is striving to reach middle-income level within the next five years.

Though initially focusing on erosion protection efforts for a few towns, Bangladesh and Assam (India) felt an increasing need to provide riverbank protection to larger, but less intensively used areas. To do this, an economic, yet sustainable riverbank protection solution was needed to protect largely agricultural areas. An advancement in geobag technology occurred when geobag revetments were tested systematically in two places in Bangladesh (ADB 2002), completing a two-year pilot phase in 2006. This development was based on experience gained from earlier works, dating back as early as 1989, when large bags were used as a filter layer for Chandpur Town protection (Halcrow 1990). This application of geobags at Chandpur, for the first time, created an appreciation for the need of a flexible filter layer, which is provided by the geobags. Subsequently, after lifting a ban on the use of geotextiles in Bangladesh in the mid-1990s, geobags were used as an apron

for pilot works at Bahadurabad in 1996 (FAP21 2001) and to repair erosion damages at Sirajganj Town Protection in 1999 (Halcrow 1998 and Halcrow 1999). Preparation for the first systematic low-cost revetment works started in 2001 for two sites, one in the Lower Jamuna and one at the confluence of Meghna and Padma rivers (ADB 2002).

Since the early 2000s, geobag revetments have been systematically built along more than 45 km of riverbanks (Oberhagemann & Hossain 2011). This work has performed well during repeated erosional attacks, mainly due to the self-launching behavior of the geobag aprons, which prevent the undermining of the toe and the eventual geotechnical collapse of the riverbanks. Based on their successful performance, geobags are currently implemented for the river training works of the Padma Bridge, one of the largest river bridges on earth (Maunsell|AECOM 2011). The geobags used for the bridge have a design lifetime of 100-years, in the form of a filter layer under rock riprap, and as riverbank protection on dredged slopes and toe aprons. Since 2015, the Bangladesh Water Development Board (BWDB) is expanding the use of geobag revetments for localized riverbank protection towards river training works of larger river reaches (ADB 2014, NHC and EMM 2016). Table 1-1 summarizes the key developments of geobag revetments in Bangladesh since 1989.

Table 1-1: Historical use of geobags in the Brahmaputra basin

Location and Year	Type of Work
Chandpur, 1989	Woven geobags used as filter layer under concrete blocks (Halcrow 1990)
Bahadurabad, 1996	Different sized geobags used as a falling apron (FAP21 2001)
Sirajganj, 1999	Repair of town protection damage in layers with different sized geobags (Halcrow 1998, Halcrow 1999)
Kaitola, Lower Jamuna, Mohanpur, Meghna-Padma confluence, 2002	Various sizes of geobags used for systematically dumped revetment works (ADB 2002, NHC 2006b)
Countrywide, 2004 onwards	BWDB uses geobags as riverbank protection (undocumented)
Padma bridge, 2010	Geobag application for bridge training works with a 100 year life time (Maunsell|AECOM 2011)
Dibrugarh, Palasbari, 2011	125 kg bags for long guiding revetments (ADB 2010)
Lower Jamuna, Upper Padma, 2017	Geobag revetments for systematic stabilization of Jamuna and Padma rivers (ADB 2014, NHC & EMM 2016)

Since the first systematic implementation of geobag revetments in Bangladesh during the dry season in early 2004, geobag revetments have been built extensively along the ~1150 km long braided Brahmaputra course. Starting with the work on the Lower Jamuna and Meghna Padma confluence in 2004 (ADB 2002), systematic works of more than 60 km has been built at 9 locations, shown in Figure 1-1and Table 1-2. The work mostly consists of geobag revetments consisting of three to five layers of geobags systematically placed on the existing under water slopes with concrete blocks above water. Exceptions are at Palasbari and Gumi, where rock riprap constitutes the above water protection and at Padma Bridge where the work is built on dredged 1V:6H (1 vertical and 6 horizontal) underwater slopes and covered with rock riprap in the bridge area. In Assam, India the use of geobags has also increased as rock is more and more discouraged due to the environmental impact of the quarry activities.

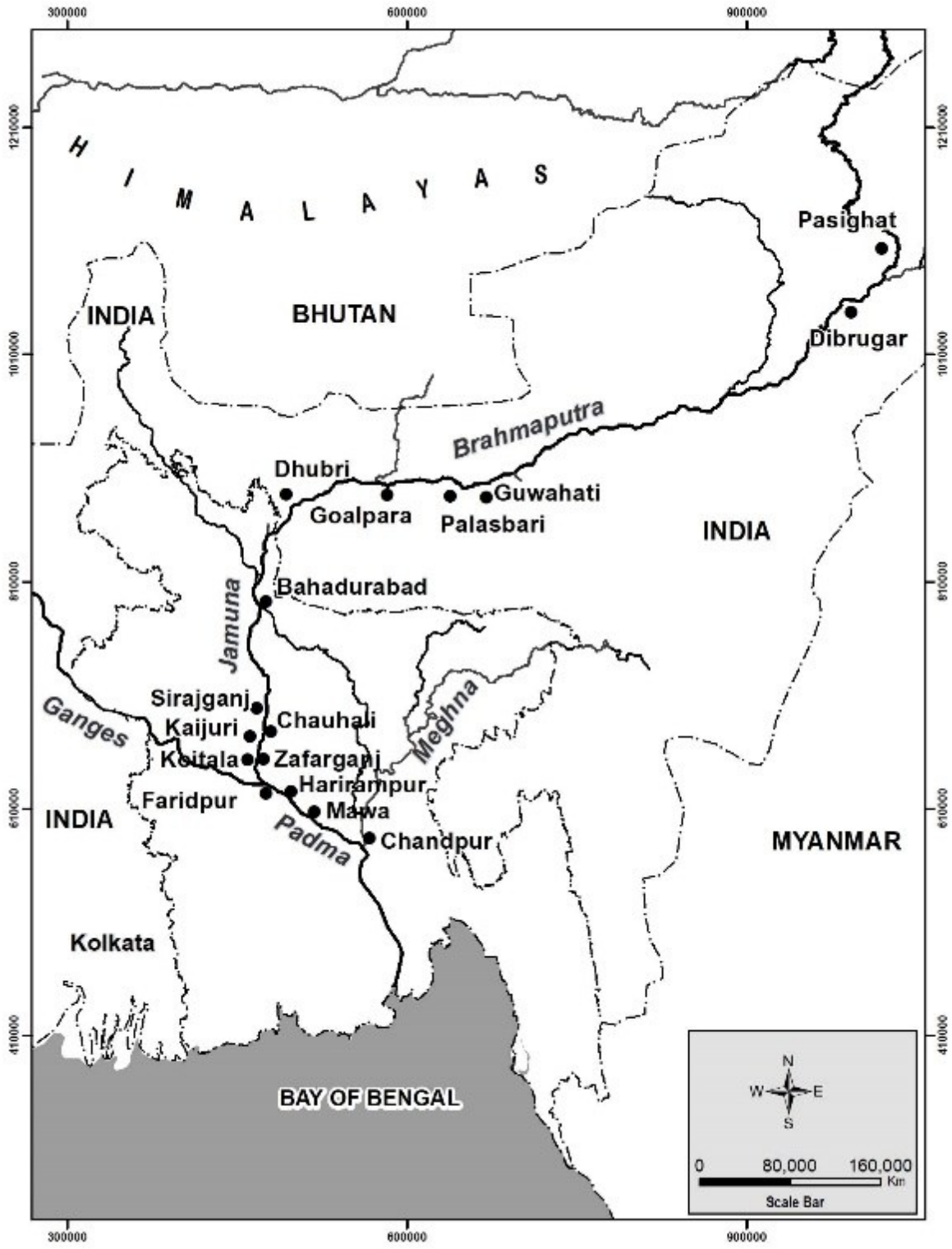

Figure 1-1: Map of locations of geobag revetments within the Brahmaputra river basin.

Table 1-2: Summary of systematically built underwater works alongside the braided Brahmaputra.

Location and Year	Work Details
Motholla, 2012-15	2.4 km, 125 kg bags, three layers
Palasbari, 2012-17	4.9 km, 125 kg bags, three layers
Gumi, 2012-17	4.5 km, 125 kg bags, three layers
Chauhali, 2016-17	7.0 km, 250 kg bags, five layers
Kaijuir, 2009-11	10.0 km, 126 kg bags, three layers
Kaitola, 2004-08	7.0 km, 126 and 78 kg bags, three layers
Zaffarganj, 2016-17	2.0 km, 250 kg bags, five layers
Harirampur, 2016	9.8 km, 250 kg bags, five layers
Padma Bridge at Mawa, 2015-20	13 km, three layers of 126 kg bags under rock riprap, five layers of 800 kg bags on slope and apron
Mohanpur, 2004-06	4.2 km, 126 and 78 kg bags, three layers, "fascine work" consisting of geotextile sheet sunken with 36 kg bags and loaded with 78 and 126 kg bags.

1.2 Dimensioning geobags

If geobags are to be used extensively for large scale river stabilization works, it is justifiable to revisit the hydraulic design of the bags. Systematic diving observations indicate that some of the geobags may be oversized (ADB 2003). During diving investigations, divers have pulled on the geobags with the intentions of displacing them. The bags are extremely resistant to movement, even 78 kg bags with additional hydraulic forces from flow velocities of approximately 2 m/s. Bag sizes have increased over time in line with increased design loads (Table 1-3). During first implementation in Bangladesh from 2004 to 2007 mixes of six 78 kg and two 126 kg bags (three 78 kg bags or two 126 kg bags providing coverage of one square meter each) have been used. Model studies conducted in 2005 at the Northwest Hydraulic Consultants (NHC) laboratories in Vancouver (NHC, 2006a) indicated that uniform bag sizes also result in good coverage. Therefore, later implementation at Kaijuri and in Assam made use of only the 126 kg bag. Different from earlier work, the work implemented since 2016 has been redesigned to use

250 kg bags (covering an area of one square meter) based on an increased hydraulic loads (3.5 m/s as opposed to 3 m/s, depth averaged velocity). At Padma Bridge 800 kg bags are used to cope with the design flow velocities of up to 5 m/s.

Large bags can slow down construction drastically, and therefore reduce the number of kilometers that can be protected each year. Larger bags also cost more, being that they require more dredged sand. The most time and cost-effective construction technique fills and dumps the geobags by hand from a barge. Once the bags are too large for two men to handle, a mechanized dumping process is required to build the revetments, which drastically increases the construction costs and prolongs the construction time. Given that larger bags are more difficult to fill and construct, and therefore reducing the amount of protection that can be provided in a dry season, optimizing the sizing process is desirable.

Extensive research has been done regarding the stability of geosystems under hydraulic loads in coastal applications (for example, Recio & Oumeraci 2009, Dassanayake 2013); however, the study of geobags used for systematic riverbank protection structures is still in its infancy. The average bottom shear stress for a current with waves is three to five times greater than that without waves (Pilarczyk 1991); therefore, design criteria intended for coastal protection applications may not be entirely suitable for underwater works in rivers, where the loading is strictly the result of currents.

There have been a number of studies which have researched geobags incipient motion in rivers. Pilarczyk (2000) discussed resistance of geobags against current attack and the need for more experimental data for final design recommendations and

recommended stability coefficient for geobags based on applied engineering judgement. Bezuijen and Vastenburg (2013) provided a guideline for sizing geobags against current loading based on Pilarczyk's formula. Akter et al. (2013a and b) has also studied the failure mechanisms of geobag revetments using Discrete Element Modelling but did not provide a design formula for geobag resistance again incipient motion. The study used the model to capture the failure mechanisms of deformable geobags and found the drag and lift coefficients for the bags, as well as analyzed the roughness values of geobag surfaces. It did not present any design formulas for resistance of incipient motion. This study's focus was limited to an orderly slope of geobags, similar to the ones found on the above-water slopes where the bags are placed, but unlike the dumped bags found in deeper sections. Zhu (2004) has theoretically derived two formulas to describe the onset of incipient motion of sandbags (similar to geobags) in open channel flow. Zhu approached the problem of the initiation of geobag incipient motion with an extremely simplified approach using rectangular block shaped bags on a flat surface, and applying the depth average velocity as the critical velocity. The simplified bags do not represent the various bag shapes found in the field, which occurs because of the dumping construction process. Elkholy and Chaudhry (2011) studied the mechanics of motion of spherical shaped bags in a failing dyke using laboratory experiments. The research looked at the effects of bed roughness, particle roughness, shape factor and the initiation of particle motion. The bags used in this study do not replicate the shape of the geobags of interest used in revetments.

At the moment, 250 kg geobags are predominately used along the banks of the Brahmaputra, which have been sized based on the USACE formula (USACE 1991), presented by NHC's physical model test (NHC 2006a and NHC 1010). The current design

formula has an exponential relationship between flow velocities and bag size. In addition, the bags size decrease as depth increases. As a result, in sections of the river with high flow velocities or deep depths, such as the Upper Meghna and Padma river confluence where depths can reach 70 m, the formula can produce unrealistic bag sizes.

The design formulas all use vertically-averaged velocity for sizing geobags without considering the local shear stresses acting on the bags. In large, braided rivers such as the Brahmaputra, depth averaged velocities may not accurately describe the velocity gradients in the water column, and therefore, the shear stress. Shear stresses have also been used to describe the incipient motion of sediment in open channel flow. Shields (1936) developed his relationship that related the shear stress to the characteristic diameter of an element using a Shields parameter. Since Shields' work other studies have looked at the critical shear stresses to instigate movement; however, to the author's knowledge, none of these studies have looked directly at the shear stresses acting on a geobag surface. Dey and Papanicolaou (2008) have provided a comprehensive overview of studies concerning incipient motion of sediment.

Diving investigations have also shown that the surface of the revetment slopes can be quite rough with elements protruding into the flow, and geobags stacked underwater, protruding over 1 m into the flow. Observations from shore have also shown that the surface flow characteristics of the river are different over the geobag covered section compared to the natural river bed. It is clear that the roughness of the geobag surface is drastically different from the natural bed, and warrants further study to understand how the shear stresses are distributed across the geobag surface.

Table 1-3: Overview of geobag sizes used in the Brahmaputra basin

Location and Year	Geobag dimensions used
Chandpur, 1989	1.31 x 0.94 x 0.46 m 1.01 x 1.04 x 0.46 m 883 kg in air, 543 kg in water (Halcrow 1990)
Bahadurabad, 1996	1.04 x 0.52 m, 90 kg 0.96 x 0.88 m, 125 kg 1.20 x 0.88 m, 180 kg 1.60 x 0.85 m, 250 kg 2.15 x 1.27 m, 900 kg (FAP21 2001)
Sirajganj, 1999	0.50 x 0.35 m, 0.04 m^3, 20 kg 1.20 x 0.90 m, 0.25 m^3, 250 kg 0.68 m^3, 900 kg 15 x 8 m blanket (Halcrow 1998, Halcrow 1999)
Kaitola, Lower Jamuna, Mohanpur, Meghna-Padma confluence, 2002	1.03 x 0.70 m, 126 kg 0.83 x 0.60 m, 78 kg added mass for dumping: 0.68 x 0.44 m, 36 kg 0.40 x 0.35, 11 kg (ADB 2002, NHC 2006b)
Countrywide, 2004 onwards	1.125 x 0.9 m, 175 kg 1.25 x 1.0 m, 250 kg (undocumented)
Padma bridge, 2010	1.03 x 0.7 m, 125 kg as filter 2.1 x 1.5 m, 800 kg for slope and apron (Maunsell|AECOM 2011)
Dibrugarh, Palasbari, 2011	1.03 x 0.7 m, 125 kg (ADB 2010)
Lower Jamuna, Upper Padma, 2017	1.25 x 1.0 m, 250 kg (ADB 2014, NHC & EMM 2016)

1.3 This thesis

Geobags have proved to be a cost effective solution for preventing riverbank erosion, and thus, providing safety and security to those living within the vicinity of the river. The development of the technology has an extensive history in Bangladesh, as well as in Assam, in India. Although great strides have been made in the success of the works, there

is a gap in knowledge of when geobags undergo incipient motion. The objective of this study was to address this problem, with the goal to develop an optimized sizing methodology for geobags used in river revetments. The current method of sizing geobags using permissible velocity was reviewed. Additionally, a first look at using the critical shear stresses to size geobags was included in this thesis. The study also examined how the flexibility of the geobags influences their stability.

This study used a combination of physical and numerical model studies to assess the incipient motion of the bags. Chapter 2 presents the results of the physical model study, and the reassessment of the current dimensioning formula for resistance against incipient motion. Chapter 3 presents the results from the numerical model and the initial attempt to apply a more theoretically appealing approach, using shear stresses, to describe the incipient motion of geobags. Chapter 4 provides further details on the numerical modelling procedure. Finally, the main conclusions of the study are summarized.

2 Geobag stability for riverbank erosion protection structures: Physical model study

2.1 Introduction

Geobags are sand filled, geotextile containers, which have a mass less than 1500 kg. Geobags are used to create long guiding revetments along sand-bed rivers, having the advantage of acting as both the filter layer and the protection element against scour and erosion (Heibaum et al. 2008). Geobags have been found to be a viable solution for riverbank erosion in sand-bed rivers. The success of the geobag revetments is credited to some unique qualities of the geobags, primarily, geobags' resistance against winnowing in the self-launching, underwater apron due to the flexible and porous nature of the bags. The scour that occurs at the toe of the apron undermines the covered bed, and causes the geobags to 'launch' down the eroded slope (Figure 2-1). The launched geobags protect the slope and drives the scour further away from the bank.

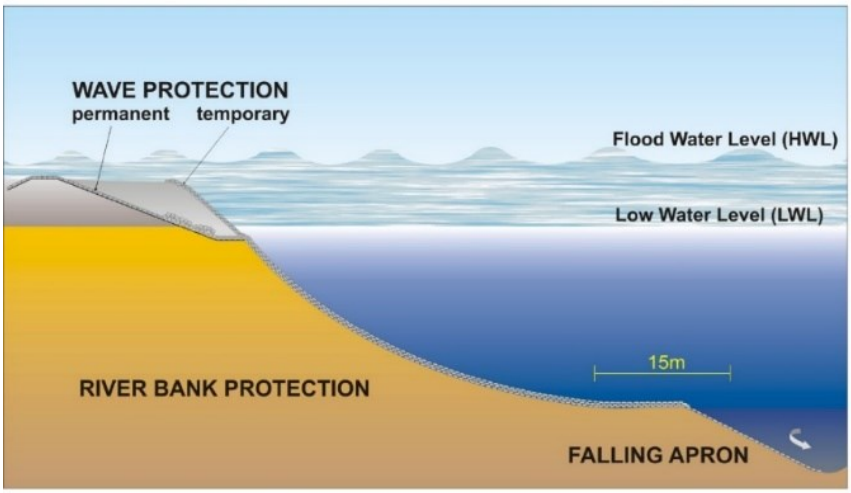

Figure 2-1: Schematic diagram of geobag revetments (Oberhagemann and Hossain 2011)

Geobags have been used extensively around the world for coastal protection (Hornsey et al. 2010) and numerous studies have focused on how geobags perform in coastal environment (e.g. Dassanayake 2013, Recio and Oumeraci 2009). However, the hydraulic loads exerted on the geobags used for coastal work differ from the loads exerted in an open channel flow. Wave loading dominates in coastal environments, while current loading is the primary source of hydraulic forces for geobags used in riverbank protection. Pilarczyk (1991) showed how the average bottom shear stress for a current with waves is 3 to 5 times greater than that without waves. Design criteria intended for coastal protection applications therefore is not suitable for underwater works in rivers, where the loading is strictly from the current.

Understanding the incipient motion of protective elements for riverbank protection due to hydraulic forces can be a thorny problem to tackle when considering the complexities which arise due to turbulent fluctuations and geometric variabilities. Particle movement may occur with low values of applied shear stresses because although the average shear stress may be low, the instantaneous component of shear stress may be high (Neill 1968). The problem of incipient motion becomes inherently a statistical problem, which is dependent on the turbulent shear stress and the bed and inter-granular geometry (Buffington and Montgomery 1997).

Element transport in rivers has been studied extensively, most notably starting with Shields' study of sediment motion using bed shear stresses (Shields, 1936). Pilarczyk (2000), Neill (1968) and the United States Army Corps of Engineers (USACE) (1991) all published further developments in the research of incipient motion of particles in a river.

These studies created semi-empirical relationships to describe incipient motion of sediment and protective elements. In contrast to traditionally used hard riverbank protection elements, geobags are flexible elements which deform, thus the kinematics of the bag's motion are more complicated; however, relationships derived for hard materials provide the basis for understanding the stability of geobags. A number of studies have previously studied geobag stability under current loading.

In 2005 Northwest Hydraulic Consultants (NHC) performed physical model tests to analyze geobag stability (NHC 2006). Further physical model studies were performed by NHC in 2010 (NHC 2010). Both studies used very small geobags elements, which have an approximate scale of 1:20 for a 126 kg, 90 kg and 38 kg geobag (38 x 28 x 9.5 mm, 34 x 25 x 9 mm and 25 x 19 x 7 mm, respectively). The small-scale model geobags lacked flexibility, most likely because the grain size of the filled sand was too large compared to the size of the scaled bags (Neill 2008). As a result of these studies, the USACE formula has been used in Bangladesh to size geobags for riverbank protection (Bangladesh Water Development Board 2010).

Pilarczyk (2000) discussed resistance of geobags against current attack and the need for more experimental data for final design recommendations and recommended stability coefficient for geobags based on applied engineering judgement. Bezuijen and Vastenburg (2013) provided a guideline for sizing geobags against current loading based on Pilarczyk's formula. The sizes of bags suggested by the guideline are more conservative than those suggested by the USACE formula. Observations of constructed revetments show that smaller bags are stable at higher velocities than the guideline suggests. Figure 2-2

shows the probability density of the surface velocity over existing geobag revetments, collected from float track data. It can be seen in the figure that velocity measurements as high as 3.4 m/s have been recorded over stable 125 kg geobag revetments. According to the relationship provided by Bezuijen and Vastenburg (2013) a 125 kg bag becomes unstable at a surface velocity of 3 m/s.

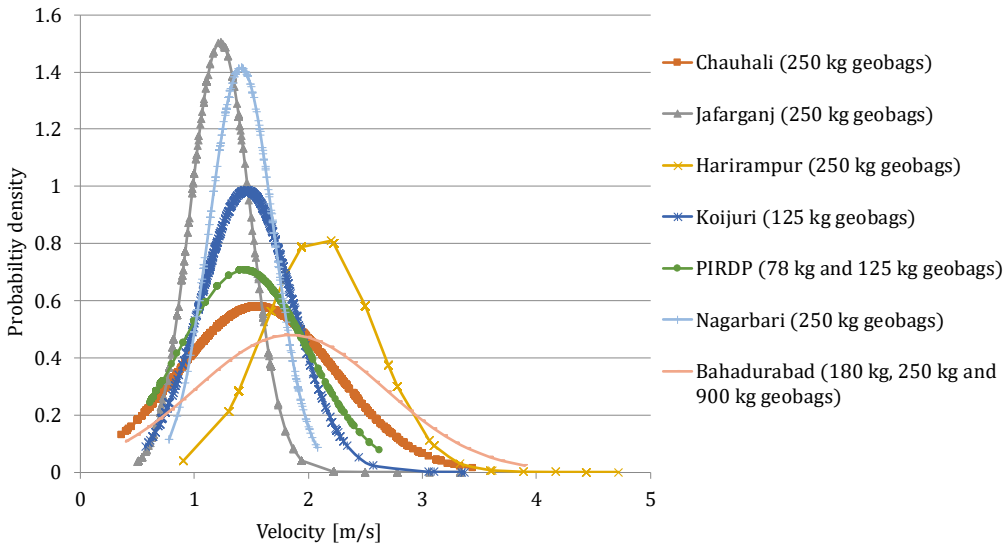

Figure 2-2: Surface velocity distributions from float track survey data over seven different geobag revetments located in the Lower Brahmaputra

Other studies have been performed pertaining to geobag behavior in open channel flow. Zhu et al. (2004) theoretically derived two formulas to describe the onset of incipient motion of sandbags. They approached the problem of the initiation of geobag incipient motion with an extremely simplified approach using rectangular block shaped bags on a flat surface, and applying the depth average velocity as the critical velocity. Elkholy and Chaudhry (2011) studied the mechanics of motion of spherical shaped bags in a failing dyke using laboratory experiments. Akter et al. (2013a, b) published the results of the

application of Discrete Element Modelling of geobag revetments. The model captured the failure mechanisms of deformable geobags and found the drag and lift coefficients for the bags, as well as analyzed the roughness values of geobag surfaces. It did not present any design formulas for resistance of incipient motion. As well, the study focused on an orderly slope of geobags, similar to the ones found on the above-water slopes where the bags are placed, but unlike the dumped bags found in deeper sections. A simple drag and lift coefficient cannot be applied to dumped bags because the elements are of non-uniform shape. In addition, small scaled bags were used, with a size of 103 x 70 mm to replicate a 1.03 x 0.70 m, 126 kg field bags.

With large-scale applications of geobags such as those used on the powerful Brahmaputra River in India and Bangladesh, there is a great need to understand how the river flow and the bags interact, and to optimize the sizing of the bags to prevent incipient motion. If the individual elements that comprise the revetment fail, local scour could occur and cause failures in the structure. Using physical models tests, this study analyzed what velocity incurs incipient motion of geobag elements and re-examined how the geobags are sized. Opposed to previous work, this study used larger geobags in the scaled model in order to better capture the behavior of the bags. In this paper, following a discussion of geobag applications on the Brahmaputra River, the experimental set up is described. Example measured data and detailed analyses are presented next. Implications of the findings to sizing geobags are also discussed and future research needs identified.

2.2 Geobag revetments on the Brahmaputra River

2.2.1 The Brahmaputra River

Draining the lower half of the Brahmaputra basin, the Brahmaputra is the largest braided sand bed river of the world. The river flows mostly through India and Bangladesh, with a 100 year return period flood season discharge of ~100,000 m^3/s (NHC 2013). The Brahmaputra River has a total length of ~1,150 km from Pasighat to the Bay of Bengal (Figure 2-3). Since the 1950s the Brahmaputra has widened dramatically, causing Assam (in India) and Bangladesh to lose approximately 3,000 km^2 of land alongside the banks of the river. This widening is largely the consequence of the Great Assam Earthquake of 1950, which dislodged ~45 billion cubic meters of sediment and, over time, transported it through the river system. The unpredictable riverbank erosion, which can cause the banks to recede up to 1 km in a year, is a major limitation to the area's development. Riverbank erosion casts marginal farmers into poverty, and so, riverbank protection schemes become more important as population densities rise.

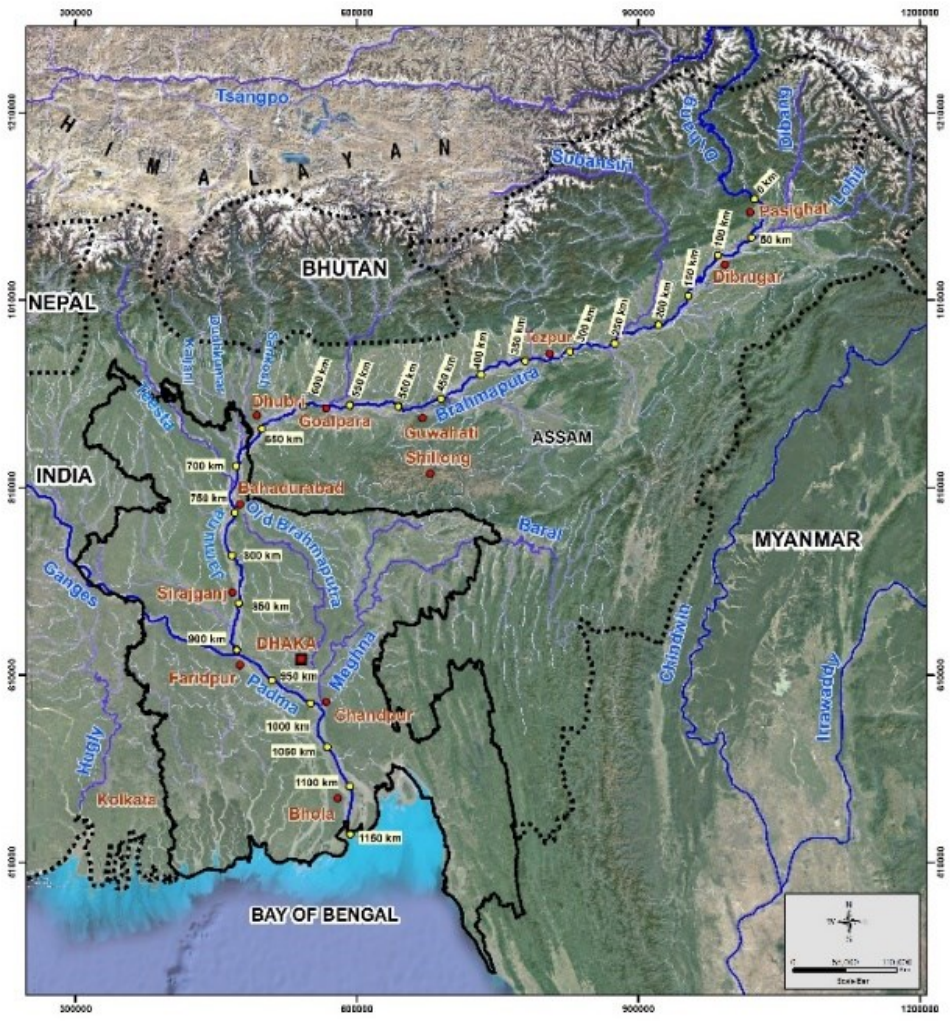

Figure 2-3: The Lower Brahmaputra Basin, with 1150 km of braided Brahmaputra River system (note that the river changes its name as it crosses country borders and joins with tributaries)

2.2.2 Implementation of geobag revetments

Geobags have emerged as a solution to this problem. Since the early 2000s, geobags have been widely used in Bangladesh to create long guiding revetments, up to 10 km in length, systematically protecting more than 60 km of riverbanks (Oberhagemann and Hossain 2011, Thompson et al. 2018). The technology has been further applied in Assam,

India since 2010. Apart from protecting the riverbanks locally, these revetments guide the flow and stabilize the channel pattern of the wide braided river belt, overall stabilizing the river system and enabling land reclamation. Geobag revetments have become an affordable solution to riverbank erosion in Bangladesh since the country has little access to hard, traditional construction material, such as rock. Whereas in Assam transport distances and mining problems are the main reason for the application of geobags. Geobag revetments are relatively cost effective at around $3 million USD per kilometer because of the use of abundantly available local resources: geobags, sand and labor. Despite positive implementation experience and good performance, there remain unresolved issues pertaining to the design of geobag revetments. Sizing of the geobags has been inconsistent. In Bangladesh, initially (2004 to 2008) a mixture of 78 and 126 kg geobags were used (Oberhagemann and Hossain 2011). From 2009 to 2011, 125 kg geobags were solely used, all designed for 3 m/s depth-averaged design velocity. Most recently (2015 to 2018) 250 kg geobags in five layers were used, designed for 3.5 m/s depth-averaged design flow velocity. In Assam, work built from 2010 until recently makes use of solely 125 kg geobags.

2.2.3 Current design methodology

Currently an adapted sizing methodology, originally proposed by the USACE for riprap is being used to size geobags (Neill et al. 2008). The USACE method for determining the required stone size using the depth-averaged local velocity is based on data gathered by Maynord in 1988 (Maynord 1988). The relationship reads,

$$\frac{D_{30}}{y} = S_f C_s C_V C_T \left[\left(\frac{\rho_w}{\rho_s - \rho_w} \right)^{\frac{1}{2}} \frac{V_{cr}}{\sqrt{K_1 g y}} \right]^{2.5} \qquad (2-1)$$

where S_F is a safety factor, C_s is a stability coefficient, C_V is a vertical velocity distribution coefficient, C_T is a thickness coefficient, ρ_w is the density of water, ρ_s is the element density, V_{cr} is the local depth averaged velocity, K_1 is the side slope correction factor, g is the acceleration due to gravity, y is the depth and D_{30} is the characteristic diameter (where 30% of graded material is finer; however, geobag revetments are typically built with one size of bag and so the characteristic diameter can be represented by D). The characteristic diameter is commonly taken as the cube root of the element's volume.

2.3 Experimental set up and method

2.3.1 Scaling geobags

It is very important for laboratory experiment to use scaled elements which reproduce important characteristics of geobags that influence their motion. Pilarczyk (2000) mentioned that when doing physical model tests on geotextile containers, the model dimensions should be made as large as possible to retain the characteristics of the geotextile container. Four different sizes of geobags were tested in the experiment (Table 2-1 and Figure 2-4). These four geobag sizes replicate common sizes used in the Brahmaputra River, scaled at 1:7.

Scaled geobags must not only mimic prototype bags' weight and dimensions, but also their flexibility. Flexibility of a geobag is governed by the fabric and the sand filling percentage. Geobags in the field ranging from 36 to 250 kg are made of non-woven geotextile material, weighing 400 g/m^2. However, because of limitations in the manufacturing process, geotextile fabric cannot be scaled below around 150 g/m^2 as it

then become too porous to retain the fine sand-fill. For this reason, geobags using both non-woven geotextile fabric and woven linen fabric were used in the experiment, weighing 150 g/m^2 and 80 g/m^2 respectively.

Table 2-1: Four different sized geobags used in the physical model experiment

Geobag	Mass [kg]	Length [m]	Width [m]	Density [kg/m^3]	Fill	Thickness [m]	Material
125 kg cloth	0.364	0.15	0.10	1732	84%*	0.031	80 g/m^2 woven linen
250 kg cloth	0.729	0.18	0.14	1881	66%*	0.040	80 g/m^2 woven linen
250 kg geotextile	0.729	0.18	0.14	1632	66%	0.040	150 g/m^2 non-woven geotextile
800 kg geotextile	2.332	0.29	0.21	1626	58%	0.055	150 g/m^2 non-woven geotextile

*Note: Because of the flexibility of the cloth fabric, the 125 and 250 kg cloth geobags have the potential to hold more sand than the equivalent geotextile bag, considered to be 120% filled of the bag size for this experiment.

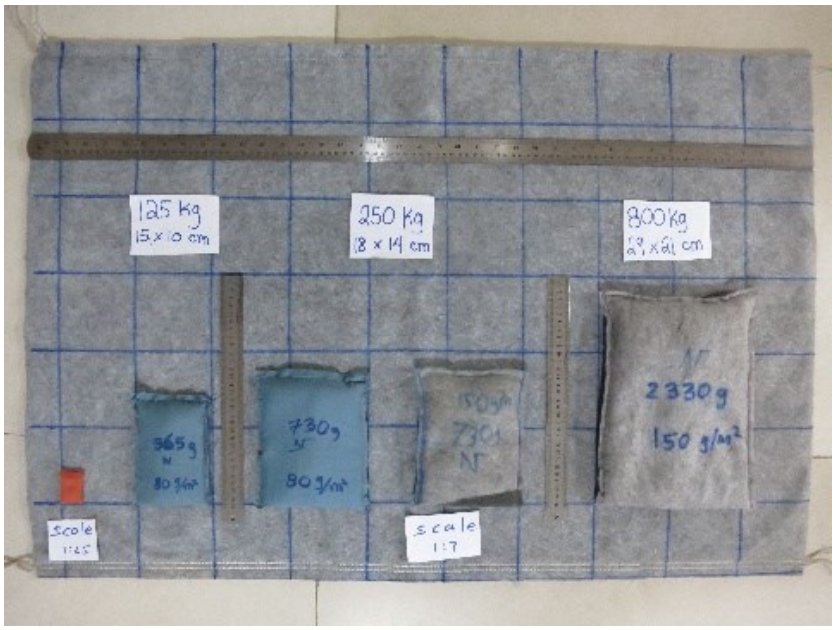

Figure 2-4: Four different sized geobags used in the physical model experiment (the orange bag was used in the 2010 NHC study)

Before the flume test commenced a simple test was performed to understand how the flexibility of geobags change as the dimensions, fill percentage and fabric change (Figure 2-5). Bags were filled with various degrees of filling and allowed to overhang with half of their length unsupported off a table and the angle at which they hung from the horizontal was measured (Thompson et al. 2018). Figure 2-5 shows the results non-dimensionalized by comparing the mass and angle of flexibility, ϕ, to those of a 125 kg prototype sized bag. It can be seen that larger bags are more flexible. Additionally, heavier fabric reduces the flexibility of a geobag. Bags with less fill also become more flexible because there is more space for the sand to move inside the bags. The geobags used in experiments of this study (Table 2-1 and Figure 2-5) better replicate the flexibility of prototype sized geobags compared to the geobags used in the earlier NHC scaled models. The NHC scaled bags (shown on the far left of Figure 2-5) only have 10% of the flexibility of a prototype sized bag, while the geobags used in this study have a range from 53% to 124% of the flexibility of a prototype sized bag.

Density is an important parameter for any incipient motion study. The density of geobags depends on the filling sand and the filling methodology. In the field, geobags 250 kg and below are filled manually by unloading baskets of sand into each bag. Consequently, geobag densities will have a degree of variability. To measure the saturated density of the filling sand, the volume of the scaled bags was obtained by soaking the bags with water and freezing them. It was found that the larger bags tended to have a lower density, possibly because they have a lower fill percentage and so the sand is not as tightly packed. The densities found in the current study (shown in Table 2-1) are close to previous densities

found by past studies. Zellweger (2007) found a density of 1760 kg/m^3 and NHC (2010) found a density of 1778 kg/m^3.

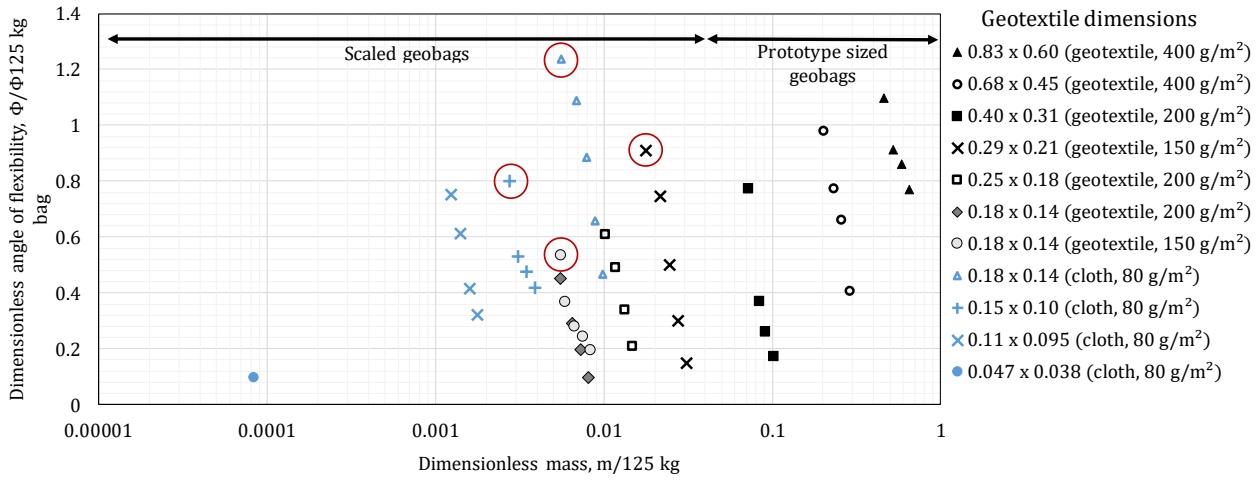

Figure 2-5: Flexibility of geobags with varying bag dimensions (measured in meters), degrees of fill percentage and material (circled points show the bags used in the flume tests, NHC (2010) bag is 0.047 x 0.038 m)

2.3.2 Experimental set up

The physical model study was performed in the NHC physical model laboratory in Vancouver, Canada. The flume was 1.2 m wide and 5.7 m long. The bed of the flume was covered with the protective elements. A schematic of the flat bed flume can be seen in Figure 2-6. Rock was placed upstream as a control section, followed by the four different types of geobags. The rock has a D_{50} of 0.064 m, and a D_{15} to D_{85} ratio of 0.5, similar to the rock used in the 2010 NHC tests. Each element section was approximately the same length. Five test series were performed, varying the slope of the bed, the order of the elements in the flume and the placement process (Table 2-2). The slope was varied in order to replicate the behavior of geobags on both flatbed scenarios and sloped surfaces that occur after

launching. Depending on the test series, the geobags were either orderly placed longitudinally on the bed of the flume or dropped into approximately 30 cm of water and allowed to settle on the bottom of the flume in order to replicate the "dumping" implementation process used in the field. A water depth of 30 cm corresponds to 2.1 m prototype depth. Zellweger (2007) showed that 126 kg bags have the same orientation when landing on the bed's surface after falling approximately 1.5 m through the water column.

Table 2-2: The five experiment series performed

Series	Placement method	Bed slope	Order of elements (from upstream to downstream)
1	Placed	Flat	Rock→250 kg cloth→125 kg cloth→250 kg geotextile→800 kg geotextile
2	Dumped	Flat	Rock→250 kg cloth→125 kg cloth→250 kg geotextile→800 kg geotextile
3	Dumped	Flat	Rock→250 kg geotextile→800 kg geotextile→125 kg cloth→250 kg cloth
4	Placed	Launched slope 1V:2H	Rock→125 kg cloth→250 kg geotextile→250 kg cloth→800 kg geotextile
5	Dumped	Launched slope 1V:2H	Rock→125 kg cloth→250 kg geotextile→250 kg cloth→800 kg geotextile

The bed was covered with two layers of placed geobags. When dumped, the same number of geobags covered the test area in what visually appeared to be a little less than two complete layers. On the flat bed, the elements were positioned on a layer of pea gravel. A grid was placed under the elements on the sloped bed to prevent them from sliding down the slope. The order of the geobag were varied in order to help account for influences from the element's position in the flume. Three larger geobags (36 kg prototype weight) were placed at the end of the entire test section to stabilize the test section and the underlying gravel bed.

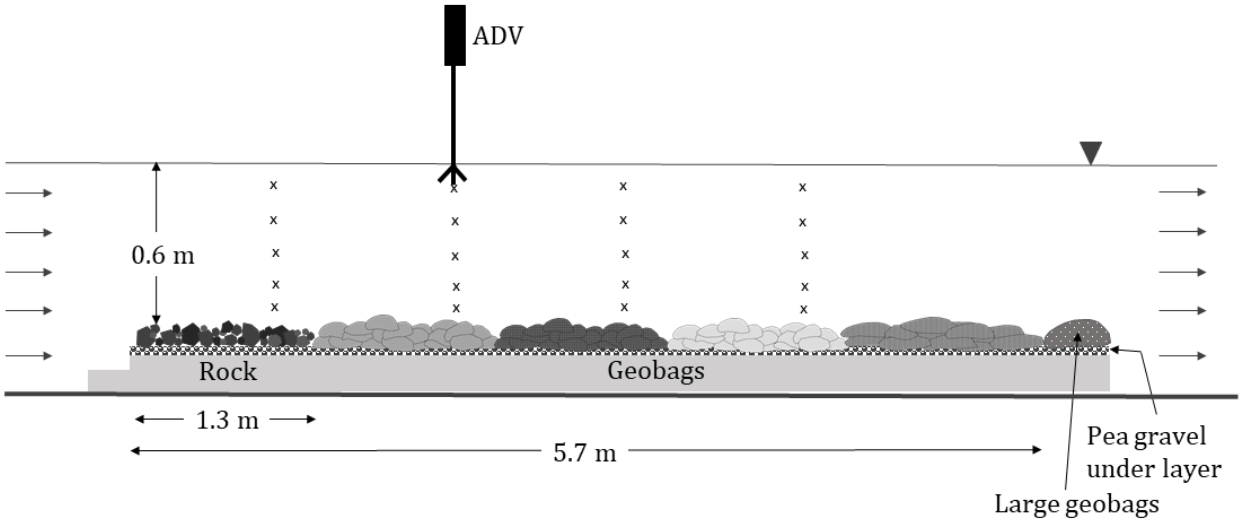

Figure 2-6: Schematic of flat-bed flume experiment, where an 'x' marks a measurement point

In all test series the flume was filled to a water depth of approximately 60 cm. The velocity in the flume was increased in steps of 0.5 m/s (ranging from 0.6 m/s to 2.1 m/s, prototype velocity) until failure of the test sections was reached. For this study, the point of failure, or incipient motion, has been defined when 5% of the elements are displaced, in line with the definition NHC's 2010 geobag tests used. Movement is specified as, when an element is displaced from its original position, not simply readjusting in place. The moved bags have been visually identified.

At every velocity increment, velocity measurements were taken at the downstream end of each element section, with the exception of the farthest downstream element section because of the physical limitations of the flume construction. The velocity measurements on the sloped bed were taken at a quarter of the slope length from the lowest point on the slope. At each velocity measurement location, five measurements were taken over the depth of the water column using an Acoustic Doppler velocimeter (ADV). The ADV ran for

approximately two minutes at each measurement location. Measurement data was checked to ensure that the ADV had collected enough data to converge and find the average velocity at each point. All of the data had a signal to noise ratio above 15. The majority of the data had a correlation above 70%, with the exception of a few points closest to the bed due to the lack of debris in the water.

Additionally, after each velocity increment, photos of the bed were taken in order to create an elevation data point cloud (done by nhc). The point cloud was converted into a three-dimensional, 1 mm resolution workable surface with ArcGIS. Differential images were created from these computer generated surfaces, enabling the surface elevation to be compared before and after a velocity run and the precise movement of elements could then be documented. The bed was also filmed in order to capture the movement of the elements. During the experiments, dye was also used to confirm that there were no irregular flow patterns in the flume, for example large-scale flow separation and reattachment points.

2.4 Results and Discussion

2.4.1 Incipient motion

Observations can be made by visually inspecting the differential images and velocity profiles collected from the experiments. Example differential images, and the corresponding velocity profiles over the different protective elements can be seen in Figure 2-7 and Figure 2-8. The figures show differential images of the bed elevations with a 0.2 m and 0.02 m range of movement shown. Although the differential image showing the finer range of motion shows slight shifts in the elevations data set (< 5 mm), sand movement

within the bags can be seen. Sand inside the bags was observed moving within the bags when flow velocities were as low as 1.2 m/s. Pilarczyk (2000) also had similar observations of sand inside geotextile bags moving at low velocities (1.5 m/s). Sand also appeared to move towards the downslope side of each bag during the tests on the slope.

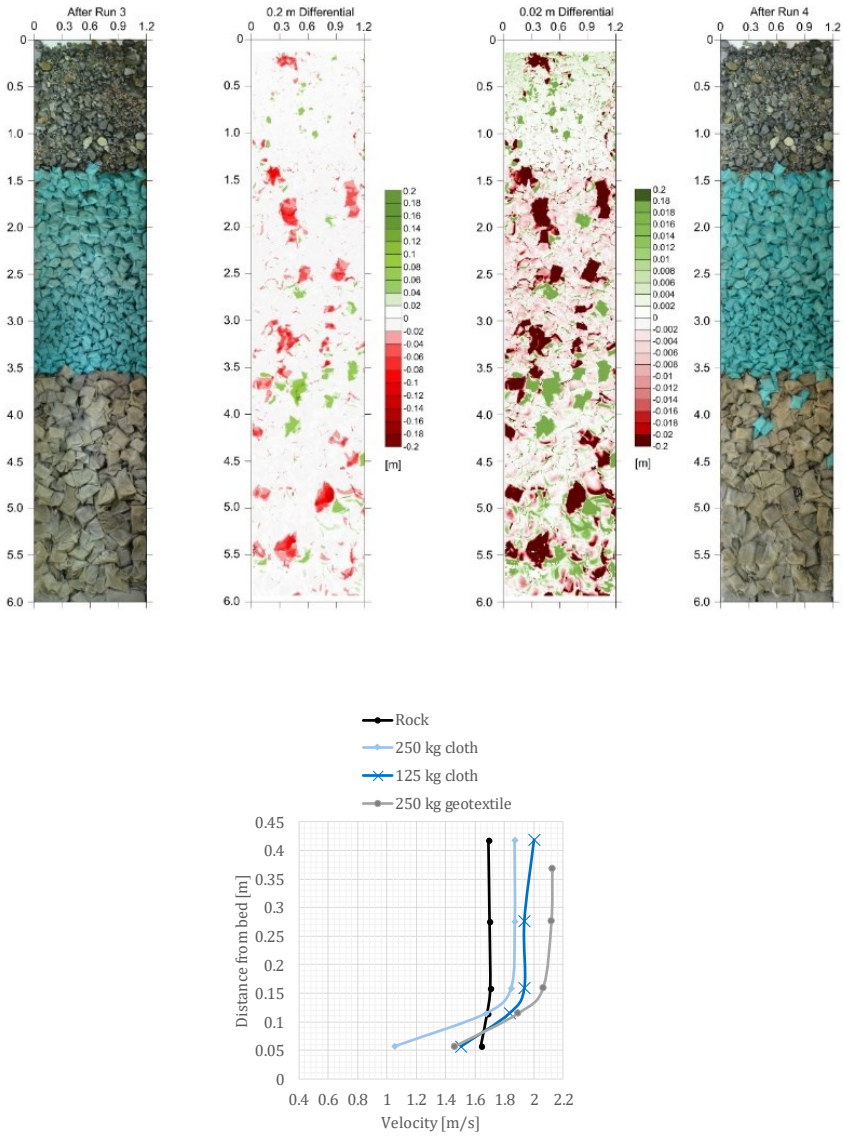

Figure 2-7: Differential image of the before and after bed elevations of an experimental run (left) and the corresponding measured velocity profiles (right) for Series 2 with dumped bags

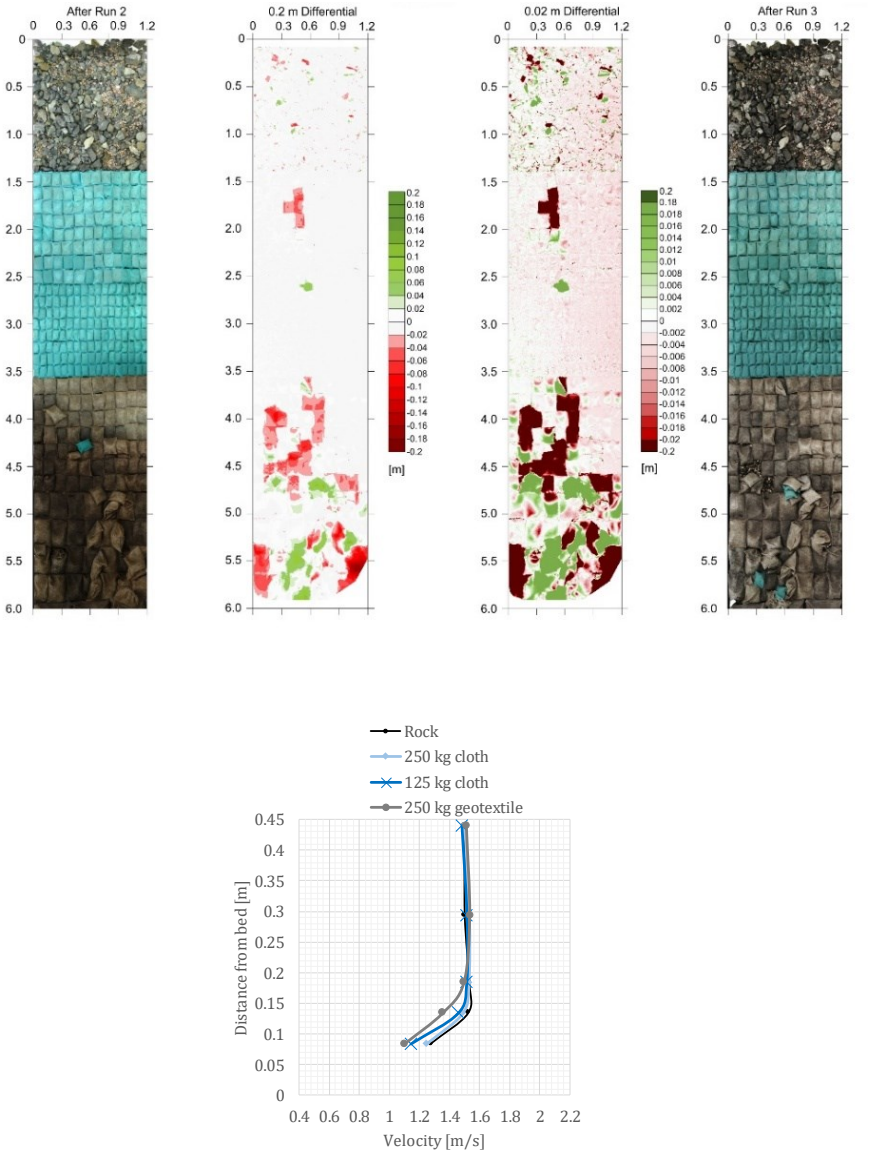

Figure 2-8: Differential image of the before and after bed elevations of an experimental run (left) and the corresponding measured velocity profiles (right) for Series 1 with placed bags

At the point of failure, the bags appeared to tumble or roll down the bed of the flume. The bags rotate along an axis normal to the flow. Their flexible bodies prevented any long periods of suspension in the flow. The larger, emptier bags appeared to fold first

before eventual movement occurs. Video recordings show geobags in the NHC 2010 model tests appear to have longer periods of suspension than the geobags used in this study, potentially due to the higher filling percentage and increased flexibility. The geobags appeared to have a readjustment phase at a relatively low velocity, and then remain stable until higher velocities caused failure. When geobags did fail, they tended to fail suddenly and in long sections, especially the placed geobags.

Figure 2-9 shows the percentage of moved elements for each test series and the correlating depth-averaged velocity. The moved bags have been identified using the differential images of the bed. Because of the limitations in velocity measurements, some approximations in velocity measurements have been taken. The depth averaged velocity of the most downstream section of the series has been approximated as the same velocity as the upstream adjacent element section. Additionally the maximum velocities for Series 1 and 3 have been approximated using the increase in measured velocity at the most upstream portion of the flume because of the risk of moving elements damaging the equipment in the flume (see Figure 2-9).

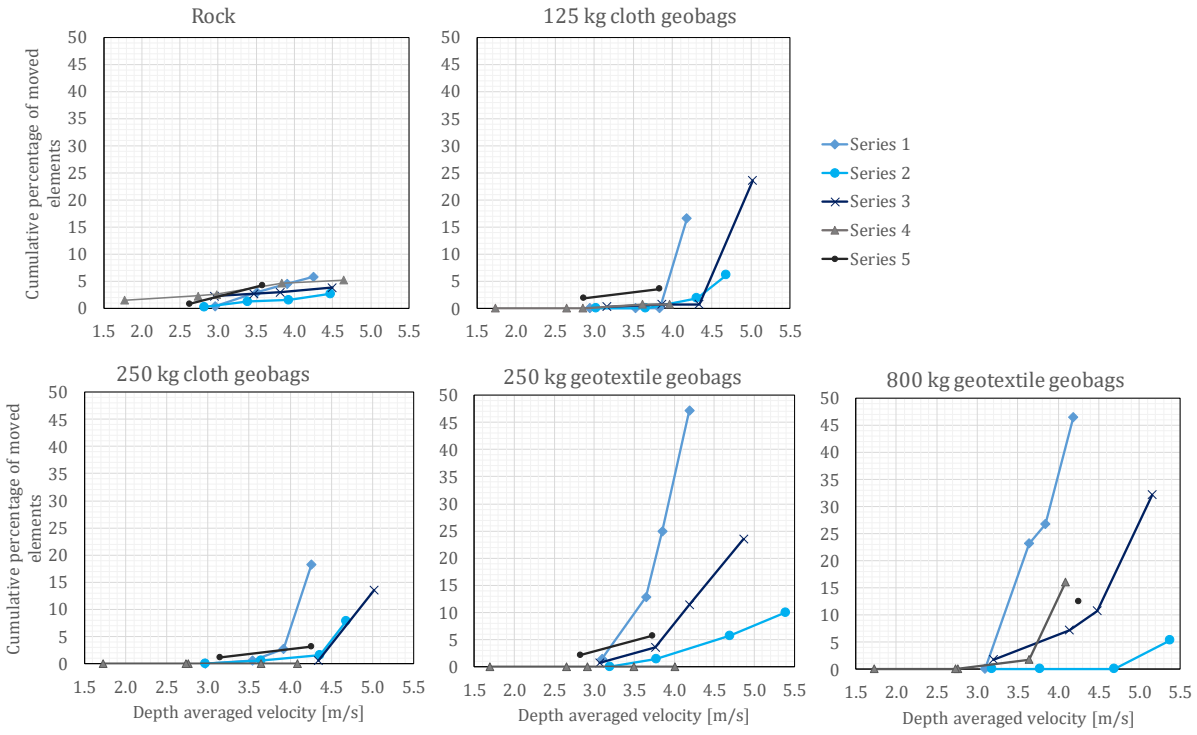

Figure 2-9: Percentage of elements moved and the corresponding depth averaged velocity

It can be noted that the geobags appear to be more stable for Series 2, compared to those for Series 3 (both being dumped bags on a flat surface). This could possibly be an effect of the position of the elements in the flume. Elements located farther downstream tended to have a more logarithmic velocity profile with a steeper gradient near the bed (see velocity profiles shown in Figure 2-7). The forces at the bed, which move the elements, are dependent on the near-bed velocity gradient. Flows with comparable depth averaged velocities can exert different shear stresses on the bed.

Series 2 may also appear to be more stable than other runs because the dumped elements were mistakenly under flow attack for a period of time before the test started and were not re-dumped. It is possible that the readjustment of the geobags occurred during

this time creating more stable geobags for the test. It is probable that geobags become more stable after a flood season because of the compaction process of the sand in the bags and the readjustment of the bags. Diving observations over geobag aprons constructed in previous years contain geobags that are harder and more difficult to move than recently dumped geobags, which have not been subjected to the hydraulic loading of the river.

The 125 kg geobags in this study failed at a velocity of approximately 4.2 m/s. This is the same as the critical velocity for 125 kg geobags in the 2010 NHC tests. Delft Hydraulics Laboratory (1985) found that clay filled jute bags weighing 42-50 kg used in a closure dam moved at 2.6 m/s. This correlates to ~3.1 m/s for a 125 kg bag. Pilarczyk (2001) found that 45 kg bags moved at 2.0 m/s. This correlates to ~2.4 m/s for a 125 kg bag. However, since the depths and density of the bags of the latter two studies are not known the direct comparison of the results cannot be made.

2.4.2 Review of USACE formula

The results have been compared to the existing sizing formula (Figure 2-10 and Figure 2-11). The stable and failure conditions which have been measured during the experiment along with historic data are plotted using the non-dimensionalized terms in the USACE stability formula (Eq. 2-1). The stable conditions are the maximum velocity measured before 5% of the elements incur movement. When incipient motion for an element section has not been achieved, the stable condition is documented as the highest velocity measured.

The lines on the figures show the USACE relationship, with the coefficient being the stability coefficient, C_s. A higher coefficient represents a less stable element. NHC (2010)

calibrated the stability coefficient to be 0.31 for geobags. The stability coefficient for riprap is commonly taken as 0.30 (USACE 1991). The rock section performed as expected and agrees with the USACE formula (Figure 2-10); however, the formula does not appear to describe the incipient motion behavior of the geobags well (Figure 2-11). While the 250 kg cloth and geotextile bags appear to behave as expected, the 800 kg geotextile bags appear to be less stable than the formula predicts and the 125 kg cloth bags appear to be more stable than the formula predicts.

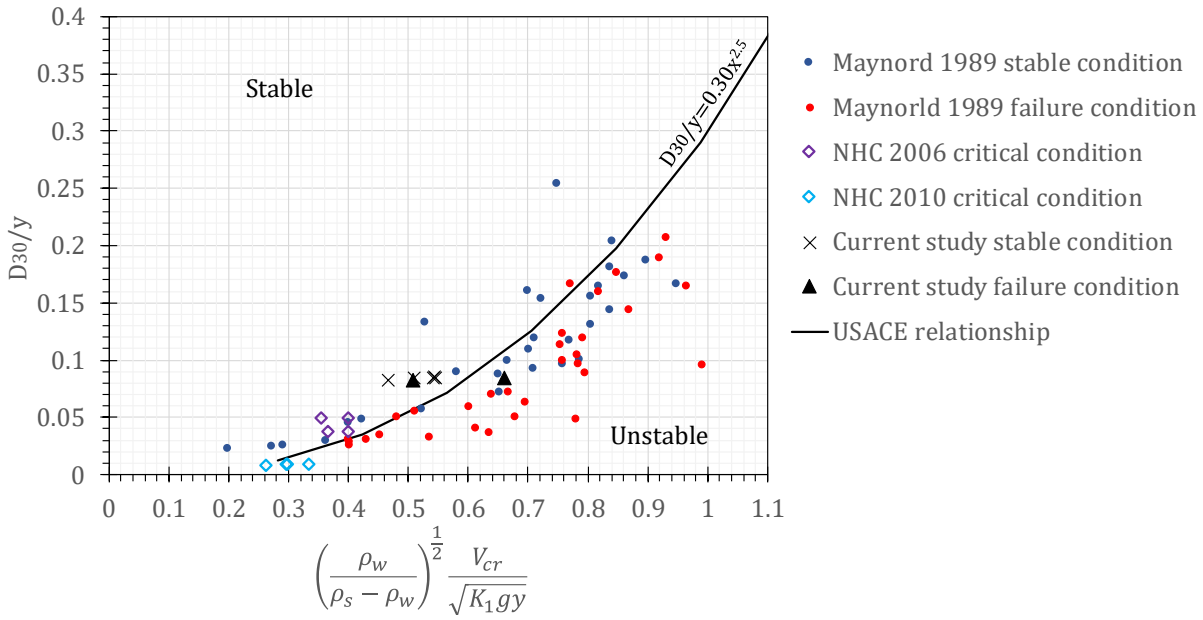

Figure 2-10: Experimental results for rock and its comparison with historic data and the USACE relationship with a stability coefficient of 0.30 (where y represents the vertical axis and x represents the horizontal axis)

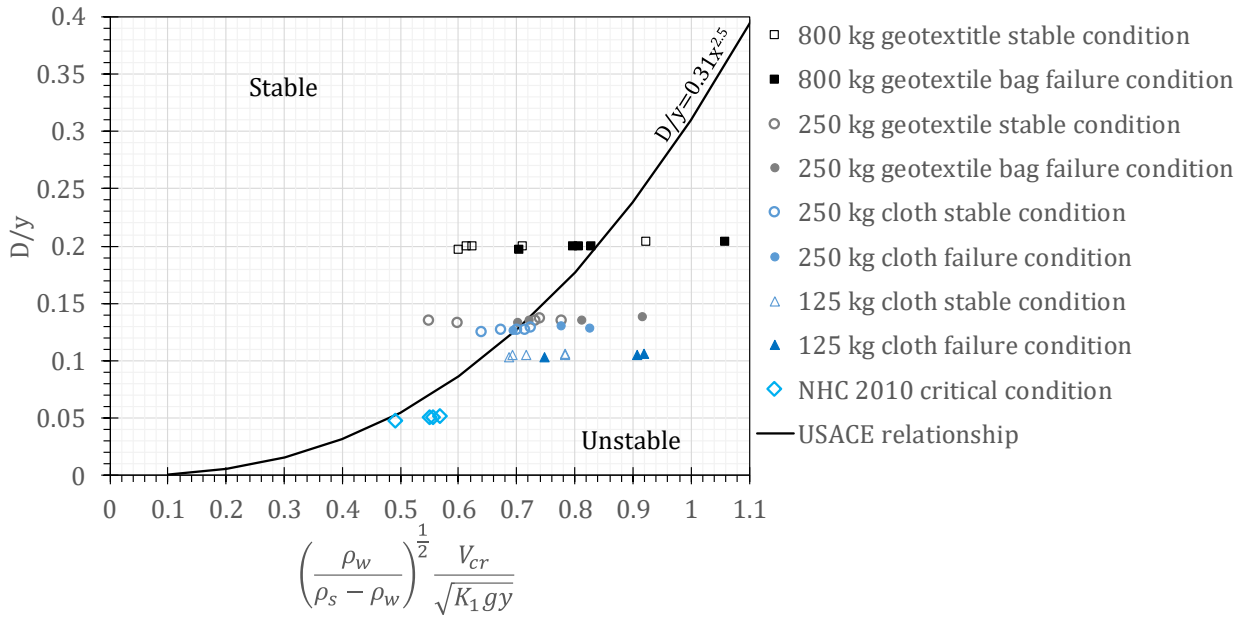

Figure 2-11: Experimental results for geobags and its comparison to previous studies and the USACE relationship with a stability coefficient of 0.31 (where y represents the vertical axis and x represents the horizontal axis)

The USACE formula uses the cube root of the volume to describe the elements characteristic diameter. This is an unintuitive way to describe the shape of geobags, which are relatively flat. Moreover, both measuring and calculating the volume of a large geobag is a difficult task. Measurements from both this study and Zellweger's (2007) along with theoretical calculations of geobag volumes can be seen in Figure 2-12. The closed and open Robin formula calculate the maximum volume able to fit into a sealed bag or a bag open at one end (Oberhagemann et al. 2017). The closed and open Robin formulas read, respectively,

$$\forall = w^3\left(\frac{h}{\pi w} - 0.142\left(1 - 10^{\frac{-h}{w}}\right)\right) \qquad (2-2)$$

$$\forall = w^3\left(\frac{h}{\pi w} - 0.071\left(1 - 10^{\frac{-2h}{w}}\right)\right) \qquad (2-3)$$

where ∀ is the bag volume, l is the length of the bag, w is the width of the bag. Bezuijen and Vastenburg (2013) provided a table for calculating the volume of a geotube based on the filling percentage. The volumes derived from the approach presented by Bezuijen and Vastenburg (2013) fail to account for the reduction in volume caused by the tapering of the geobag ends and consequently, overestimate the volume slightly. It can be seen in Figure 2-12 that there is large scatter and no clear agreement between the different methods.

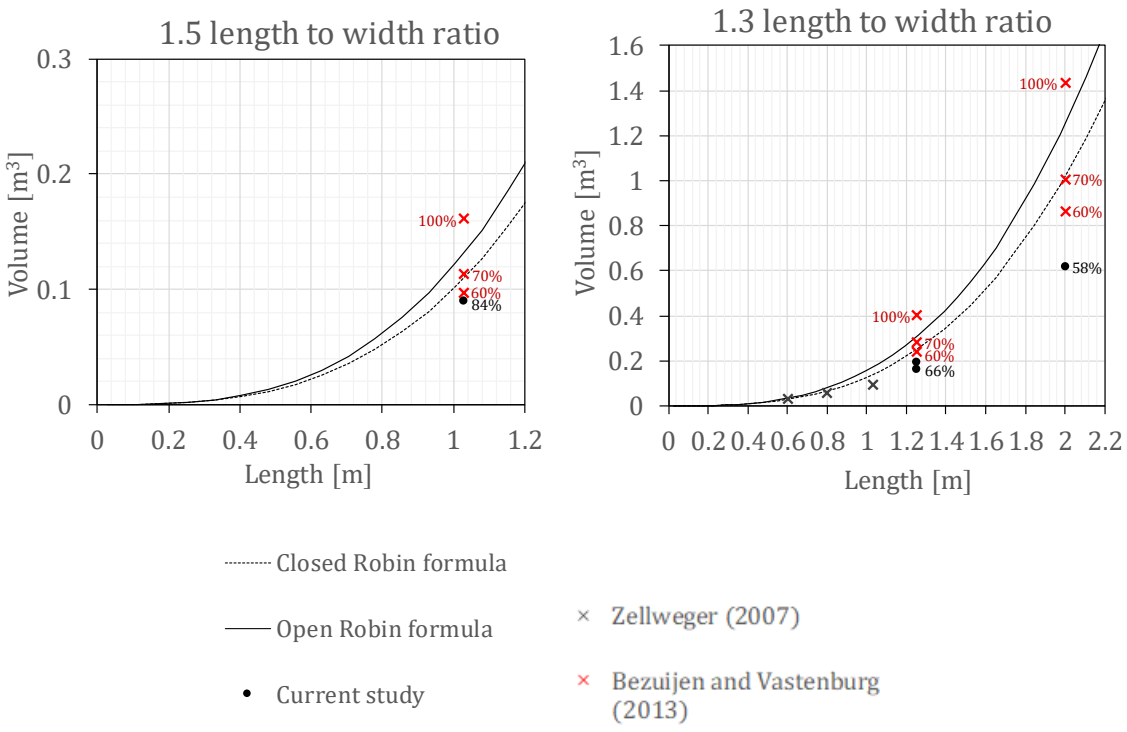

Figure 2-12: Measured and theoretical volumes of geobags (percentages show the fill percentage of the bags)

To avoid having to use the volume of the geobags, the authors propose using the thickness of the filled geobag as the characteristic diameter. In addition to correlating to the amount of obstruction the bag causes to the flow, the thickness is an easy measurement to obtain, and prevents the uncertainty of using the volume of a geobag, which is especially important considering that the USACE formula is sensitive to errors in measurements. A 10% change in the velocity will result in a nearly 100% change in the weight limits of the rock and a 10% change in the unit weight of rock will result in a 70% change in the weight limits of the riprap gradation and about a 20% change in the riprap thickness (USACE 1991). Thickness has been previously used as the characteristic diameter by Pilarczyk (2000).

Figure 2-13 and Figure 2-14 shows the results using the new characteristic diameter (the thickness) for both dumped and placed bags. The stability coefficients have been adjusted to correlate to the smallest failure velocity for a given bag size. It can be observed that the placed bags are less stable than the equivalently sized dumped bags. This could possibly be the result of the change in velocity profile (Figure 2-7 and Figure 2-8). Placed geobags have a steeper velocity profile, which may result in higher bed shear stresses, despite having comparable depth averaged velocities. This result confirms that the current construction methodology of dumping the geobags from barges is beneficial for their stability.

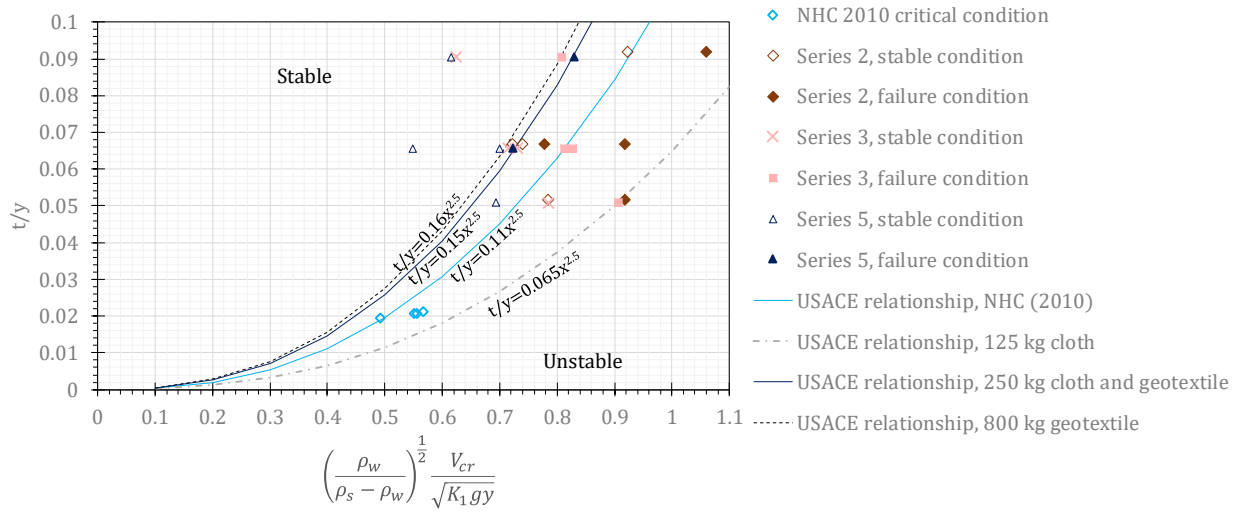

Figure 2-13: Dumped geobag incipient motion results presented with thickness, t, used as the characteristic diameter (where y represents the vertical axis and x represents the horizontal axis)

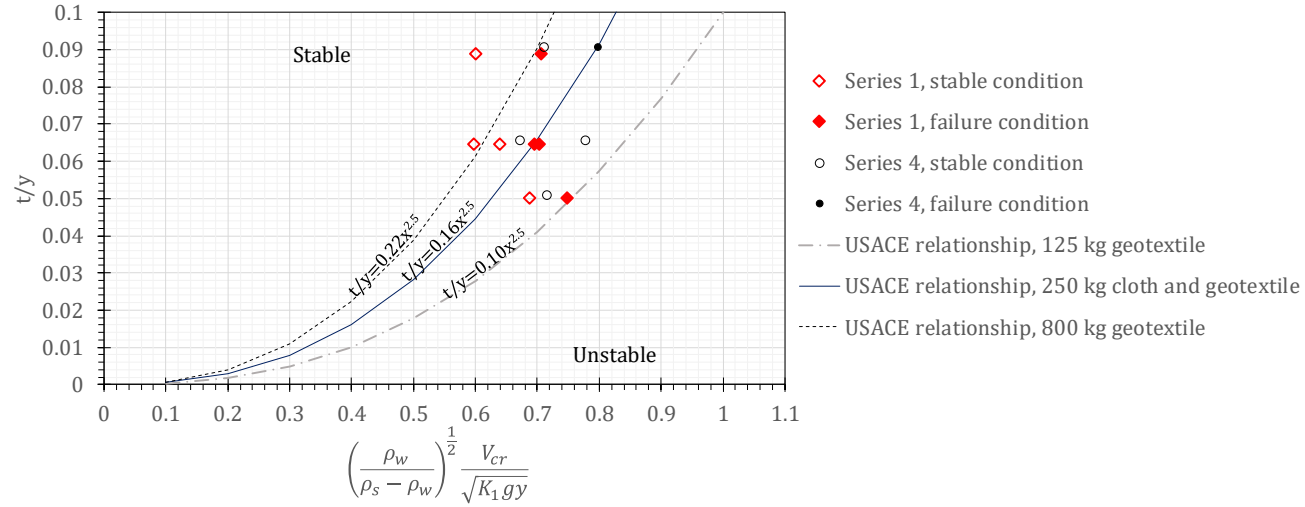

Figure 2-14: Placed geobag incipient motion results presented with thickness, t, used as the characteristic diameter (where y represents the vertical axis and x represents the horizontal axis)

It also appears that an increase in mass does not necessarily lead to a direct increase in element stability against incipient motion. The authors suggest that this is due to the filling percentage of the geobags. The stability coefficient is not a constant but rather dependent on the filling percentage, as it influences how readily the sand in the geobag can move (Figure 2-15). Bags which have lower filling percentages allow for too much sand movement in the bags, and does not force the entire mass of sand to move as one unit. It appears that bags also lose stability if they are extremely full, possibly because of the reduced contact forces between the elements. In Figure 2-15 the 2010 NHC bags have been assumed to be 95% full and have a lower stability than the 84% 125 kg filled bags. There appears to be a range of optimal filling percentages for geobags. When sizing geobags with an approximate aspect ratio of 1:3, the authors recommend using a stability coefficient of 0.15 for fill percentages ~60% and a stability coefficient of 0.07 for fill percentages above ~80%. These stability coefficients are only applicable when the thickness is used as the characteristic diameter.

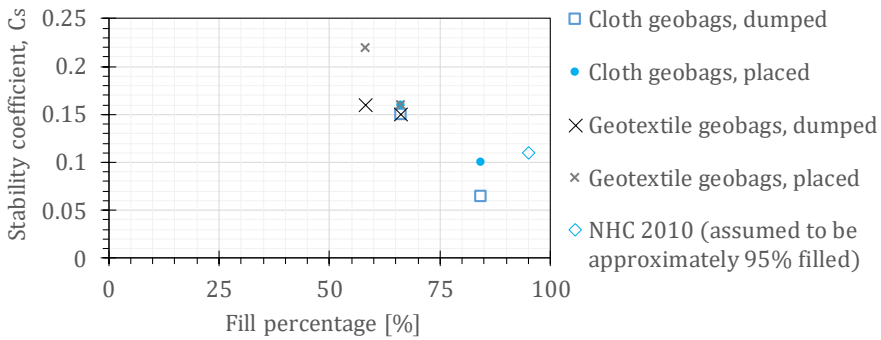

Figure 2-15: Relationship between stability coefficient and filling percentage

Other studies have found similar findings regarding the importance of filling percentages of geobags. Grüne and Oumeraci (2007) conducted a study for geobags used as

monopile scour protection and concluded that the stability of the elements under wave attack was dependent on the filling percentage. The study tested geobags filled to 56%, 80% and 100% and found that depending on the type of wave loading, either the 100% or 80% filled geobags were the most stable. For all cases the 56% filled geobags were the least stable. Additionally, Pilarcyzk (2000) suggested filling bags to 80% fill to prevent the sand from moving inside, while maximizing contact area between elements.

Filling large geobags in the field can be difficult because of the slumping of the fabric, which reduces the potential volume available to fill. Because of this, under-filling rather than over-filling the large geobags is more likely to be a problem. Geobags are sewn on three sides before reaching the construction site. The open edge is later shut after the bag has been filled. Potentially bags could be filled to a higher degree of filling if the fourth edge is partially closed before the filling process.

2.5 Conclusion

Using physical model tests, this study re-examines the stability of geobags under current loading. The study used larger scaled elements than previous tests in order to capture the flexibility of the geobags in the experiment. The following conclusions have been made from this study. First, dumped geobags are more stable than orderly placed bags. Second, the study found that the current USACE stability formula can be improved in order to better predict the incipient motion of geobags. The geobag thickness can be used as the characteristic diameter rather the cube root of the volume. The volume of a geobag is a difficult value to acquire, and using the cube root of the volume is not an intuitive way to describe how the geobag obstructs the oncoming flow. Additionally, the stability coefficient

in the USACE formula should be adjusted to account for the filling percentage of the bags. The stability of geobags is not purely dependent on the mass of the bags, but also a function of the filling percentage. Too little fill, and the sand is able to move independently of the entire element. Too much fill, and the contact points between bag elements reduce, thus reducing the overall stability of the elements. These results confirm suggestions originally proposed by Pilarczyk (2000).

These results are preliminary and further testing needs to be done to collect more data for a more complete understanding of how the fill percentage effects the stability coefficient. For bags with an approximate aspect ratio of 1:3 and using a thickness as the characteristic diameter, the authors recommend using a stability coefficient of 0.15 for fill percentages ~60% and a stability coefficient of 0.07 for fill percentages above ~80%. The authors do not recommend filling the bags beyond ~90% fill capacity.

Although these adjustments may fix some of the issues designers face using the USACE sizing formula, there are still limitations to its applicability. The USACE relationship suggests that bag sizes get smaller as the channel becomes deeper. Points in the Brahmaputra can be extremely deep (up to 70 m depth has been recorded at Chandpur, at the confluence of the Upper Meghna and Brahmaputra). At great depths the USACE formula suggests unrealistic bag sizes. As well, the formula uses the depth-averaged velocity. Different velocity profiles with the same depth-averaged velocity can have different shear stresses. Although shear stresses are difficult to work with, using the Shields relationship may be a more theoretically appealing approach for sizing geobags at locations such as Chandpur.

2.6 References

Akter, A., Pender, G., Wright, G., Crapper, M., 2013a. Performance of a geobag revetment I: Quasi- physical modeling. Journal of Hydraulic Engineering. 129(8), 865-876.

Akter, A., Crapper, M., Pender, G., Wright, G., Wong, W., 2013b. Performance of a geobag revetment II: Numerical modeling. Journal of Hydraulic Engineering. 139(8), 877-885.

Bangladesh Water Development Board, 2010. Guidelines for River Bank Protection. Jamuna-Meghna River Erosion Mitigation Project, Bangladesh.

Bezuijen, A., Vastenburg, E. W., 2013. Geosystems. Design Rules and Applications, first ed. Taylor & Francis Group, London.

Buffington, J. M., Montgomery, D. R., 1997. A systematic analysis of eight decades of incipient motion studies, with special reference to gravel-bedded rivers. Water resources research. 11(8), 1993-2029.

Dassanayake Mudiyanselage, D. T. B. D., 2013. Experimental and numerical modelling of the hydraulic stability of geotextile sand containers for coastal protection (Doctoral dissertation). Retrieved from https://publikationsserver.tu-braunschweig.de/servlets/MCRFileNodeServlet/digibib_derivate_00032409/Diss_Dassanayake.pdf

Delft Hydraulics Laboratory, 1985. Stability of clay-filled gunny bags. Feasibility study Sandwhip Crossdam R 1331-40, Delft.

Elkholy, M., Chaudhry, M. H., 2011. Drag and added-mass coefficients of large sandbags. Journal of Hydraulic Engineering. 137(11), 1441-1451.

Grüne, J., Oumeraci, H., 2007. Stability tests of geotextile sand containers for monopile scour protection. International Conference on Coastal Engineering, San Diego. 5, 5093-5105.

Heibaum, M., Oberhagemann, K., Faisal, M.A., Haque, S., 2008. Geotextile Bags for sole permanent Bank Protection. 4th European Geosynthetics Conference, Edinburgh.

Hornsey, W. P., Carley, J. T., Coghlan, I. R., Cox, R. J., 2011. Geotextile sand container shoreline protection systems: Design and application. Geotextiles and Geomembranes. doi:10.1016/j.geotexmem.2011.01.009

Maynord, S. T., 1988. Stable riprap size for open channel flows. US Army Corps of Engineers, Washington.

Neill, C. R., 1968. A re-examination of the beginning of movement for coarse granular bed material. Hydraulics Research Station, Wallingford.

Neill C. R., Mannerström, M., Azad, A. K., 2008. Model tests on geobags for erosion protection. Fourth International Conference on Scour and Erosion, Tokyo.

NHC, 2006. Jamuna-Meghna River Erosion Mitigation Project Part B Special Report 11 Physical Model Study. Prepared for Bangladesh Water Development Board.

NHC, 2010. Padma Multipurpose Bridge Design Project RT23 Geobag Flume Model Study. Prepared for Maunsell/AECOM and Bangladesh Bridge Authority.

Oberhagemann, K., Diggelmann, P., Mukhles-uz-zaman, 2008. Understanding Falling Aprons. – Experience from the Lower Brahmaputra / Jamuna River. 4th International Conference on Scour and Erosion, Tokyo.

Oberhagemann, K., Hossain, M. M., 2011. Geotextile bag revetments for large rivers in Bangladesh. Geotextiles and Geomembranes. 29(4), 402-414.

Oberhagemann, K., Thompson, A., Walsh, B., 2017. Lecture Note on Geotextile Bag Revetments. Prepared for training courses for Bangladesh Water Development Board staff, conducted at the Bangladesh University for Engineering and Technology under the Flood and Riverbank Erosion Management Investment Program Tranche-1, Bangladesh.

Pilarczyk, K. W., 1991. Coastal Protection Short Course Rijkswaterstaat. Road and Hydraulic Engineering Division Van der Burghweg, Delft.

Pilarczyk, K. W., 2000. Geosynthetics and geosystems in hydraulic and coastal engineering. A. A. Balkema, Rotterdam.

Recio, J., Oumeraci, H., 2009. Process based stability formulae for coastal structures made of geotextile sand containers. Coastal Engineering. 632–658. doi:10.1016/j.coastaleng.2009.01.011

Shields, A., 1936. Application of similarity principles and turbulence research to bedload movement English translation. W.M. Keck Laboratory of Hydraulics and Water Resources, California Institute of Technology.

Thompson, A., Oberhagemann, K., She, Y., Haque, A.M.A., 2018. The behavior of self-launching geotextile bag aprons – latest investigations from the Lower Brahmaputra in Bangladesh. 9th International Conference on Scour and Erosion, Taipei.

USACE, 1991. Hydraulic design of flood control channels, Engineer Manual. U.S. Army Corps of Engineers, Washington.

Zellweger, H., 2007. Geotextile bags for river erosion control in Bangladesh. Swiss Federal Institute of Technology, Zürich.

Zhu, L., Wang, J., Cheng, N. S., Ying, Q., Zhang, D., 2004. Settling distance and incipient motion of sandbags in open channel flows. Journal of Waterway, Port, Coastal and Ocean Engineering. 130(2), 98-103.

3 Geobag stability for riverbank erosion protection structures: Numerical model study

3.1 Introduction

Since the early 2000's geobags have been used to protect the banks of the Brahmaputra River from erosion (Oberhagemann and Hossain 2011). Long guiding revetments comprised of geobags prevent local erosion, and guide the river into a more predictable, stable planform. The stability provided by the geobag revetments provide security to the people who live along the riverbanks and enable economic development of the adjacent land. An overview of the use of geobags in Bangladesh and India can be found in Thompson et al. (2018).

Quantifying the conditions of incipient motion has been studied extensively for sediment particles, most notably starting with Shields' study of sediment motion (Shields 1936). Shields demonstrated that the critical shear stress for the onset of incipient motion varied with the critical boundary Reynolds number, the dimensionless variable $\rho u^* D/\mu$, where ρ is the fluid density, u* is the shear velocity, D is the characteristic diameter and μ is the dynamic viscosity (Buffington and Montgomery 1997). Shields developed the relationship by equating the gravitational forces moment acting on a particle with the drag moment (Shields 1936). Dey and Papanicolaou (2008) provide a comprehensive overview of studies concerning incipient motion of sediment.

While, the onset of incipient motion can be analyzed using the bed shear stresses, it can also be analyzed using the method of permissible velocity. Currently, geobags are sized using an adapted United States Army Corps of Engineers (USACE) stability formula for riprap (NHC 2010, Oberhagemann et al. 2017). This formula uses the design depth

averaged velocity to calculate the required geobag size. While velocity is typically more convenient to work with for engineering purposes because of the relative ease of gathering velocity data, shear stresses are more theoretically acceptable when describing the incipient motion of protective elements because they include the basic grain mechanics (Pilarczyk 1991). Additionally, the USACE formula fails to calculate realistic bag sizes when design velocities and depths become large, both of which can occur in the Brahmaputra. That being said, there has been little research about the shear stresses which act on geobag surfaces.

River currents exert forces on the elements which comprise of the river bed. When the applied lift and drag forces become greater than the stabilizing forces (the submerged weight, cohesion or contact forces) the bed particles will undergo incipient motion (Pilarczyk 1991) (Figure 3-1). Cohesion is only significant for clay and silt; therefore, it is neglected when considering geobags. The force acting on an element in the stream wise direction, called the drag force, is comprised of two parts: the friction drag, caused from the 'pulling' of the flow, and the form drag, caused from the pressure differences of the upstream and downstream points of an element. The form drag is heavily influenced by the degree of flow separation on the downstream portion of the geobag. The friction drag is dependent on the shape of the velocity profile and where the shear stresses reside in the water column. Schlichting (1979) describes how the resistance of a rough bed in turbulent flow (such as a geobag surface) is primarily due to the form drag and is independent of Reynolds number. This is a result of all of the protrusions lying outside of the laminar sublayer. The fully rough regime is classified as when the ratio of the product of the

Nikuradse roughness and shear velocity to the kinematic viscosity is greater than 70 (Schlichting 1979).

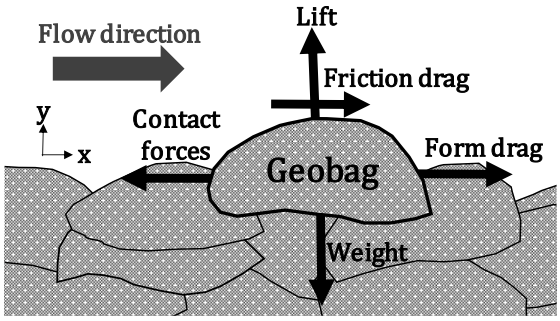

Figure 3-1: Forces acting on a submerged geobag under current loading

There are a number of methods of estimating the total shear stress, which is associated with the total drag force. For example, in an open channel, uniform flow scenario, the reduction in energy grade can be used (Chanson 2004). The shear stress can also be derived by assuming a logarithmic velocity profile (Schlichting 1979) or using the turbulent kinetic energy, widely applied in oceanography studies, where a calibrated coefficient is required (Biron et al. 2004). All of these methods have shortcomings. For example, using the reduction in energy grade line produces a reach-averaged bed shear stress, and is not appropriate for local, small scale estimates of the variation in shear stress (Biron et al. 2004). Furthermore complex flow fields may not conform to a logarithmic velocity field.

Advanced modelling techniques have previously been applied to study incipient motion of riprap. The U.S. Department of Transportation has used fluid structure interaction (FSI) for riprap design in order to use site specific conditions for determining riprap size (U.S. Department of Transportation Federal Highway Administration 2017). By

coupling CFD with computational structural mechanics the study was able to model the initiation of individual rock motion. This approach was very demanding, both in terms of time and modelling capability.

Akter et al. (2013a and b) modelled geobag revetments using Discrete Element Modelling. The modelling exercise coupled a physical model study with a numerical model study. The model strictly studied the failure mechanisms of the geobags found on the above low water level slopes where the elements are orderly placed. Recio (2007) also used physical and numerical modelling to study the stability of geobags, focusing primarily on stacked bags for coastal applications. The study coupled fluid dynamic and structural models to examine the behavior of geobags under wave loading. Both of these studies found a drag and lift coefficient for geobags. The majority of revetments along the Brahmaputra are comprised of of geobags that have been "dumped" from a barge, resulting in variations in the geometry of the flexible bags, and so, the drag and lift coefficient of each bag will vary as well.

The objective of this study was to obtain a formula that is based on shear stress for sizing geobags used in river revetments. Using data collected from a flume experiment (Thompson, et.al submitted), a three-dimensional (3-D) computational fluid dynamics (CFD) modelling tool was employed to quantify the critical shear stress on geobags at incipient motion and to estimate the Shields parameter to apply the Shields formulae to geobags. This paper first provides an overview of the flume experiments. Afterwards details of the numerical modelling methodology are provided and finally, first results and initial conclusions of the study are presented.

3.2 Methodology

3.2.1 Flume experiment

A 1:7 scaled flume experiment was performed in the Northwest Hydraulic Consultants (NHC) laboratory. The flume was 1.2 m wide and 5.7 m long. Using four different scaled model geobags, in addition to rock (D_{50}=0.064 m), the incipient motion of the elements was found by systematically increasing the flow velocity in the flume. Details of the scaled geobags can be seen in Table 3-1. Velocity measurements were taken with an Acoustic Doppler velocimeter (ADV) at the downstream end of each element section. Additionally, photos before and after each velocity run were taken in order to track the movement of the elements. For this study, the threshold for incipient motion is defined as when 5% of the elements move. Thompson et al. (submitted) provides a detailed overview of the flume experimental procedure and results, as well as a review of the USACE stability formula.

Table 3-1: Details of the geobags used in the flume experiments (using a scaled of 1:7)

Geobag	Mass [kg]	Length [m]	Width [m]	Density [kg/m^3]	Fill	Thickness [m]	Material
125 kg cloth	0.364	0.15	0.10	1732	84%*	0.031	80 g/m^2 woven linen
250 kg cloth	0.729	0.18	0.14	1881	66%*	0.040	80 g/m^2 woven linen
250 kg geotextile	0.729	0.18	0.14	1632	66%	0.040	150 g/m^2 non-woven geotextile
800 kg geotextile	2.332	0.29	0.21	1626	58%	0.055	150 g/m^2 non-woven geotextile

*Note: Because of the flexibility of the cloth fabric, the 125 and 250 kg cloth geobags have the potential to hold more sand than the equivalent geotextile bag, considered to be 120% filled of the bag size for this experiment.

3.2.2 Numerical model description

The numerical models were created using ANSYS CFX. The modelling software solves the 3-D Reynolds Averaged Navier-Stokes equations using a discretized fluid domain and time step and, in turn, describes the transfer of mass and momentum through the fluid domain. The k-ω shear stress transport (SST) turbulence model was used to address the turbulence closure problem. The k-ω SST turbulence model was chosen because of the model's competency in predicting separation points without requiring additional computational effort. Two additional transport equations are solved: one for the turbulence kinetic energy, k, and one for the turbulence eddy frequency, ω. The shear stresses are determined from the 3-D stress tensor. Background theory can be found in ANSYS (2009). The model assumed a steady state regime with an automatic timescale factor. The model used a high resolution advection scheme, and an Euler discretization. As the drag force on the geobag surface is of particular interest, convergence was confirmed by ensuring that the change in the drag force over subsequent time steps was less than 2%. Because of the complexity of the flow, a number of assumptions had to be made in the numerical model. The porosity of the bags has been neglected. The particulate in the water column has also been neglected and was not included in the model. The water was at a uniform temperature and therefore buoyancy within the fluid has been neglected.

Two sequential velocity runs of the flume experiments were modelled (Table 3-2). The two cases modelled are the final two velocity runs of Series 2. These cases were chosen because the 125 kg cloth, 250 kg cloth and 800 kg cloth geobags all surpassed the threshold of incipient motion during these cases. The two cases have a flat-bed covered in

approximately two layers of dumped geobags. The domain and boundary conditions of the models can be seen in Figure 3-2. Because of restrictions in computing power, each element section was modelled in a separate domain, wide enough to contain a minimum of three geobags across the width of the model. The upstream boundary of each element domain was assigned a velocity profile taken from the upstream ADV measurement data. The downstream boundary was assigned an average static pressure of 0 Pa, approximately 1 meter away from the end of the element section. The bathymetry of the bed was resolved with a 2 cm gridded surface in order to balance geometric accuracy with an efficient use of computational resources. The comparison of a 0.1 cm grid to a 2 cm grid can be seen in Figure 3-3. The grids have been created using triangulation and bilinear interpolation resampling using ArcGIS. The gridded surface covers each 125 kg, 250 kg and 800 kg bag with approximately 36, 63 and 153 grid points respectively. The D_{50} rock (0.064 m) is covered by 8 points. The boundary water levels along the length of the flume were calibrated to ensure the majority of the stream wise velocity component values were within 10% of the measured values, with the exception of a few points close to the bed (Figure 3-4).

An unstructured, tetrahedron mesh has been created using ~2 million nodes with a grid size of 1.3 cm. Mesh independence has been tested, implying that the results will not change with further mesh refinement (Table 3-3). The boundary layer over the elements has been resolved with fifty inflation layers with a growth rate of 1.15 and a first element height of 1×10^{-4} m (with a typical Y+ range between 0.2 to 13.9). To reduce the aspect ratio of mesh elements close to the bed, a mesh size of 0.8 cm has been applied just above the bed.

Table 3-2: Numerical models created and measured data from the flume experiments (Thompson et al. submitted)

	Case 1		Case 2	
	Cumulative percentage of failed elements	Depth averaged velocity* [m/s]	Cumulative percentage of failed elements	Depth averaged velocity* [m/s]
Rock	1.6%	3.9	2.7%	4.5
125 kg cloth	1.8%	4.3	6.3%	4.7
250 kg cloth	1.6%	4.4	7.8%	4.7
250 kg geotextile	5.7%	4.7	10.0%	5.4
800 kg geotextile	0.0%	4.7	5.4%	5.4

*converted to prototype scale

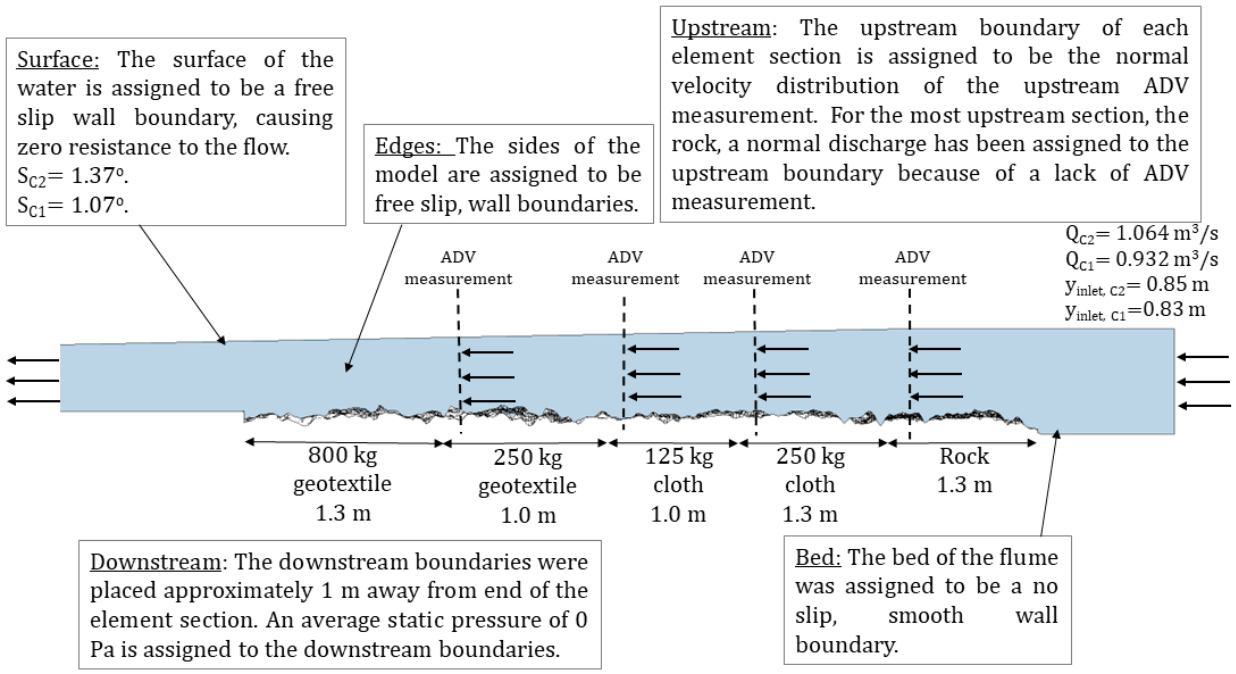

Figure 3-2: Domain and boundary conditions of the numerical models

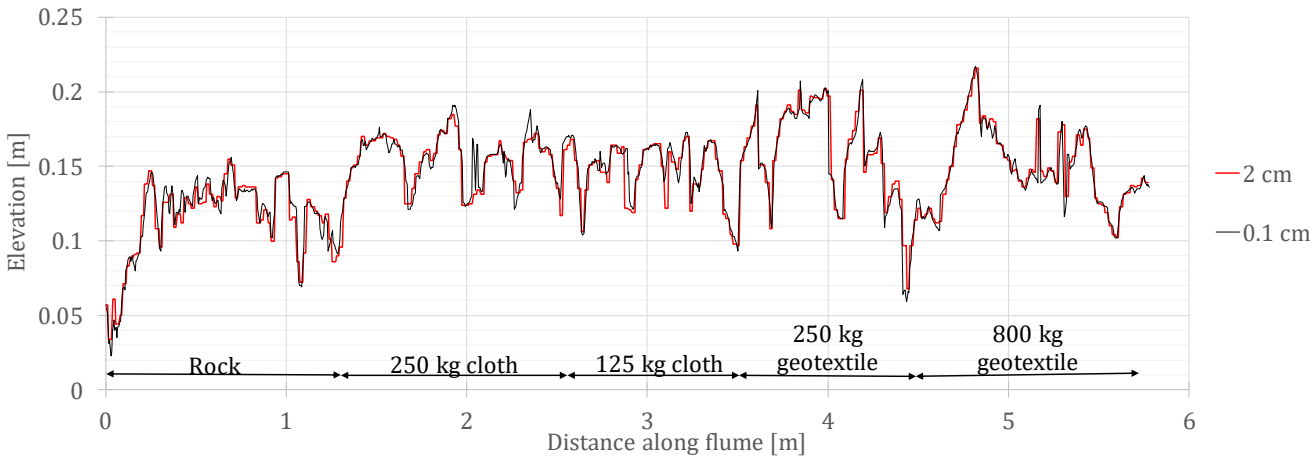

Figure 3-3: Example longitudinal cross section of flume showing loss in resolution from using a 2 cm grid

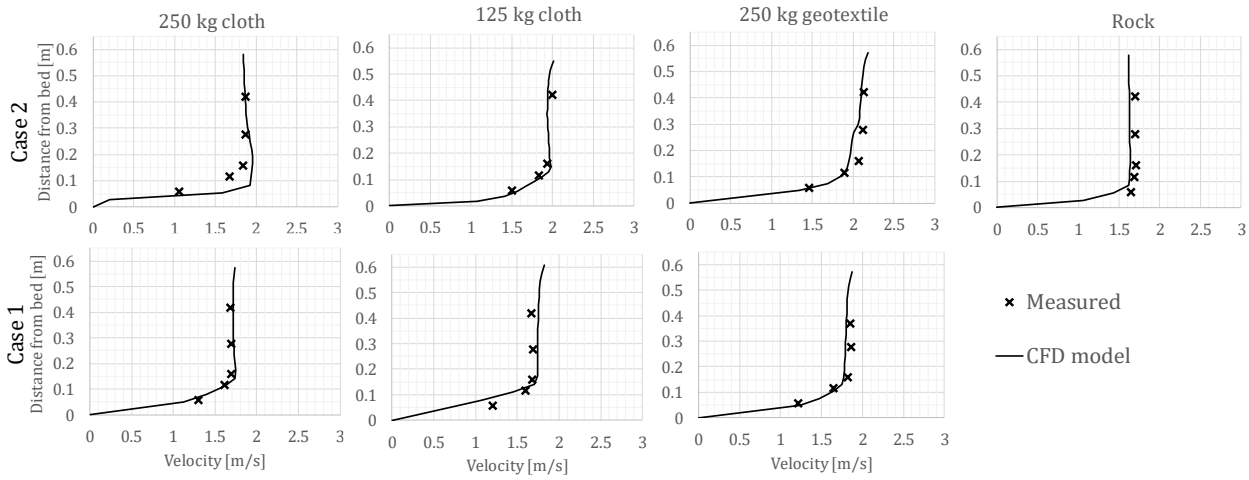

Figure 3-4: Calibrated velocity profiles for Case 1 and 2

Table 3-3: Mesh independence using 250 kg cloth bags for Case 2

Number of nodes	Total drag force on bed [N]	Percent difference
189 000	47.44	-
548 000	50.15	5.6
1 933 000	51.64	2.9
2 400 000	51.64	0

3.3 Results and Discussion

3.3.1 Discussion of shear stresses

The shear stresses found in the model can be compared to shear stresses found using analytical methods. The shear stresses on the geobag surface has been compared to the average shear stress from the energy grade line. The model has also been validated by testing how the drag coefficient of a cube is reproduced. The following section discusses these comparisons.

An approximation for the shear stress on the flume bed has been derived from the decrease in the energy grade line. The relation reads,

$$\tau = g\rho S_F y \qquad (3-1)$$

where τ is the shear stress, g is the acceleration due to gravity, ρ is the density of water, S_F is the friction slope of the bed, taken to be the slope of the water surface and y is the depth. This relation has been applied to the middle section (from the 250 kg cloth to the 250 kg geotextile element sections) of the flume to avoid any adverse effects of the entrance or exit of the flume. Since the flume has a low aspect ratio (width/depth~2), the influence of the sidewalls on the shear stress has been accounted for using the flow depth method (Guo 2015). This method states that the shear stress acting on the bed, τ_{bed}, can be derived from the following relationship,

$$\tau_{bed} = g\rho S_F y - \frac{2y}{b}\tau_{wall} \qquad (3-2)$$

where b is the width of the flume and τ_{wall} is the shear stress acting on the walls of the flume. The resulting total shear stress acting on the bed is 35 Pa and 29 Pa for Case 2 and 1 respectively. Figure 3-5 shows the total shear stress derived from the CFD model. The shear stresses derived from the CFD model have been found by taking the sum of the forces acting on the element section (an output of the numerical model) and dividing them by the area of the associated element section. The shear stresses derived from the energy grade line is within the range of the shear stresses found from the numerical model.

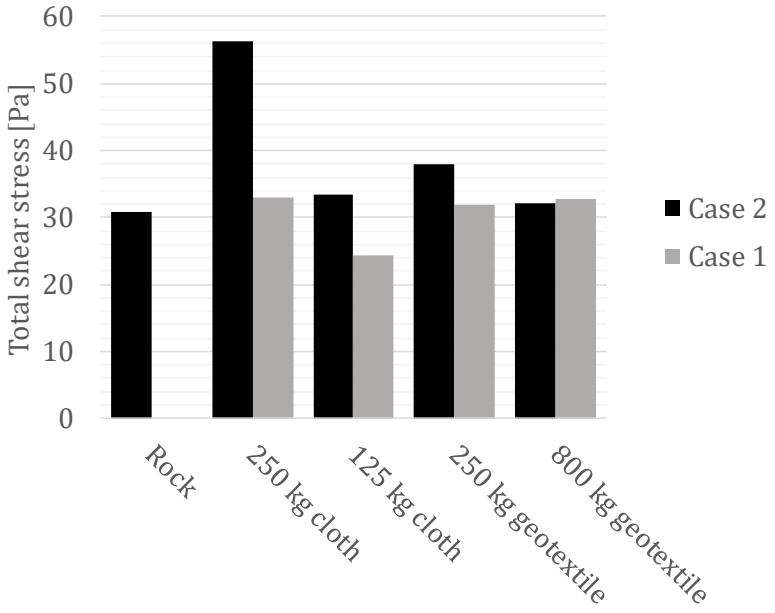

Figure 3-5: Total shear stress from the CFD model for each element section

Since the drag force is the main variable of interest in this study, the CFD model was tested on its ability to recreate the drag created from flow over a blunt object, a cube. A cube was suspended in the flow conditions of Case 2. The cube has approximately the same dimension of the roughness height of the geobag surface, 5 x 5 x 5 cm. Using the meshing and modelling parameters of the numerical model, the drag force was computed and the

corresponding drag coefficient was compared to the known drag coefficient value of 1.05 (Hoerner 1965). The drag coefficient is expressed as,

$$C_D = \frac{2F_D}{AV^2\rho} \qquad (3-3)$$

where C_D is the drag coefficient, F_D is the drag force, A is the cube area, V is the free stream velocity and ρ is the density of the fluid. The model found a drag coefficient of 0.98, having an error of 6.7%. For the purpose of extracting the Shields parameter from the model, this is an adequate reproduction of drag forces around a blunt object in the flow. The total drag forces acting on the cube was comprised of 99.8% form drag and 0.2% friction drag.

3.3.2 Hydraulic forces acting on a geobag surface

Figure 3-6 shows the velocity, pressure and drag force distribution on a portion of the 250 kg cloth geobag surface. It can be seen that the water is constricted and speeds up as it flows over the humps of the geobags creating high pressure regions on the upstream sides of the bags. If the flow is unable to follow the contours of the bag surface it separates on the downstream side, creating a recirculation region before reattaching once again downstream. These recirculation regions create areas of low pressure on the downstream sides of the bags. The difference in pressure from the upstream and downstream portion of the bags creates form drag. The pressure differences, and therefore, the forces are much lower in Case 1 (Figure 3-7) where the flow is slower.

The total drag force is also constituted of friction drag. Higher friction drag occurs where the flow is constricted and the near bed velocity profile becomes steeper. That being said, the friction drag was found to comprise of only ~5% of the total drag force. The

advanced modelling study done by the U.S. Department of Transportation Federal Highway Administration (2017) found similar results in that the pressure component of the drag force was 2-3 orders of magnitude higher than the shear forces. These results are expected for protruding objects in flows with high Reynolds numbers because of the flow separation points. The lift forces cannot be assessed from the model because the conditions of the underside of the geobags was not recreated in the model.

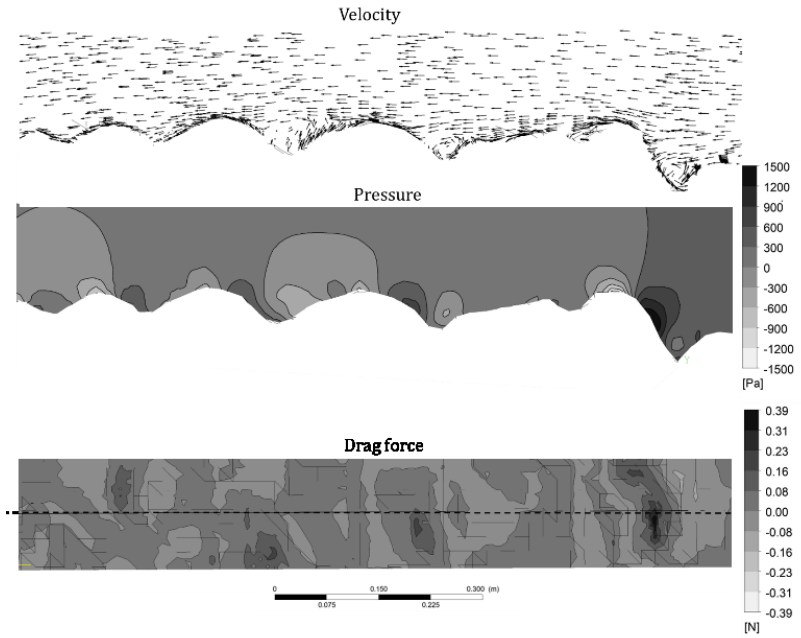

Figure 3-6: Velocity, pressure (both side view), and drag force (top view), over 250 kg cloth geobags for Case 2, where flow is from right to left

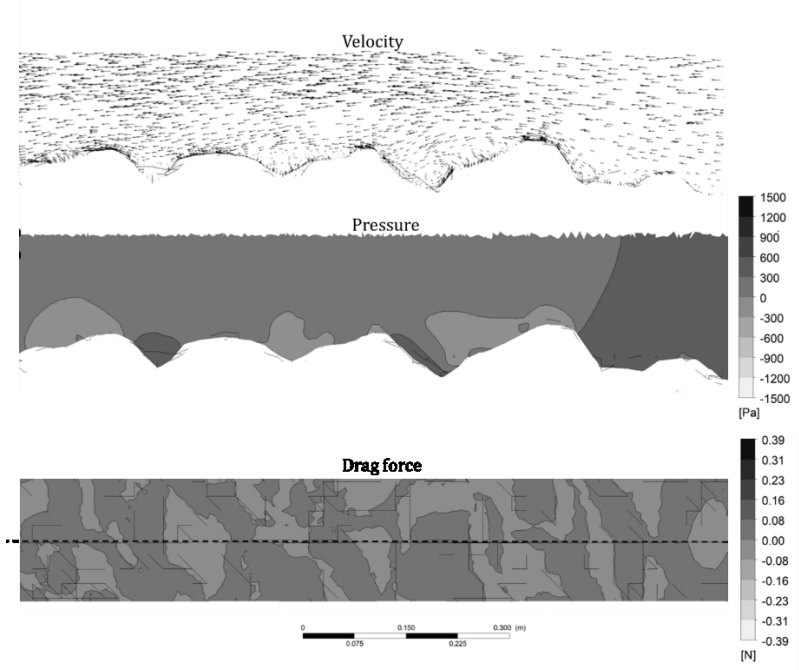

Figure 3-7: Velocity, pressure (both side view), and drag force (bottom view) over 250 kg cloth geobags for Case 1, where flow is from right to left

Although a drag coefficient for an individual geobag cannot be found because they vary in geometry (Figure 3-8), an average drag coefficient for the entire geobag surface can be found using Equation 3-3. The found drag coefficient of 0.02 resides between the drag coefficients of a flat plate under turbulent flow (0.005) and one half of a streamlined body protruding from a flat plane (0.07) (Hoerner 1965). Recio (2007) shows how previous studies have found drag coefficients for submerged stone structures vary from 0.045 to 0.35.

Figure 3-8: Surface of each element section in the flume experiment

A number of geobags have been identified in Figure 3-9 for Case 1 and 2. The total shear stress acting on these random, individual bags can be seen in Figure 3-10. The shear stress has been found by taking the total forces acting on the geobag and dividing them by the area of the geobag. It appears that the bags which underwent incipient motion typically had higher shear stresses acting on their surface.

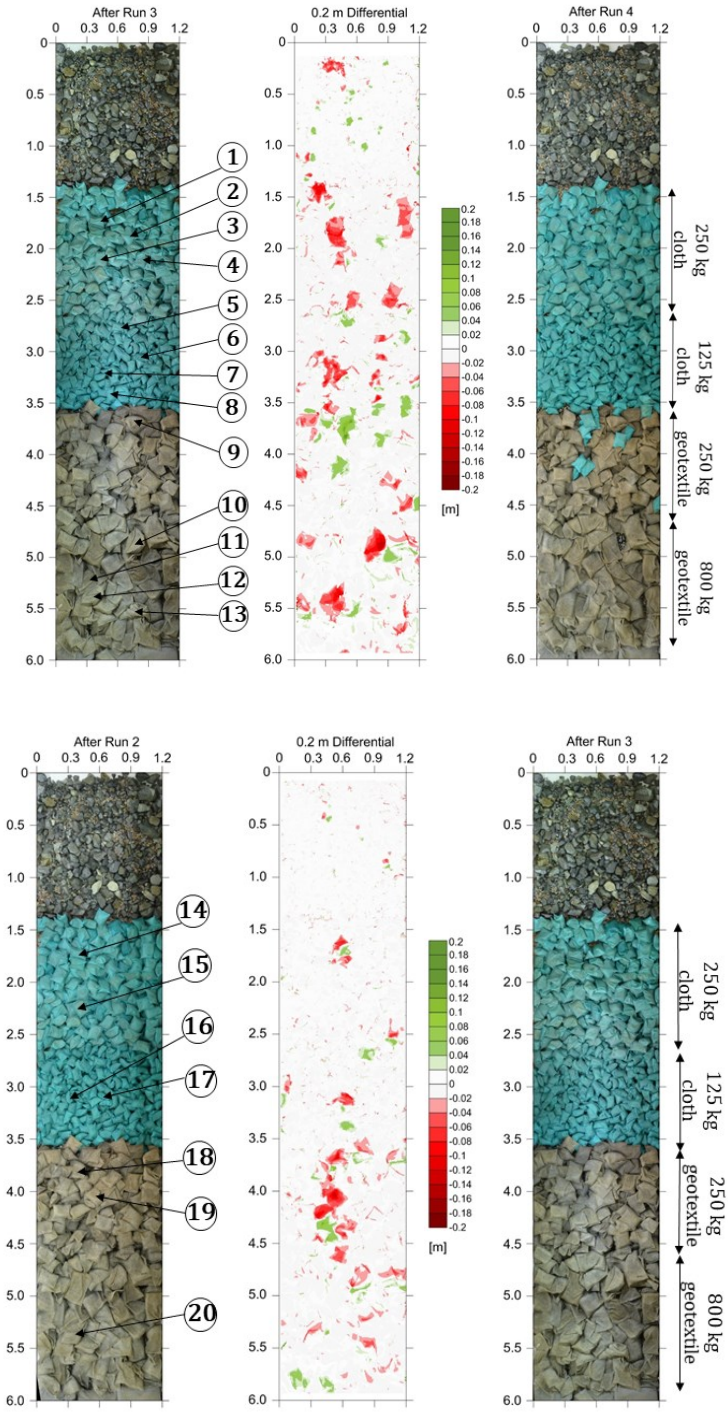

Figure 3-9: Image of the bed before and after velocity run and the difference in bed elevation for Case 2 (top) and Case 1 (bottom) where stresses on numbered bags are shown in the following figure (flow from top to bottom)

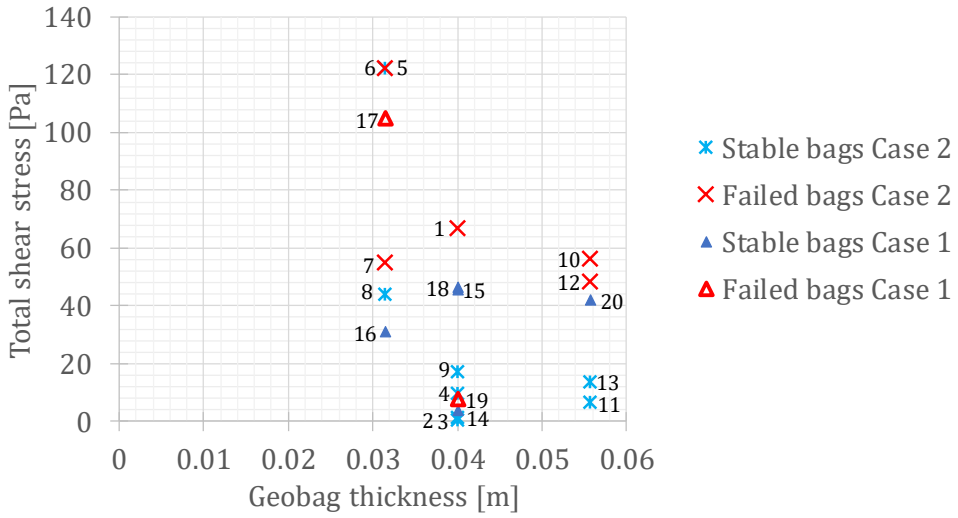

Figure 3-10: The correlating total shear stress for a number of failed and stable geobags (bag locations are shown in the previous figure)

3.3.3 Shields parameter

The Shields parameter, θ, or dimensionless critical shear stress, is defined as,

$$\theta = \frac{\tau_{cr}}{(\rho_s - \rho)gD} \qquad (3-4)$$

where ρ_s is the density of the element, and D is the characteristic diameter. The Shields parameter is a function of grain geometry and the boundary Reynolds number. A summary of the forces acting on the elements and the correlating shear stresses and Shields parameters can be found in Table 3-4.

Table 3-4: Summary of forces, stresses and Shields parameters from CFD results

Element type	Rock	125 kg cloth		250 kg cloth		250 kg geotextile		800 kg geotextile	
Case	2	2	1	2	1	2	1	2	1
Total force	17	18.4	19.2	49.6	24.1	37.7	26.6	31.3	33.1
Total shear	30.9	33.4	24.3	56.4	32.9	38.0	32.0	32.0	32.8
Shields parameter	0.041	0.15	0.11	0.16	0.095	0.15	0.13	0.094	0.096

The rock section did not undergo incipient motion in either of the Cases modelled. Only 2.7% of the rock section in Case 2 moved. The shear stresses computed in the rock section of Case 2 correlates to a Shields parameter of 0.041. The Shields parameter for rock is around 0.045 (Buffington and Montgomery 1997).The computed value rightly lies beneath the critical Shields parameter for rock since the section did not undergo incipient motion. That being said, the definition for incipient motion varies depending on the study and the method of detection (Buffington and Montgomery 1997). Because of this, there is a degree of uncertainty when comparing results to other studies.

A first estimate for the Shields parameter of geobags has been made using the shear stresses generated by the numerical model (Figure 3-11). All of the results of the study are well above the boundary Reynolds number of ~1000, where the Shields parameter becomes a constant. The Shields parameters shown in Figure 3-11 have been found using the thickness as the characteristic diameter (Thompson et al. submitted). Although there is not enough data to confidently find the lower bound of the critical Shields parameter, the value appears to be around 0.09. The Shields parameter of 0.09 is much higher than the critical Shields parameter for rock, 0.045. Since the shear stresses acting on the geobag

sections are comparable to the shear stresses acting on the rock section (Figure 3-5), the higher Shields parameter is attributed to the lower submerged density of the geobags. The added stability of the geobags is possibly due to the flexibility of the elements. Recio (2007) found that the lift forces are largely effected by the deformable nature of the geobags, reducing the lift moment by approximately 20%.

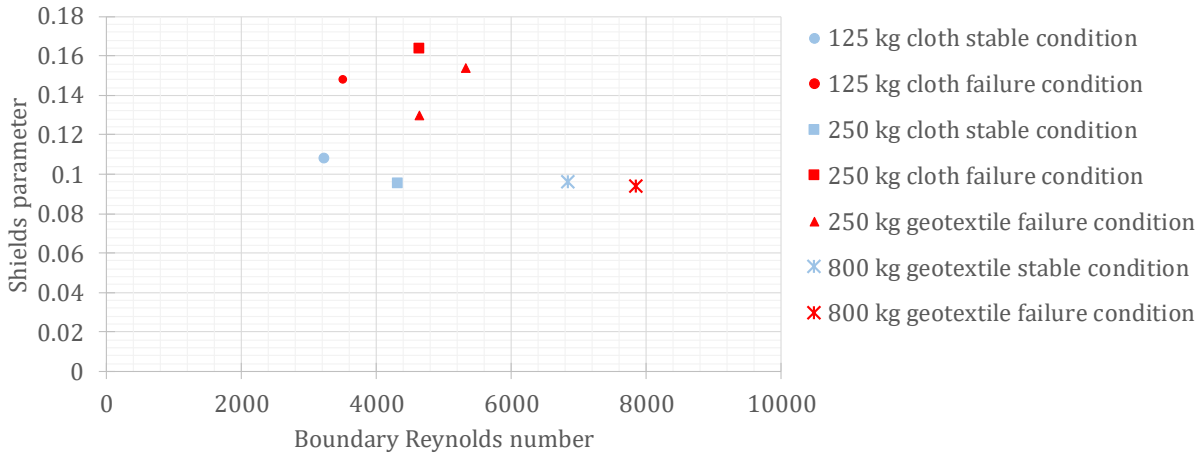

Figure 3-11: Corresponding Shields parameter for the stable and unstable geobag sections (the 250 kg geotextile bag was not stable in either Case 1 or 2; however, it was stable in the lower velocity runs)

It can also be noted from Figure 3-11 that it appears that the larger, 800 kg geobags appear to fail at lower shear stresses than the smaller 125 kg geobags and therefore have a lower critical Shields parameter. This is possibly attributed to the lower fill percentage of the larger bags (Table 3-1). With a lower fill percentage, the sand is able to move within the bags at lower shear stresses, failing to force the sand in the bags to move as one body. Similar conclusions have been observed by Thompson et al. (submitted). The study found

that geobags have a range of fill percentage which optimizes the stability of the elements. Elements which were under filled moved at lower critical velocities.

3.3.4 Contemplating the roughness of a geobag surface

The relative roughness of a surface influences the acting shear stresses, and therefore influences the stability of surface elements. A number of approaches can be utilized to quantify the roughness of a geobag surface. A hydraulic analysis can be used to determine the Nikuradse roughness using Prandlt von Kàrmàn universal velocity distribution law for turbulent flow over a rough surface (Chow 1959). Since the velocity profile does not fit this relationship, the method has not been used. Roughness has also been described using Manning's n value, found from Manning's equation,

$$V = \frac{1}{n} R^{\frac{2}{3}} S_F^{\frac{1}{2}} \qquad (3-5)$$

where R is the hydraulic radius and S_F is the energy slope of the channel. The energy slope is used rather than the bed slope in Manning's equation because of the flat bed of the flume. Andersson et al. (2014) have described the physical height of the surface protrusions, called the Nikuradse roughness, k_s, using the standard deviation of the surface elevations. Pilarczyk (1991) and the USACE (1991) describe riprap roughness with the protective element size, represented by the characteristic diameter, D. Pilarczyk (1991) suggests the relationship, $k_s = (1\text{-}2)\cdot D$, for uniform sediment. In this analysis, the Pilarczyk relationship was assigned to be $k_s = 1\cdot D$. The USACE (1991) uses Strickler's equation for uniformly sized riprap, $n=0.034\cdot D^{1/6}$ to find Manning's n.

The roughness of the surfaces in the flume experiments (seen in Figure 3 8) have been compared to surfaces constructed in the field. In order to analyze geobag surfaces constructed in the field multibeam survey data from nine different geobag aprons have been collected. The geobag aprons in the field all lie on relatively flat beds and have been constructed by systematic dumping (Figure 3 12). During the construction process geobags, positioned in rows one meter apart, are pushed off the side of a barge. Details of the nine field location can be seen in Table 3 5.

Table 3 6 shows how the roughness can vary depending on the method used to calculate the roughness. The table also shows the average and maximum deviation of the surface from a datum, set at the minimum elevation value over the sample. A few conclusions can be drawn from the results shown in Table 3-6. Placed geobags create a smoother surface than dumped geobags because of the flat shape of the bags. Using the characteristic diameter to find the roughness of the elements does not account for the placement method. Additionally, the larger geobags do not necessarily create a rougher surface. Using the characteristic diameter to find the surface roughness does not reflect this. It also appears that the geobag surfaces found in the field are typically rougher than those in the flume experiment. This is due to the dumping process creating lines along the aprons, which increase the roughness of the surface. Akter et al. (2013a) found a manning's n for geobags of 0.020. While this roughness is lower than the ones presented in the geobags used in the study were orderly placed along the length of an above water revetment structure.

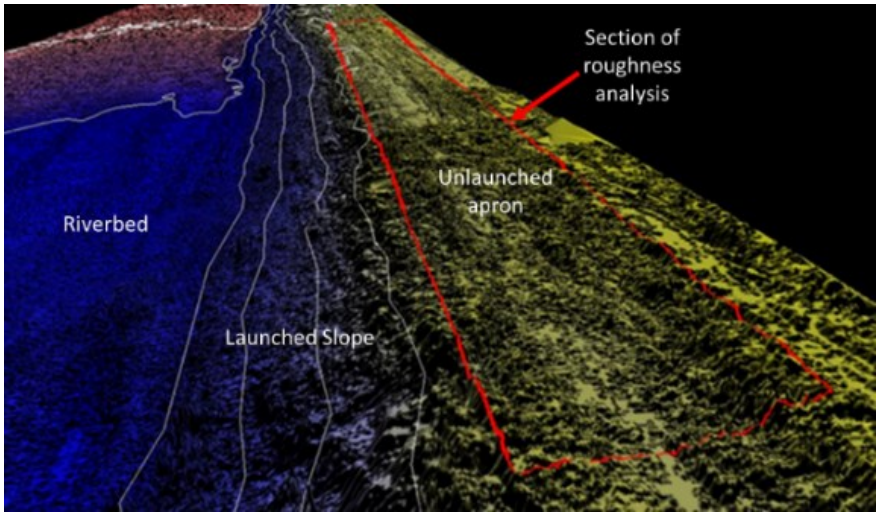

Figure 3-12: Multibeam image of underwater geobag apron

Table 3-5: Field multibeam data used to analyze geobag surface roughness

Location	Section size [m]	Resolution [cm]	Geobag mass [kg]	Construction methodology	Year of apron completion	Survey date
Chauhali Chauhali Chauhali	40 x 5 60 x 5 120 x 5	10 x 10	250	Individually dumped bags on a natural bed	2016	November 5th-8th, 2017
Koijuri Koijuri Koijuri	80 x 5 80 x 5 42 x 2.5	10 x 10	125	Bags dumped in groups of 6 on a natural bed	2010	November 9th-10th, 2017
Mawa Mawa Mawa	70 x 5 70 x 5 70 x 5	20 x 20	800	Individually dumped bags on a dredged 1V:6H surface	2016	November 25th, 2016

Table 3-6: Surface roughnesses (flume Nikuradse roughnesses scaled to prototype height)

		Nikuradse roughness, k_s [m]				Manning's n	
		Average deviation	Maximum deviation	Standard deviation	Pilarczyk (1991)	Manning's equation	USACE (1991)
Field data	125 kg	1.53	2.67	0.47	0.22	-	0.026
	250 kg	1.13	2.27	0.28	0.28	-	0.028
	800 kg	0.89	2.18	0.41	0.39	-	0.029
Flume experiment (dumped)	125 kg cloth	0.68	1.18	0.18	0.22	0.031	0.026
	250 kg cloth	0.75	1.22	0.19	0.28	0.030	0.028
	250 kg geotextile	0.70	1.22	0.21	0.28	0.027	0.028
	800 kg geotextile	0.78	2.35	0.19	0.39	0.027	0.029
	Rock	0.91	1.50	0.24	0.37	0.032	0.029
Flume experiment (placed)	125 kg cloth	0.34	0.65	0.10	0.22	-	0.026
	250 kg cloth	0.25	0.49	0.07	0.28	-	0.028
	250 kg geotextile	0.31	0.61	0.08	0.28	-	0.028
	800 kg geotextile	0.29	0.58	0.10	0.39	-	0.029

3.4 Conclusions

CFD modelling helps to provide more insight into how hydraulic forces act on geobags with the goal of improving the sizing process for designing geobag river revetments. The models have found that the drag forces acting on the bags were comprised of mostly form drag (~95%), created from the flow separating on the downstream portion of the bags. Because of the high form drag acting on the bags, the Shields parameter of geobags is around 0.09. The results also indicate the Shields parameter varies with the fill percentage of the bags. Bags with lower fill percentages appear less stable than those with

higher fill percentages, possibly because the internal movement of sand is less restricted. Similar results have been found by Thompson et al. (submitted).

The results found from this numerical model study are initial estimates and more data would be needed to confirm the results and use them in a design context. This study analyzed a limited sample size of critical shear stresses. It would be advantageous to work with a larger data set because of the inherently statistical nature of incipient motion of underwater protection elements. Measurements of pressure differences on the upstream and downstream side of a geobag, would be beneficial to add confidence to critical shear stress values. Additionally, this study only focused on geobags placed on a flat surface. Many geobags used in the field lie on the launched slopes (1 vertical: 2 horizontal). It would be valuable to look at how the shear stresses change for geobags lying on sloped surfaces.

3.5 References

Akter, A., Pender, G., Wright, G., Crapper, M., 2013a. Performance of a Geobag Revetment I: Quasi- Physical Modeling. Journal of Hydraulic Engineering, 129(8), 865-876.

Akter, A., Crapper, M., Pender, G., Wright, G., Wong, W., 2013b. Performance of a Geobag Revetment II: Numerical Modeling. Journal of Hydraulic Engineering, 139(8), 877-885.

Andersson, A. G., Hellström, J. G. I., Andreasson, P. and Lundström, T. S., 2014. Effects of spatial resolution of rough surfaces on numerically computed flow fields with application to hydraulic engineering. Engineering Applications of Computational Fluid Mechanics. 8(3), 373-381.

ANSYS, 2009. ANSYS CFX- Solver Theory Guide. Ansys inc. Canonsburg.

Biron, P., Robson, C., Lapointe, M., and Gaskin, S., 2004. Comparing different methods of bed shear stress estimates in simple and complex flow fields. Earth Surface Processes and Landforms. 29, (1403-1415)

Buffington, J. M., Montgomery, D. R., 1997. A systematic analysis of eight decades of incipient motion studies, with special reference to gravel-bedded rivers. Water resources research. 11(8), 1993-2029.

Chanson, H., 2004. The Hydraulics of Open Channel Flow: an Introduction, second edition. Elsevier.

Chow, V.T., 1959. Open-Channel Hydraulics. McGraw Hill Book Company, Inc. Kogakusha Co., Ltd. Tokyo.

Dey, S. and Papanicolaou, A., 2008. Sediment Threshold under Stream Flow: A State-of-the-Art Review. KSCE Journal of Civil Engineering. 12(1), 45-60. DOI 10.1007/s12205-008-8045-3

Guo, J., 2015. Sidewall and non-uniformity corrections for flume experiments, Journal of Hydraulic Research. 53(2), 218-229. DOI: 10.1080/00221686.2014.971449

Hoerner, S. F., 1965. Fluid-Dynamic Drag. Published by author. 148 Busteed Drive, Midland Park, New Jersey.

NHC, 2010. Padma Multipurpose Bridge Design Project RT23 Geobag Flume Model Study. Prepared for Maunsell/AECOM and Bangladesh Bridge Authority.

Oberhagemann, K., Hossain, M. M., 2011. Geotextile bag revetments for large rivers in Bangladesh. Geotextiles and Geomembranes. 29(4), 402-414.

Oberhagemann, K., Thompson, A., Walsh, B., 2017. Lecture Note on Geotextile Bag Revetments. Prepared for training courses for Bangladesh Water Development Board staff, conducted at the Bangladesh University for Engineering and Technology under the Flood and Riverbank Erosion Management Investment Program Tranche-1, Bangladesh.

Pilarczyk, K. W., 1991. Coastal Protection Short Course Rijkswaterstaat. Road and Hydraulic Engineering Division Van der Burghweg, Delft.

Recio, J., 2007. Hydraulic Stability of Geotextile Sand Containers for Coastal Structures, Effect of deformations and stability formulae. PhD dissertation. Technical University of Braunschweig, Germany.

Schlichting, H., 1979 Boundary-layer theory. Magraw Hill Book Company.

Shields, A., 1936. Application of similarity principles and turbulence research to bedload movement English translation. W.M. Keck Laboratory of Hydraulics and Water Resources, California Institute of Technology.

Thompson, A., Oberhagemann, K., She, Y., Haque, A.M.A., 2018. The behavior of self-launching geotextile bag aprons – latest investigations from the Lower Brahmaputra in Bangladesh. 9th International Conference on Scour and Erosion, Taipei.

Thompson, A., Oberhagemann, K., She, Y., Submitted for publishing. Geobag stability for riverbank erosion protection structures: Physical model study. Geotextiles and Geomembranes.

USACE, 1991. Hydraulic design of flood control channels, Engineer Manual. U.S. Army Corps of Engineers, Washington.

U.S. Department of Transportation Federal Highway Administration, 2017. Advanced Methodology to Assess Riprap Rock Stability at Bridge Piers and Abutments. Research, Development, and Technology Turner-Fairbank Highway Research Center PUBLICATION NO. FHWA-HRT-17-054 McLean

4 Treatment of the boundary layer in the numerical model

In a CFD model, the boundary layer of a fluid flow can either be resolved by computing the near wall velocity and pressure components or it can be approximated using a wall function. The wall function approximates the near wall flow using a logarithmic relationship. When modelling fluid flows the decision to use a wall function approximation can have great impacts on the results, particularly if the near wall results, such as shear stresses, are of interest. If a wall function is not used the amount of computational resources required increases. In the case of the current study, to resolve the near bed flow, the center width of each individual element section needs to be modelled separately, as opposed to including the entire length of the flume in one single domain. This adds time and complications to the modelling procedure. This chapter discusses why the decision was made to resolve the boundary layer. The two boundary layer treatments are compared by analyzing how the models reproduce the turbulent kinetic energy, the Shields parameter for the reference rock section and the well-known drag coefficient for a cube. Reynolds stresses were not used because of the wide variable of local shear stresses and the sensitivity of the probe location and orientation, as well as to deviations from two dimensional flows (Biron et al. 2004).

The two different boundary treatments have been applied to the Case 2 model. The two models both used the same modelling parameter, included in the k- ω SST turbulence model. The k- ω SST turbulence model was chosen over the commonly used k-ε turbulence model because of the model's ability to simulate flow separation points. The model resolving the boundary layer has a finer mesh close to the flume bed boundary (Table 4-1).

Mesh independence for the resolved boundary layer model has been shown in the previous chapter (Table 3-3). Table 4-2 shows the mesh independence for the wall function model.

Table 4-1: Differences between the boundary layer mesh of the two models being compared

	Resolved boundary layer	Wall function approximation
Number of inflation layers	50	10
First layer thickness	0.01 mm	3 mm
Y+ range	0.2-13.9	16-258

Table 4-2: Mesh independence study for the wall function approximation model

Number of nodes	Peak shear stress [Pa]	Percent difference
400,000	15.0	-
2,000,000	17.0	12.5%
2,700,000	17.5	2.9%

One method of confirming shear stresses is to compare the turbulent kinetic energy (TKE), k. The TKE is the mean kinetic energy per unit of mass, represented by the equation,

$$k = \frac{1}{2}\left(\overline{(u')^2} + \overline{(v')^2} + \overline{(w')^2}\right) \qquad (4-1)$$

where u', v' and w' are the variation in the fluctuations of the velocity components. A comparison of the computed TKE to the measured TKE for the two different boundary treatments can be seen in Figure 4-1. While the two models appear to compute similar TKE for the 250 kg cloth measurement point, other sections, such as the 250 kg geotextile, do not match closely. The rock section TKE in both models does not match the measured TKE. This is possibly attributed to the deviations of the computed velocity profiles over the rock section from the measured values. Deviations in the velocity fields are possibly attributed to simplifications of the geometry of the surface of the bed.

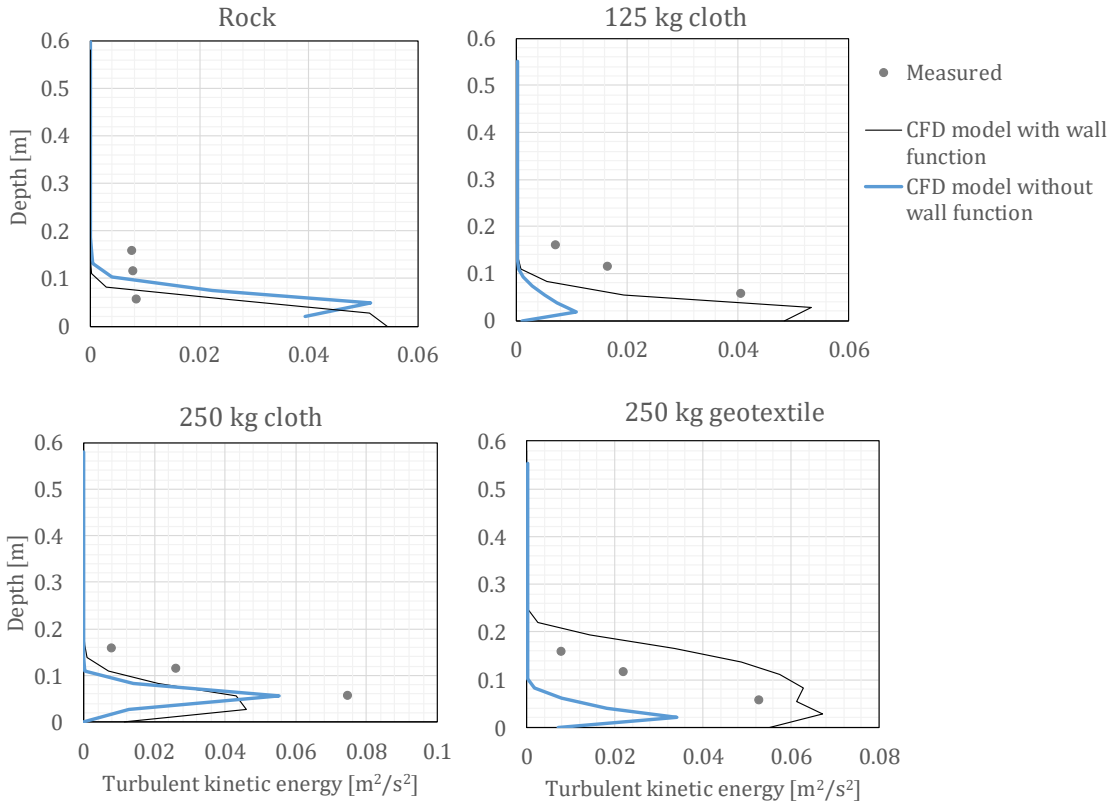

Figure 4-1: Comparison of the turbulent kinetic energy of the two models and the measured values.

While some of the TKE appears to be more accurately computed at the ADV measurement points using the wall function (125 kg cloth), other tests imply that the resolved boundary layer produces more accurate drag forces and shear stresses. As mentioned in the previous chapter, the Shields parameter for rock is commonly taken to be around 0.045 (Buffington and Montgomery 1997). Using the resolved boundary layer model, the Shields parameter for rock was found to be 0.041. Using the wall function, the Shields parameter for rock was found to be 0.26. Considering the rock section had not

undergone incipient motion, the latter Shields parameter is too large. This implies that the drag forces computed by the model using the wall function are artificially high.

Both models were also used to calculate the drag coefficient of a cube. The cube model described in the previous chapter has been modelled using the wall function approximation and the corresponding mesh. While the resolved boundary layer model produced an error of 6.7% when computing the drag coefficient of a cube, the wall function model produced a larger error of 12.3%.

While the resolved boundary layer does not appear to compute more accurate turbulent kinetic energy in the flow, it computes a more accurate Shields parameter for rock and drag coefficient for a cube. It can be concluded from the results that the resolution of the boundary layer improves the models ability to recreate flow separation points and the resulting drag forces. Since the drag forces and the corresponding shear stresses are the desired parameters from the modelling exercise, it was decided to resolve the boundary layer and not use a wall function.

5 Conclusion

Geobags have proven to be an effective technology for riverbank protection structures, replacing traditional hard protective materials in places where such materials are not available. While the technology has performed well along the banks of the Brahmaputra and Padma rivers, the methodology for sizing the geobags against hydraulic loading has room for improvement. This thesis examined how geobags behave under current loading in an attempt to improve and optimize the sizing methodology for the use of geobags in long guiding river revetments. Physical model studies were performed at the NHC laboratory in Vancouver, Canada using geobags scaled at 1:7. Using data from the physical model, CFD numerical models were created in order to obtain the forces acting on the geobags.

A number of findings have been concluded from the results. Dumped geobags are much more stable than orderly placed bags, confirming the current methodology for constructing geobag revetments is beneficial for their stability. The study also found that the current USACE stability formula can be improved in order to better predict the incipient motion of geobags. The geobag thickness can be used as the characteristic diameter rather the cube root of the volume. The volume of a geobag is a difficult value to acquire, and using the cube root of the volume is not an intuitive way to describe how the geobag obstructs the oncoming flow. Additionally, the stability coefficient in the USACE formula should be adjusted to account for the filling percentage of the bags. The stability of geobags is not purely dependent on the mass of the bags, but also a function of the filling percentage. Too little fill, and the sand is able to move independently of the entire element.

Too much fill, and the contact points between bag elements reduce, thus reducing the overall stability of the elements. These results confirm suggestions originally proposed by Pilarczyk (2000). These results are preliminary and further testing needs to be done to collect additional data for a more complete understanding of how the fill percentage effects the stability coefficient. For bags with an approximate aspect ratio of 1:3 and using a thickness as the characteristic diameter, the author recommends using a stability coefficient of 0.15 for fill percentages ~60% and a stability coefficient of 0.07 for fill percentages above ~80%. The authors do not recommend filling the bags beyond ~90% fill capacity. Further research would be needed to gain a more comprehensive idea of how the varied fill changes the geobag stability. A study using uniform geobags and only varying fill percentage would isolate the effects of filling percentage.

The numerical model results have found that the drag forces acting on the bags comprised mostly of form drag (~95%), created from the flow separating on the downstream portion of the bags. Because of the high form drag acting on the bags, the initial estimate of the Shields parameter of geobags is relatively high, around 0.09. The results of the shear stresses also indicate the Shields parameter varies with the fill percentage of the bags.

The results pertaining to the Shields parameter are initial estimates, and further research is needed in order to gain confidence in the results for use in a design context. This study analyzed a limited sample size of critical shear stresses. It would be advantageous to collect more data to gain a confidence in the lower bound of the critical shear stresses. Measurements of pressure differences on either side of a geobag, would be

beneficial to acquire local shear stress values in order to compare computed results to for more rigorous model validation. In addition, this study only focused on geobags placed on a flat surface. Many geobags used in the field lie on the launched slopes (1 vertical: 2 horizontal). It would be valuable to look at how the shear stresses change for geobags lying on sloped surfaces. Closer agreement between the turbulent kinetic energies would be desirable in order to add additional confidence in the results. Because two-equation turbulence models tend to create excessive turbulent energy, the model includes a limiting factor (ANSYS 2009). Closer agreement to the measured turbulent kinetic energy could possibly be achieved by adjusting this limiting factor.

References

ADB, 2002. Report and Recommendation of the President to the Board of Directors on a Proposed Loan to the People's Republic of Bangladesh for the Jamuna-Meghna River Erosion Mitigation Project, October.

ADB, 2003. Jamuna-Meghna River Erosion Mitigation Project Part A Geobag Protection, June.

ADB, 2010. Report and Recommendation of the President to the Board of Directors, Proposed Multitranche Financing Facility, India: Assam Integrated Flood and Riverbank Erosion Risk Management Investment Program, September.

ADB, 2014. Report and Recommendation of the President to the Board of Directors, Proposed Multitranche Financing Facility, People's Republic of Bangladesh: Flood and Riverbank Erosion Risk Management Investment Program, June.

Akter, A., Pender, G., Wright, G., Crapper, M., 2013a. Performance of a geobag revetment I: Quasi- physical modeling. Journal of Hydraulic Engineering. 129(8), 865-876.

Akter, A., Crapper, M., Pender, G., Wright, G., Wong, W., 2013b. Performance of a geobag revetment II: Numerical modeling. Journal of Hydraulic Engineering. 139(8), 877-885.

Andersson, A. G., Hellström, J. G. I., Andreasson, P. and Lundström, T. S., 2014. Effects of spatial resolution of rough surfaces on numerically computed flow fields with application to hydraulic engineering. Engineering Applications of Computational Fluid Mechanics. 8(3), 373-381.

ANSYS, 2009. ANSYS CFX- Solver Theory Guide. Ansys inc. Canonsburg.

Bangladesh Water Development Board, 2010. Guidelines for River Bank Protection. Jamuna-Meghna River Erosion Mitigation Project, Bangladesh.

Bezuijen, A., Vastenburg, E. W., 2013. Geosystems. Design Rules and Applications, first ed. Taylor & Francis Group, London.

Biron, P., Robson, C., Lapointe, M., and Gaskin, S., 2004. Comparing different methods of bed shear stress estimates in simple and complex flow fields. Earth Surface Processes and Landforms. 29, (1403-1415)

Buffington, J. M., Montgomery, D. R., 1997. A systematic analysis of eight decades of incipient motion studies, with special reference to gravel-bedded rivers. Water resources research. 11(8), 1993-2029.

Chanson, H., 2004. The Hydraulics of Open Channel Flow: an Introduction, second edition. Elsevier.

Chow, V.T., 1959. Open-Channel Hydraulics. McGraw Hill Book Company, Inc. Kogakusha Co., Ltd. Tokyo.

Dassanayake, D., 2013. Experimental and Numerical Modelling of the Hydraulic Stability of Geotextile Sand Containers for Coastal Protection (Doctoral dissertation). Retrieved from https://publikationsserver.tu-braunschweig.de/servlets/MCRFileNodeServlet/digibib_derivate_00032409/Diss_Dassanayake.pdf

Delft Hydraulics Laboratory, 1985. Stability of clay-filled gunny bags. Feasibility study Sandwhip Crossdam R 1331-40, Delft.

Dey, S. and Papanicolaou, A., 2008. Sediment Threshold under Stream Flow: A State-of-the-Art Review. KSCE Journal of Civil Engineering. 12(1), 45-60. DOI 10.1007/s12205-008-8045-3

Elkholy, M., Chaudhry, M. H., 2011. Drag and added-mass coefficients of large sandbags. Journal of Hydraulic Engineering. 137(11), 1441-1451.

FAP21, 2001. Bank Protection and River Training (AFPM) Pilot Project FAP21/22, Final Project Evaluation Report. Prepared by Jamuna Test Works Consultants, Joint Venture for Ministry of Water Resources, Water Resources Planning Organization, December.

Grüne, J., Oumeraci, H., 2007. Stability tests of geotextile sand containers for monopile scour protection. International Conference on Coastal Engineering, San Diego. 5, 5093-5105.

Guo, J., 2015. Sidewall and non-uniformity corrections for flume experiments, Journal of Hydraulic Research. 53(2), 218-229. DOI: 10.1080/00221686.2014.971449

Halcrow, 1990. Flood Damage Restoration Project, Chandpur Town Protection, Design and Construction Report. Prepared by Sir William Halcrow and Partners Ltd for Ministry of Irrigation, Water Development and Flood Control, Bangladesh Water Development Board. April.

Halcrow, 1998. River Bank Protection Project, Brahmaputra Right Bank Priority Works, Contract B2: Sirajganj, Engineer's Review and Action Plan Report on Damages in 1998 Monsoon. Prepared for Bangladesh Water Development Board, October.

Halcrow, 1999. Riverbank Protection Project, contract B2: Sirajganj; Design Report on Remedial Works to Sections A and C; Volume 2: Design Documentation. Prepared for Bangladesh Water Development Board, May.

Heibaum, M., Oberhagemann, K., Faisal, M.A., Haque, S., 2008. Geotextile Bags for sole permanent Bank Protection. 4th European Geosynthetics Conference, Edinburgh.

Hoerner, S. F., 1965. Fluid-Dynamic Drag. Published by author. 148 Busteed Drive, Midland Park, New Jersey.

Hornsey, W. P., Carley, J. T., Coghlan, I. R., Cox, R. J., 2011. Geotextile sand container shoreline protection systems: Design and application. Geotextiles and Geomembranes. doi:10.1016/j.geotexmem.2011.01.009

Maynord, S. T., 1988. Stable riprap size for open channel flows. US Army Corps of Engineers, Washington.

Maunsell|AECOM, 2011. Padma Multipurpose Bridge Design Project, River Training Works, Final Design Report. Prepared by Maunsell|AECOM in association with Northwest Hydraulic Consultants, SMEC International, ACE Consultants, for Bangladesh Bridge Authority by Maunsell|AECOM, 5 July.

Neill, C. R., 1968. A re-examination of the beginning of movement for coarse granular bed material. Hydraulics Research Station, Wallingford.

Neill C. R., Mannerström, M., Azad, A. K., 2008. Model tests on geobags for erosion protection. Fourth International Conference on Scour and Erosion, Tokyo.

NHC, 2006a. Jamuna-Meghna River Erosion Mitigation Project Part B Special Report 11 Physical Model Study. Prepared for Bangladesh Water Development Board.

NHC, 2006b. Jamuna Meghna River Erosion Mitigation Project, Part B, Special Report 23 Design Brief for Riverbank Protection Implemented under JMREMP (update). Prepared by Northwest Hydraulic Consultants in association with Beller Consult and RPMC for Bangladesh Water Development Board, December.

NHC, 2010. Padma Multipurpose Bridge Design Project RT23 Geobag Flume Model Study. Prepared for Maunsell/AECOM and Bangladesh Bridge Authority.

NHC, 2013. Main River Flood and Bank Erosion Risk Management Program, Project preparatory technical assistance Annex D. Prepared for the Bangladesh Water Development Board and the Asian Development Bank.

NHC & EMM, 2016. Strategic Framework for River Stabilization and Development: Jamuna-Padma and Dependent Areas. Prepared by the Joint Venture Northwest Hydraulic Consultants and Euroconsult Mott MacDonald, in association with Deltares, RPMC, and CEGIS, for Bangladesh Water Development Board, November.

Oberhagemann, K., Diggelmann, P., Mukhles-uz-zaman, 2008. Understanding Falling Aprons. – Experience from the Lower Brahmaputra / Jamuna River. 4th International Conference on Scour and Erosion, Tokyo.

Oberhagemann, K. & Hossain, M. M., 2011. Geotextile bag revetments for large rivers in Bangladesh. Geotextiles and Geomembranes, 29(4): 402-414.

Oberhagemann, K., Thompson, A., Walsh, B., 2017. Lecture Note on Geotextile Bag Revetments. Prepared for training courses for Bangladesh Water Development Board staff, conducted at the Bangladesh University for Engineering and Technology under the Flood and Riverbank Erosion Management Investment Program Tranche-1, Bangladesh.

Pilarczyk K. W., 1991. Coastal Protection Short Course Rijkswaterstaat. Delft: Road and Hydraulic Engineering Division Van der Burghweg.

Pilarczyk, K. W., 2000. Geosynthetics and geosystems in hydraulic and coastal engineering. A. A. Balkema, Rotterdam.

Recio, J., 2007. Hydraulic Stability of Geotextile Sand Containers for Coastal Structures, Effect of deformations and stability formulae. PhD dissertation. Technical University of Braunschweig, Germany.

Recio, J. & Oumeraci, H., 2009. Process based stability formulae for coastal structures made of geotextile sand containers. Coastal Engineering: 632–658. Retrieved from doi:10.1016/j.coastaleng.2009.01.011

Schlichting, H., 1979 Boundary-layer theory. Magraw Hill Book Company.

Shields, A., 1936. Application of similarity principles and turbulence research to bedload movement English translation. W.M. Keck Laboratory of Hydraulics and Water Resources, California Institute of Technology.

Thompson, A., Oberhagemann, K., She, Y., Haque, A.M.A., 2018. The behavior of self-launching geotextile bag aprons – latest investigations from the Lower Brahmaputra in Bangladesh. 9th International Conference on Scour and Erosion, Taipei.

Thompson, A., Oberhagemann, K., She, Y., Submitted for publishing in the journal of Geotextiles and Geomembranes. Geobag stability for riverbank erosion protection structures: Physical model study.

USACE, 1991. Hydraulic design of flood control channels, Engineer Manual. U.S. Army Corps of Engineers, Washington.

U.S. Department of Transportation Federal Highway Administration, 2017. Advanced Methodology to Assess Riprap Rock Stability at Bridge Piers and Abutments. Research, Development, and Technology Turner-Fairbank Highway Research Center PUBLICATION NO. FHWA-HRT-17-054 McLean

Zellweger, H., 2007. Geotextile bags for river erosion control in Bangladesh. Swiss Federal Institute of Technology, Zürich.

Zhu, L., Wang, J., Cheng, N. S., Ying, Q., Zhang, D., 2004. Settling distance and incipient motion of sandbags in open channel flows. Journal of Waterway, Port, Coastal and Ocean Engineering. 130(2), 98-103.

Appendix A: Differential images

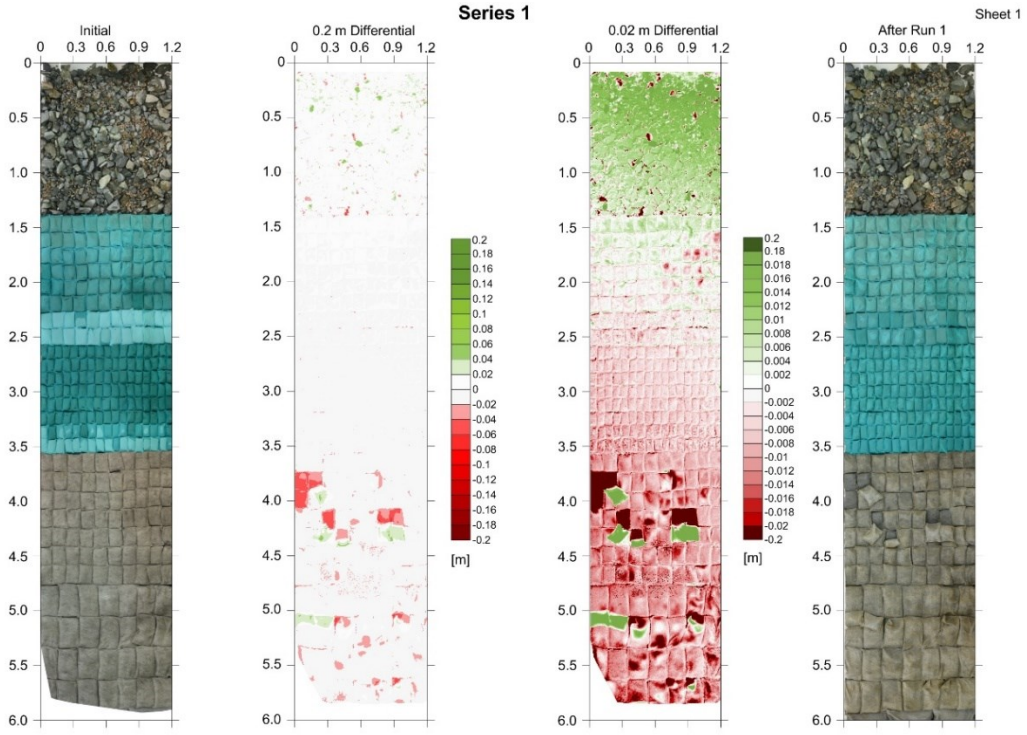

Figure A-1: Differential image for Series 1after Run 1

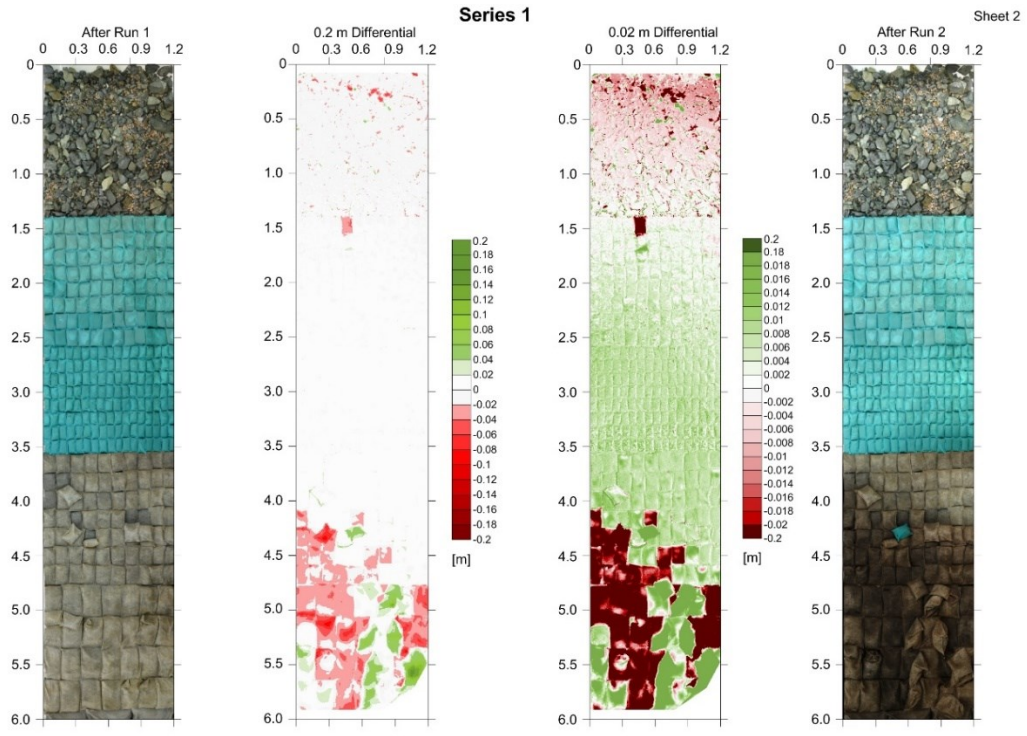

Figure A-2: Differential image for Series 1after Run 2

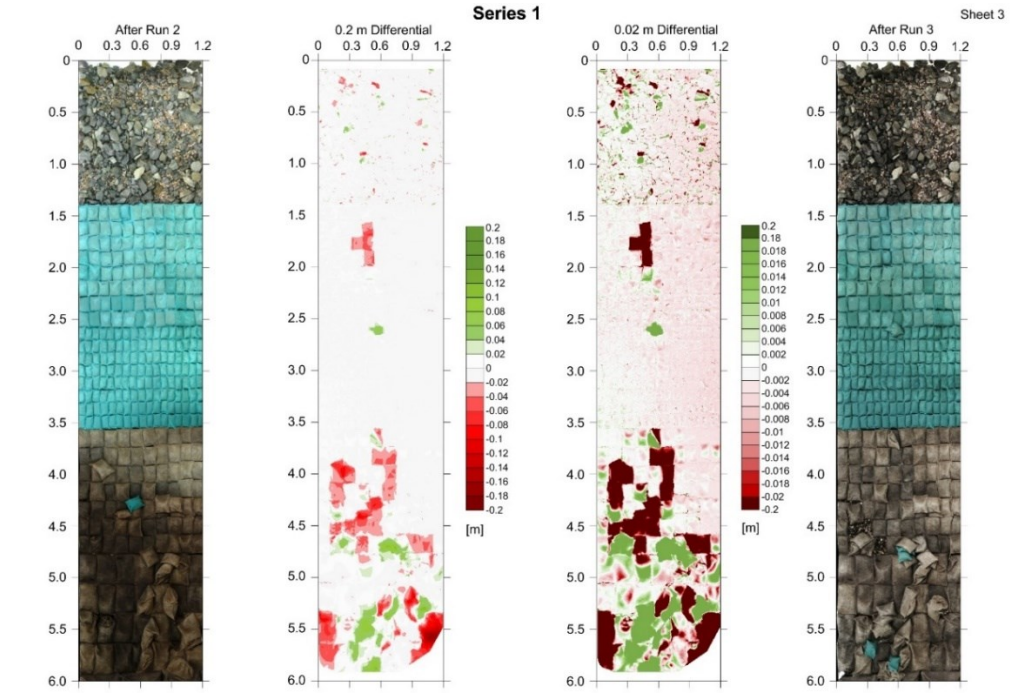

Figure A-3: Differential image for Series 1after Run 3

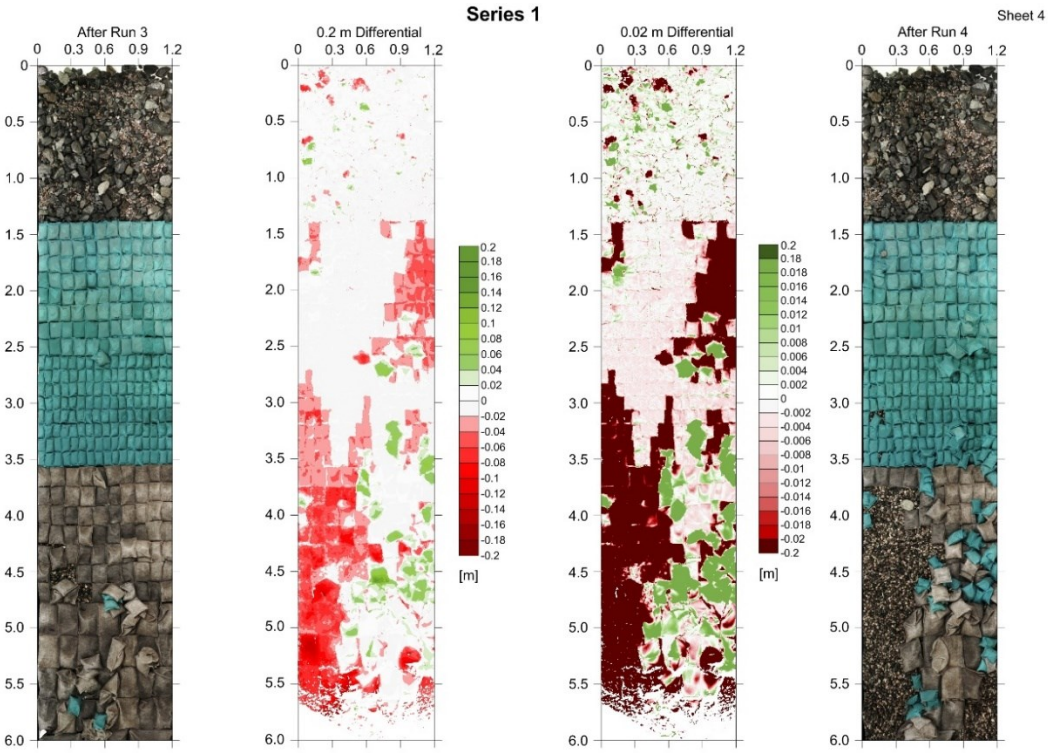

Figure A-4: Differential image for Series 1after Run 4

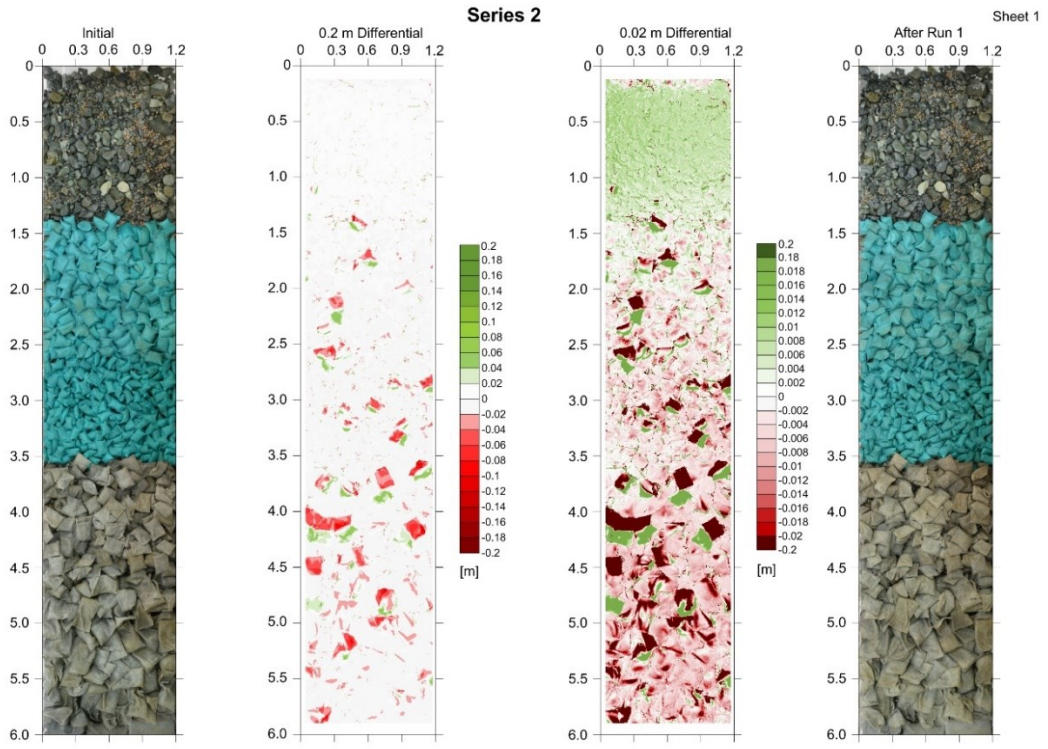

Figure A-5: Differential image for Series 2 after Run 1

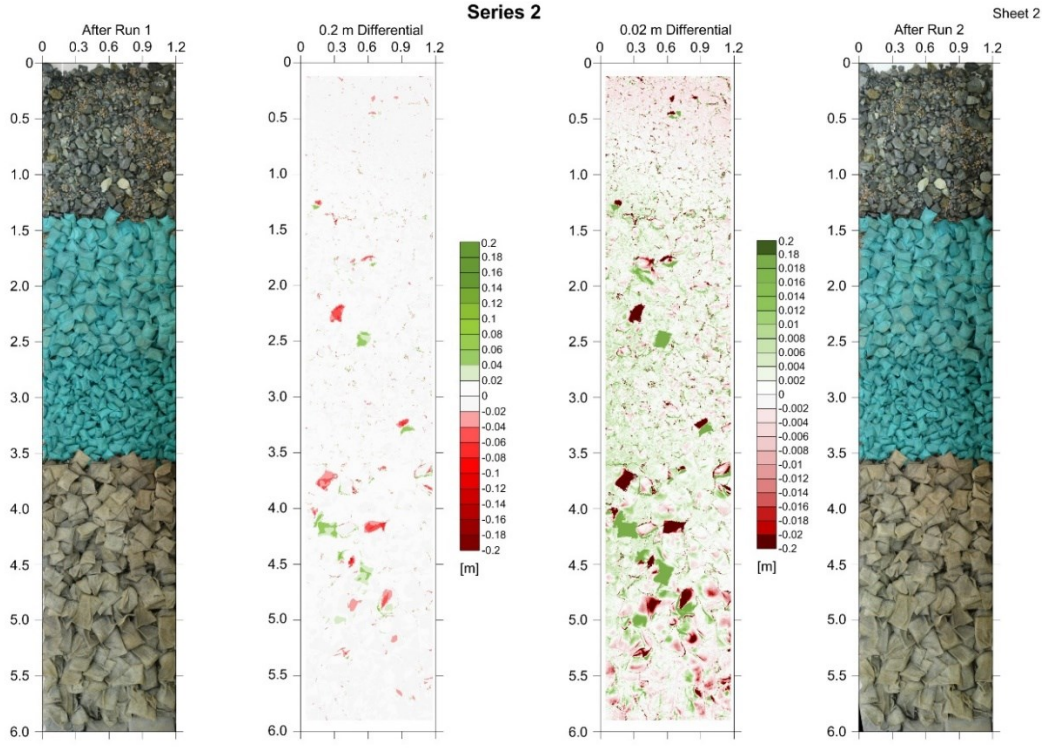

Figure A-6: Differential image for Series 2 after Run 2

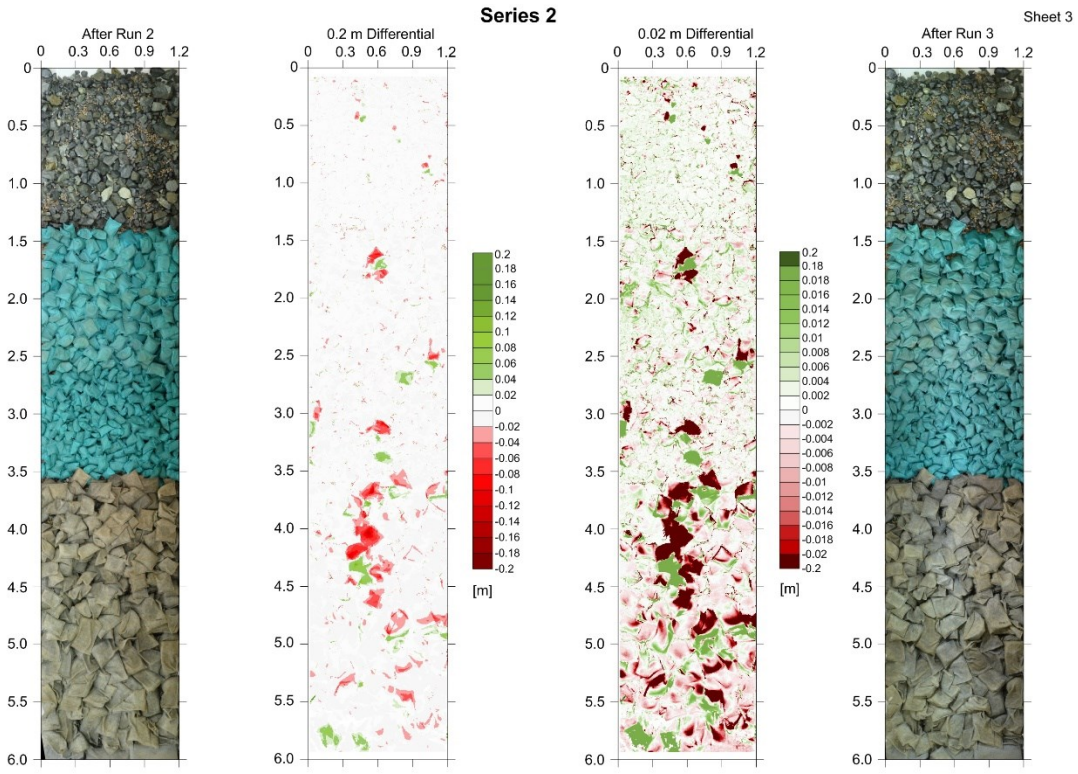

Figure A-7: Differential image for Series 2 after Run 3

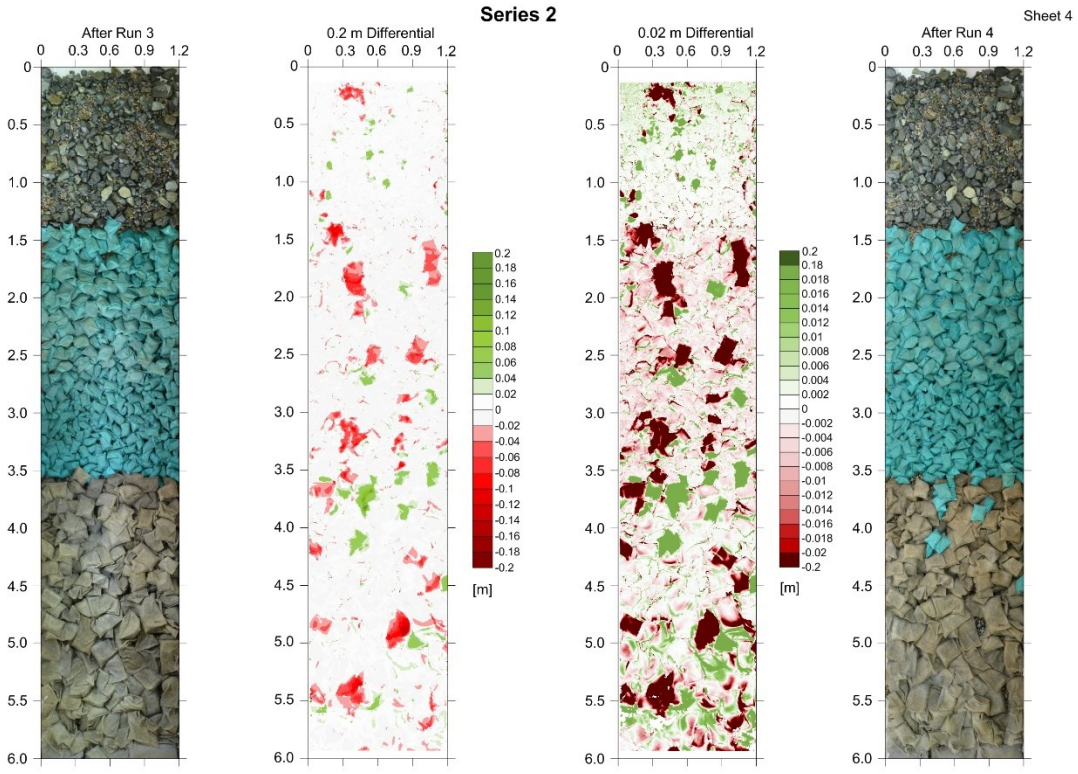

Figure A-8: Differential image for Series 2 after Run 4

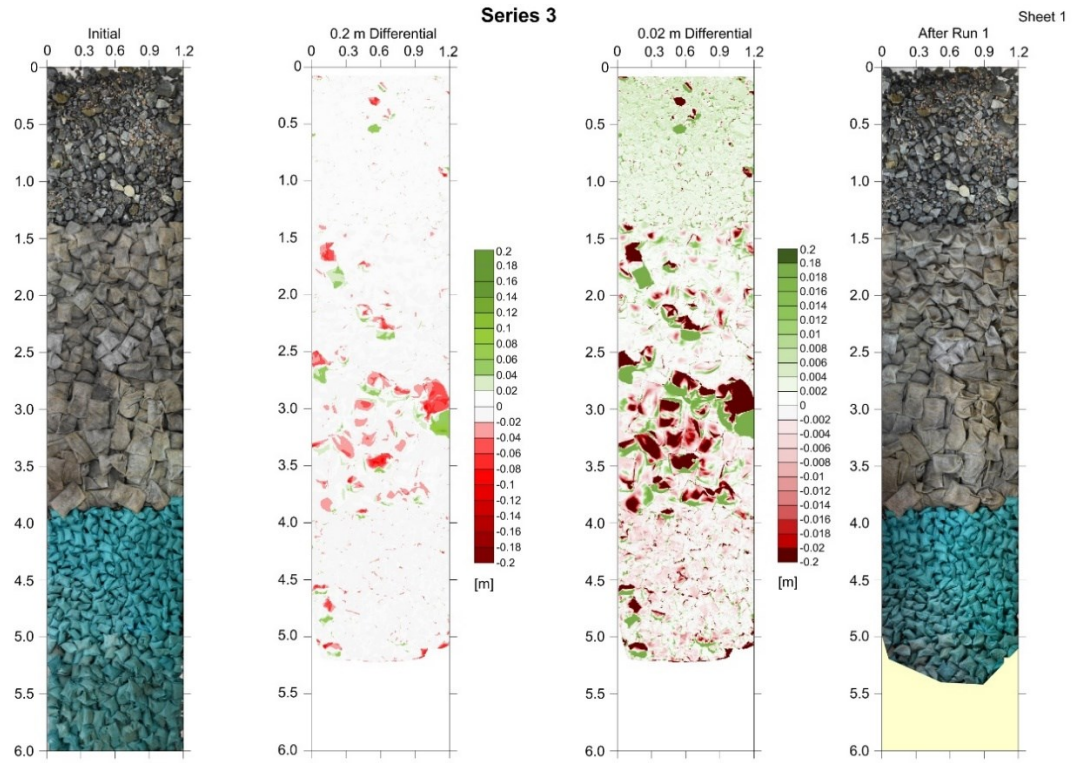

Figure A-9: Differential image for Series 3 after Run 1

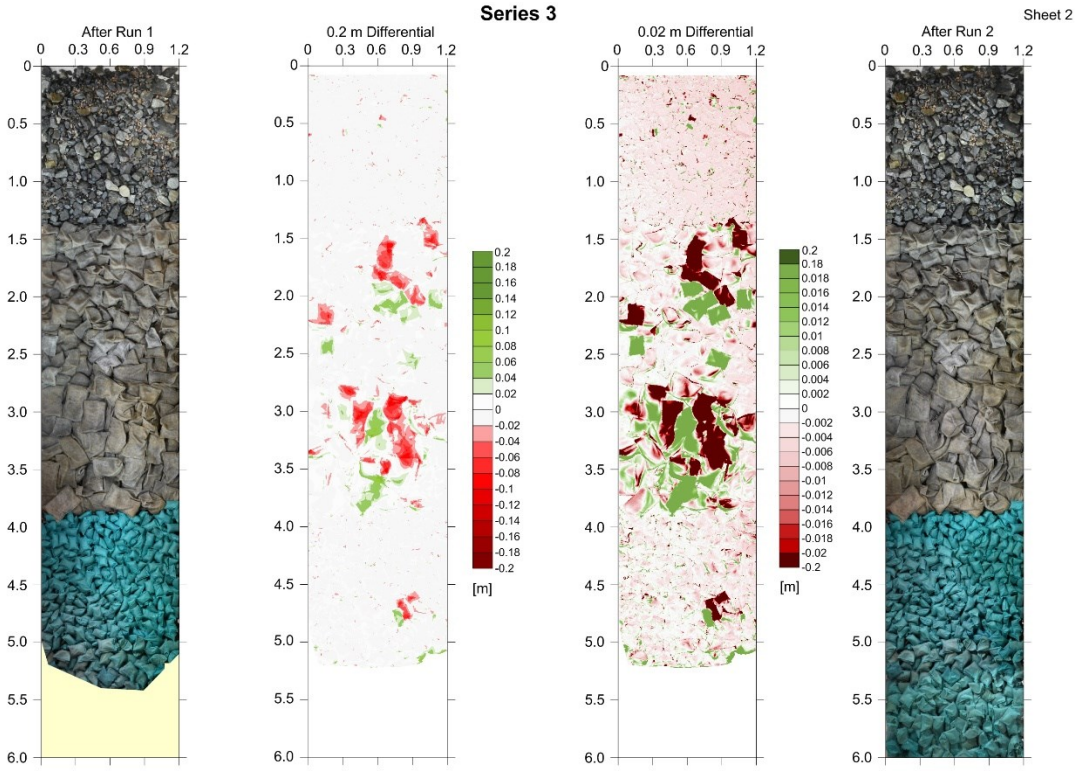

Figure A-10: Differential image for Series 3 after Run 2

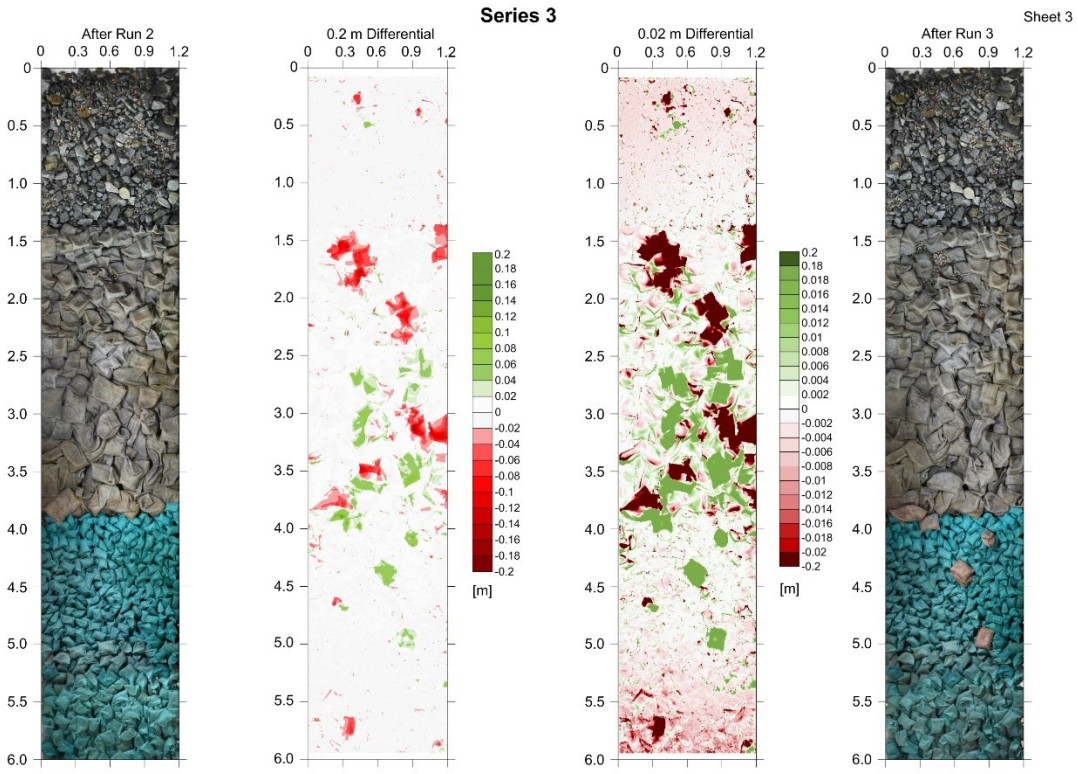

Figure A-11: Differential image for Series 3 after Run 3

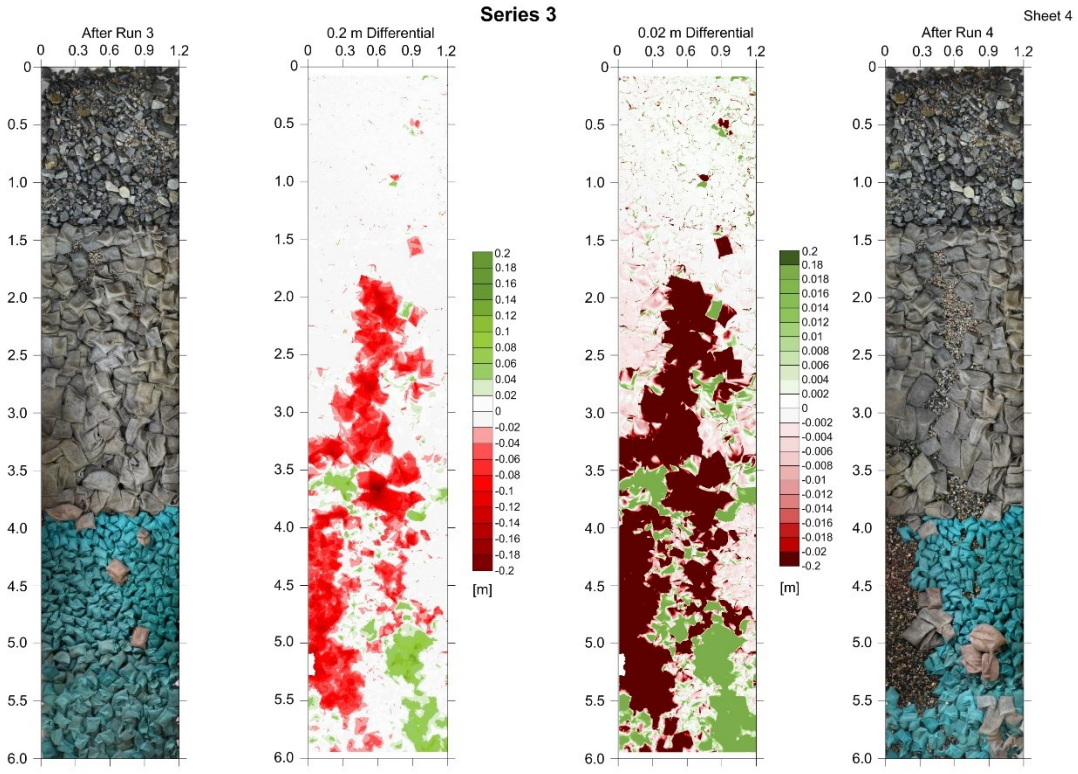

Figure A-12: Differential image for Series 3 after Run 4

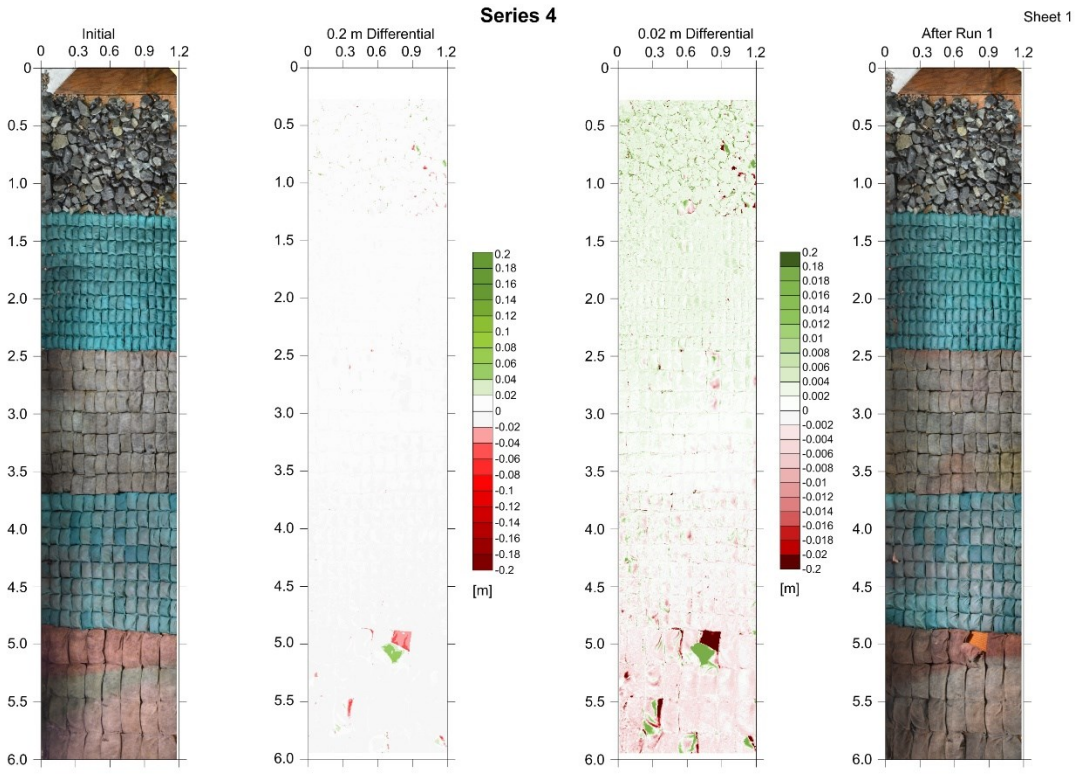

Figure A-13: Differential image for Series 4 after Run 1

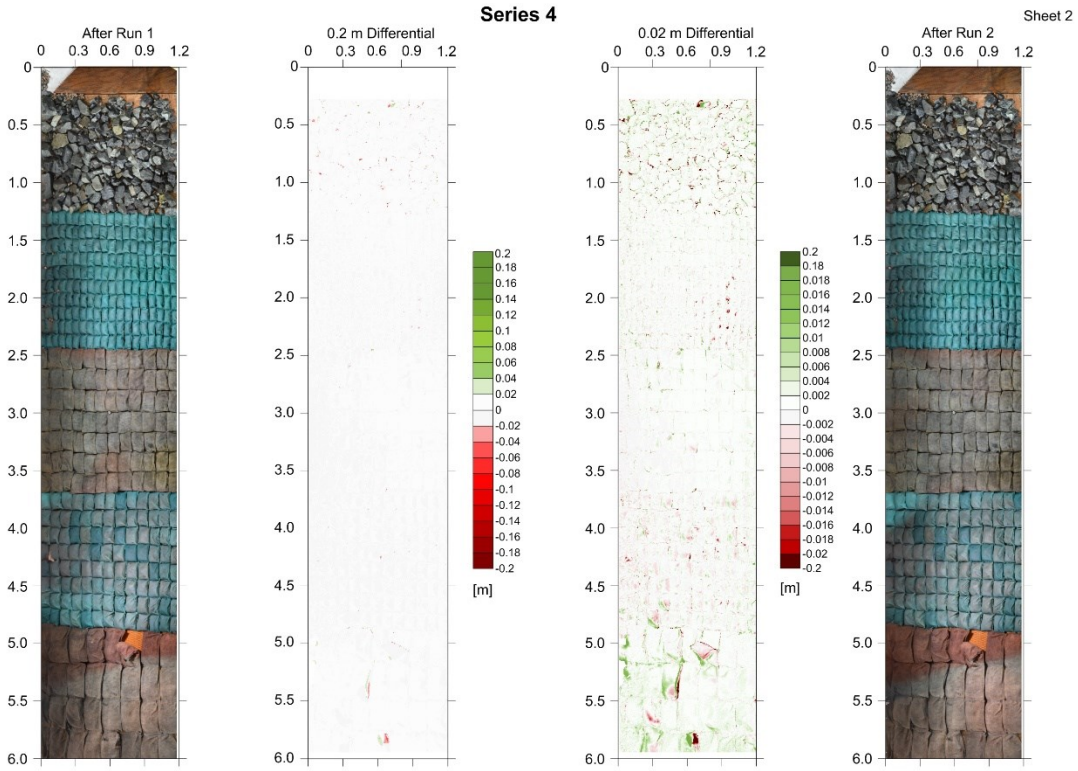

Figure A-14: Differential image for Series 4 after Run 2

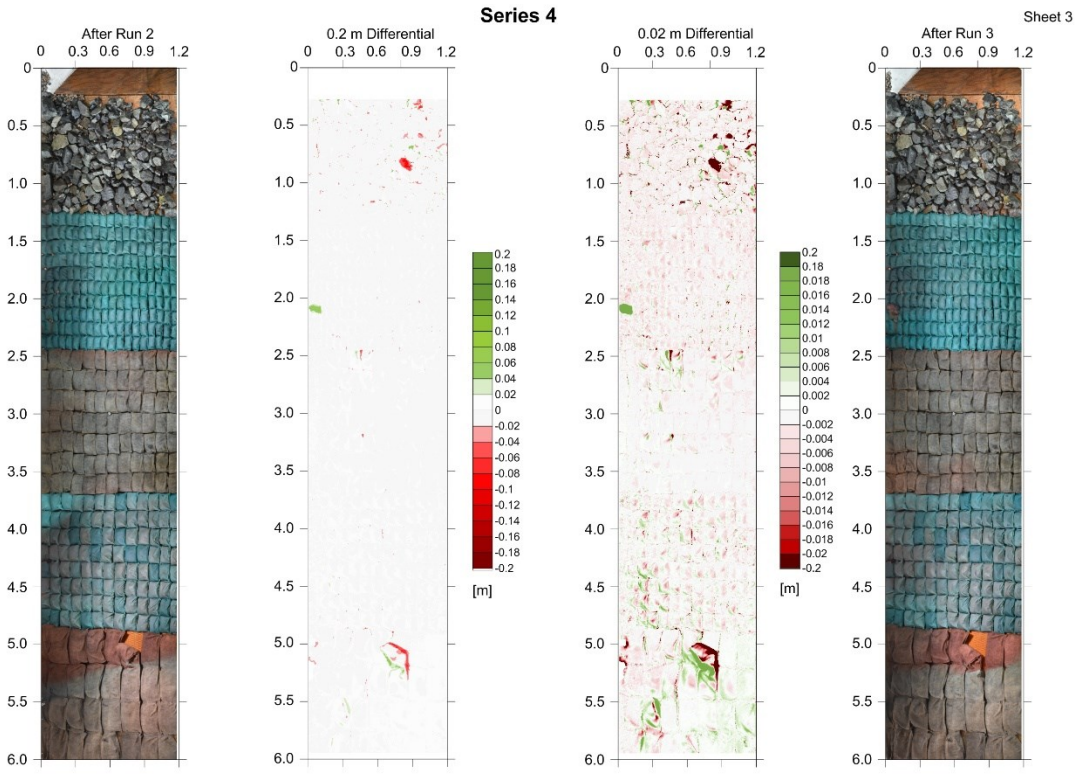

Figure A-15: Differential image for Series 4 after Run 3

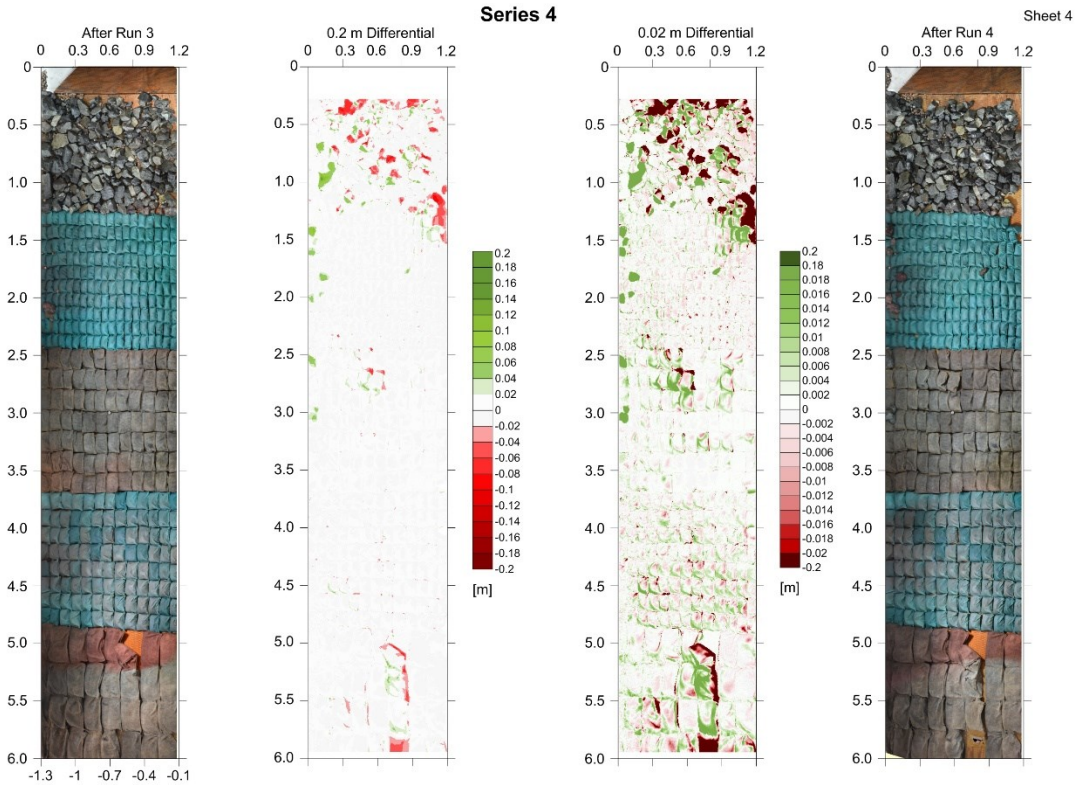

Figure A-16: Differential image for Series 4 after Run 4

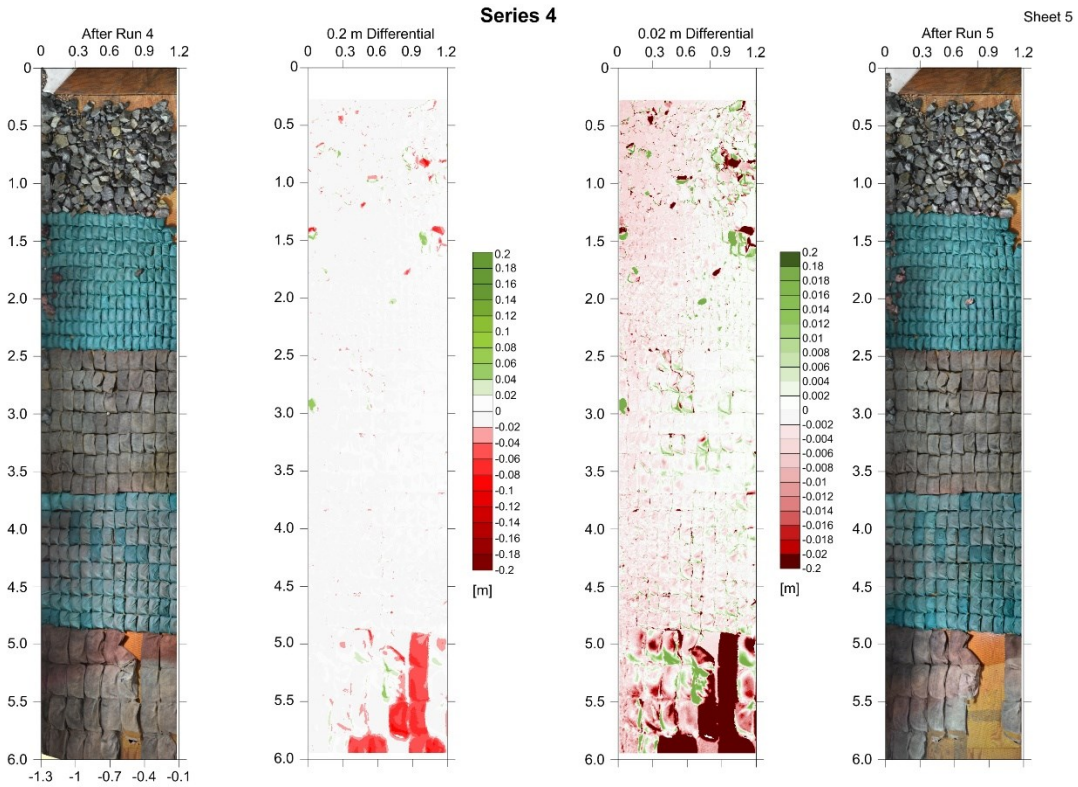

Figure A-17: Differential image for Series 4 after Run 5

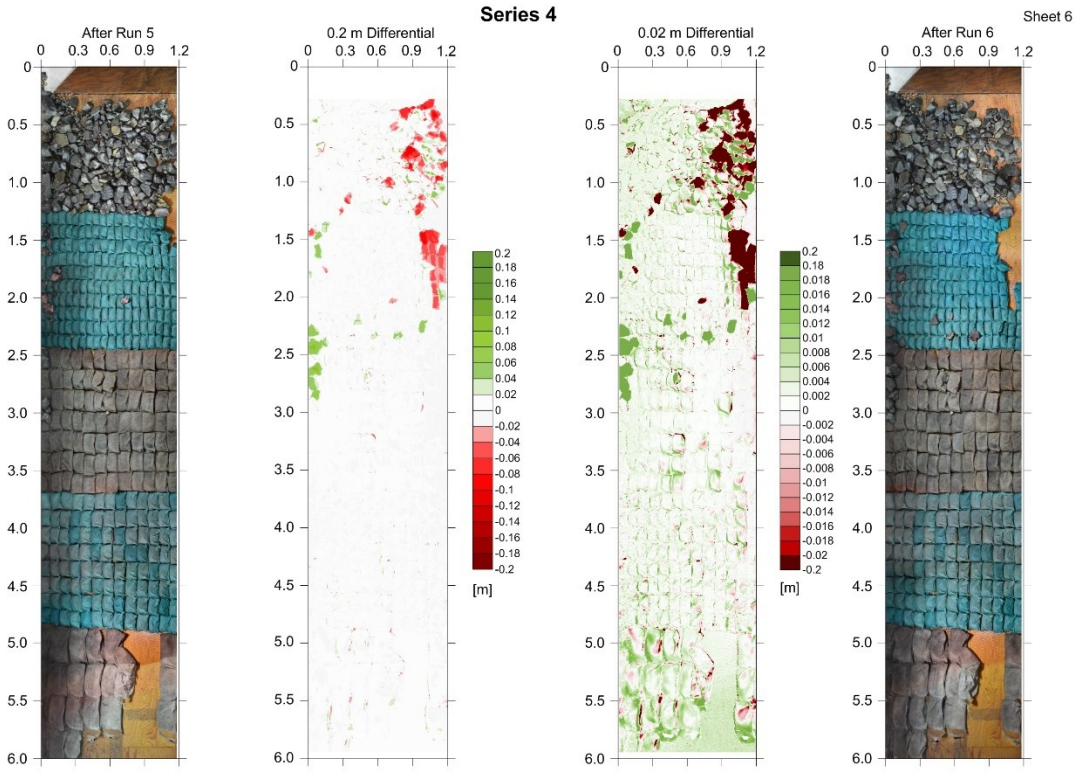

Figure A-18: Differential image for Series 4 after Run 6

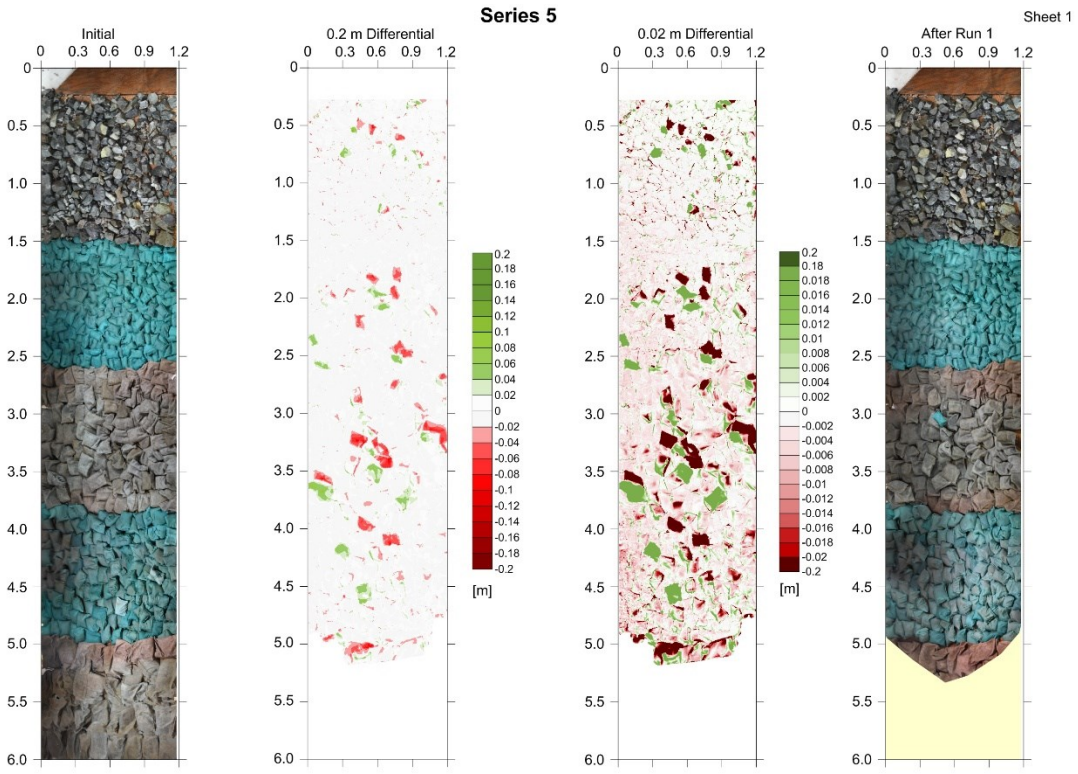

Figure A-19: Differential image for Series 5 after Run 1

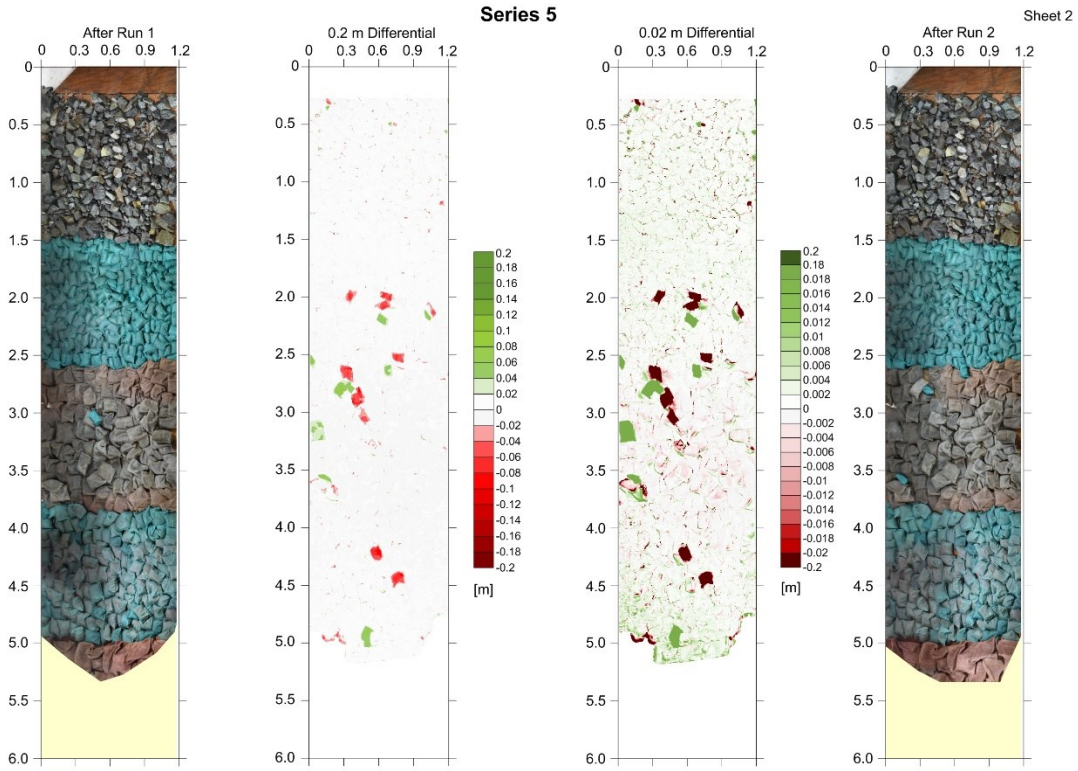

Figure A-20: Differential image for Series 5 after Run 2

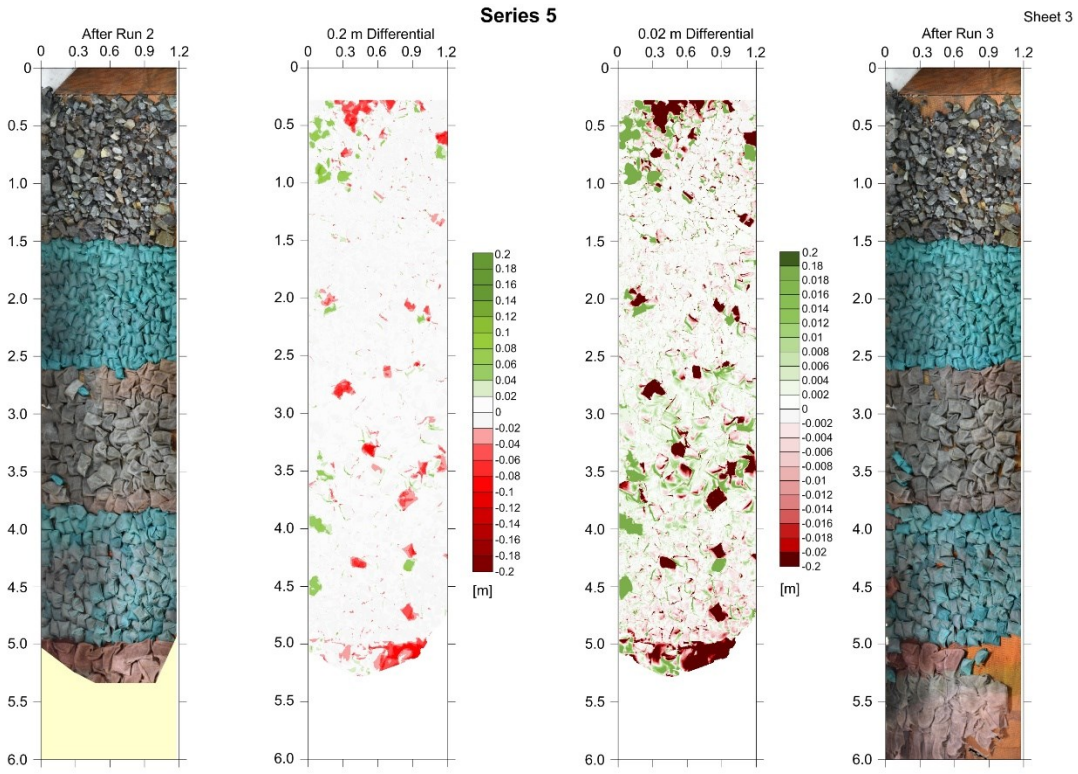

Figure A-21: Differential image for Series 5 after Run 3

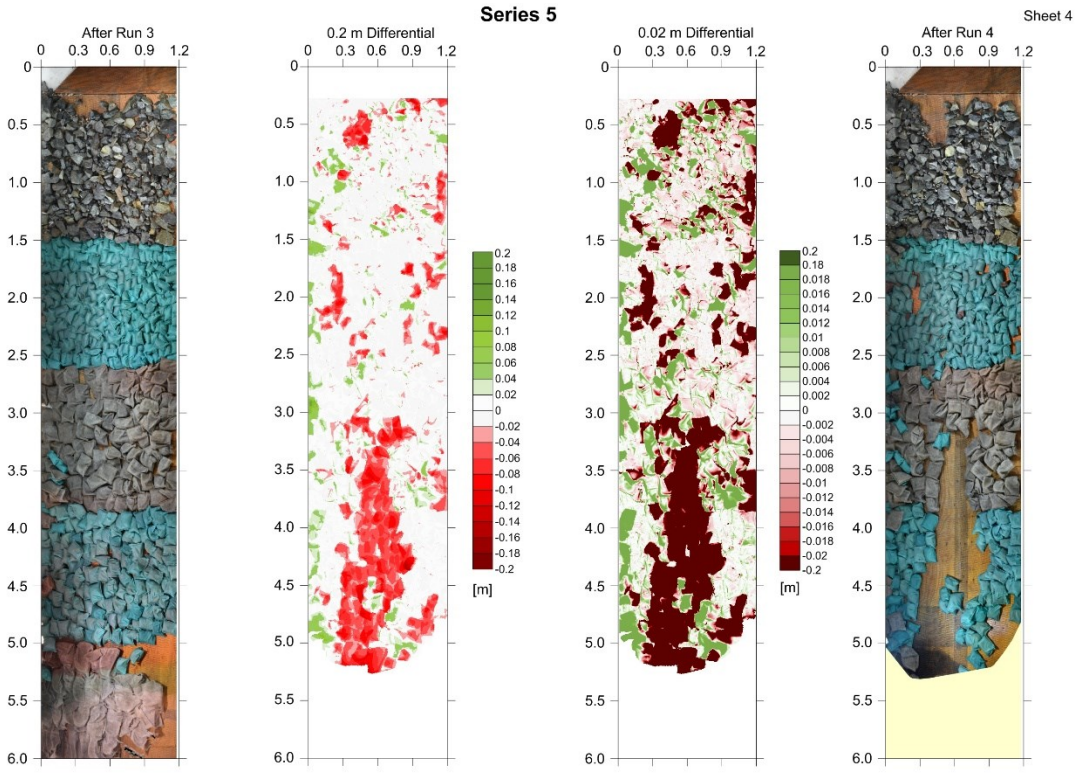

Figure A-22: Differential image for Series 5 after Run 4